Viscosity of aqueous and cyanate ester suspensions containing alumina nanoparticles

by

Katherine Ann Lawler

A thesis submitted to the graduate faculty

in partial fulfillment of the requirements for the degree of

MASTER OF SCIENCE

Major: Materials Science and Engineering

Program of Study Committee:
Mufit Akinc, Co-major Professor
Michael R. Kessler, Co-major Professor
Klaus Schmidt-Rohr

Iowa State University

Ames, Iowa

2009

Table of Contents

Acknowledgements

I would like to thank my Major Professors Dr. Mufit Akinc and Dr. Michael Kessler for their support and guidance given throughout my research work. I greatly appreciate all that they have done. Thanks also to my committee Klaus Schmidt-Rohr for help with NMR analysis. Special thanks also to Wilber Lio, Xia Sheng, Yusuf Yusufoglu, and Tim Mauldin for being there to answer my questions as well as Lisa Nielsen and Lars Ellingson for their time spent in the lab working with me for their Freshman Honors projects. Last, but certainly not least, thanks to my parents and Craig Ament, my fiancé, for their great support.

This work was partially funded by the Ames Laboratory Seed Grant Program and supported by a grant from the Strategic Environmental Research and Development Program (SERDP), under the "Environmentally Benign Repair of Composites Using High Temperature Cyanate Ester Nanocomposites" project (Project Number WP-1580). The United States government has assigned the DOE Report number IS-T 2902 to this thesis.

Chapter 1

Introduction

Organization

This thesis is composed of a general introduction and a conclusion sections surrounding two chapters, each of which is a manuscript to be submitted for publication. The common topic shared between these papers is "suspensions containing alumina nanoparticles and the viscosity reduction of highly loaded suspensions achieved through the addition of short organic molecules". At first, it would seem that these subjects are closely related, but actually the suspensions containing water as the solvent behave much differently than suspensions based on the bisphenol E cyanate ester (BECy) monomer. Consequently, the phenomena investigated in the two papers are not closely related besides the viscosity reduction aspect. It is advantageous to reduce the viscosity of highly loaded aqueous slurries of nanoparticles in order to produce high quality slip cast or tape cast advanced ceramic bodies. The addition of non-toxic, renewable saccharide molecules to these suspensions will reduce the viscosity. Also, it will be necessary to reduce the viscosity of highly loaded BECy suspensions in order to make them injectable for composite repair. Benzoic acid was found to be an appropriate additive for viscosity reduction in this case. This introduction will give background information about viscosity measurements and the systems studied.

Literature Review

Previous investigations of the rheology and effects of saccharide additions to aqueous suspensions of alumina nanoparticles have been performed by Schillinget al. Their original work with micron-sized alumina particles[1,2,3] showed that both saccharides and starches were effective at reducing the viscosity of those suspensions. When these organic molecules were added to suspensions of nanoparticles, it was found that larger saccharides (oligo- and poly-) were not effective at reducing the viscosity. Instead, these molecules increased the viscosity of the suspensions probably due to particle bridging as the long-chain saccharides connected the particles and caused an increase in viscosity. While the larger molecules were not found

to reduce the viscosity of suspensions, mono- and di-saccharides such as fructose and sucrose as well as sugar alcohols were found to work well, even at low concentration[4].

Although no flow curves were shown, their rheological measurements were fit to the Herschel-Bulkley model:

$$\tau = \tau_o + K(\dot{\gamma})^n$$

Equation 1.1

Where τ is the shear stress, τ_o is the yield stress, K is the consistency coefficient, $\dot{\gamma}$ is the strain rate and n is the flow behavior index. Their results are shown in Table 1, below.

Table 1. Effect of type and concentration of saccharide and sugar alcohol in 30 vol% alumina suspensions. Adapted from reference[4]

Additive	Concentration (wt%)	Yield stress τ_o (Pa)	Consistency coefficient K (Pa*s^n)	Flow behavior index n
None	0	13.1	5	0.4
D-mannitol	5	0	0.46	0.58
Xylitol	5	0	0.49	0.56
D-Sorbitol	5	0	0.47	0.57
Maltitol	5	0	0.43	0.58
Arabinose	5	0	0.42	0.58
Xylose	5	0	0.47	0.57
D-Galactose	5	0	0.71	0.53
D-Fructose	5	0	0.41	0.58
D-Glucose	5	12.7	6.44	0.37
Sucrose	5	0	0.67	0.55
Maltose	5	13.8	3.24	0.43

Suspensions with a yield stress were said to have no viscosity reduction. Also, a high consistency coefficient value also indicated no reduction in viscosity. Glucose and maltose did not improve rheological parameters according to this work as they showed yield stresses and consistency coefficients similar to the sample with no additive.

Analysis was done to determine which saccharides were most effective at viscosity reduction. The authors found some correlation between viscosity reduction and the presence of the 4-hydroxyl group in its axial or equatorial position on a given saccharide. However,

this analysis was not rigorous and the authors determined glucose to be ineffective, though through the work in this thesis it was found that glucose was consistently more effective than sucrose. So, the correlation between saccharide effectiveness and viscosity reduction has not been resolved, but it has been proven that some saccharides are more effective than others.

Li and Akinc[5] also explored the viscosity reduction of alumina nanoparticle suspensions achieved with fructose. It was found that fructose effectively reduced the viscosity of nanoparticle suspensions, and this was attributed to adsorbed fructose on the particle surface. NMR experiments showed that fructose was adsorbed as a function of concentration up to a limit. This was done by integrating the methanol (solvent) peak and the $-CH_2$ peak of fructose found in the supernatant of the centrifuged suspension to see how much fructose was adsorbed. Figure 2 indicates that the maximum adsorbed fructose is about 0.012 g/g Al_2O_3 for a 20 vol% suspension.

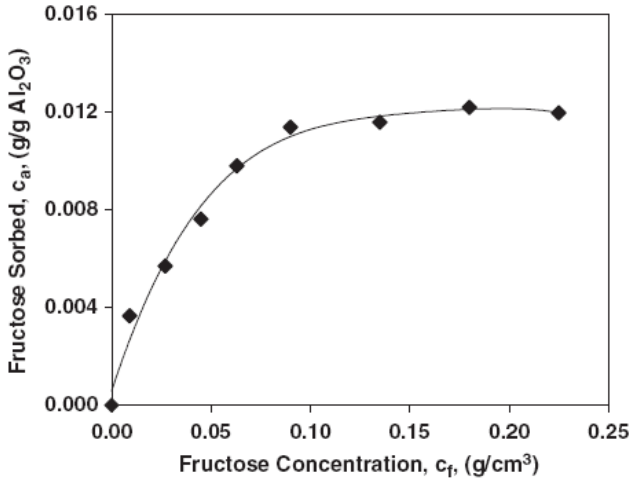

Figure 2. Results of NMR determination of fructose adsorption[5]

It is thought that the adsorption of fructose displaces bound water from the surface of the particles and increases the amount of bulk water in the suspension thereby lowering the viscosity of the suspension because bound water is associated with the particle surface and does not contribute to fluidity. The presence of bulk and free water was observed by DSC measurements. In Figure 3 this is shown by peak 1 (bound water) and peak 2 (free water).

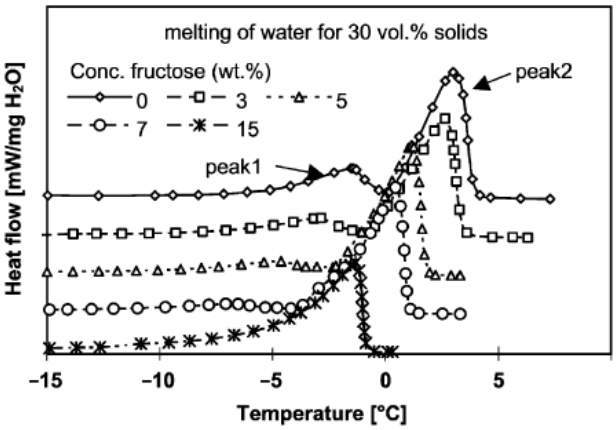

Figure 3. Melting of 30 vol% alumina suspensions measured by DSC[5].

The presence of the free and bound water in ceramic particle suspensions is also found in the work of Rennie and others[6,7] who have studied the melting of water in porous silicas. Figure 4 (b) shows the behavior of nanoporous silica particles that are saturated with bound water and no free water. The singular peak begins to melt at a lower temperature (-10^{o}C) than bulk water which is expected to melt at 0^{o}C. Curves in (c) and (d) correspond to samples with free and bulk water which is manifested in the two melting events.

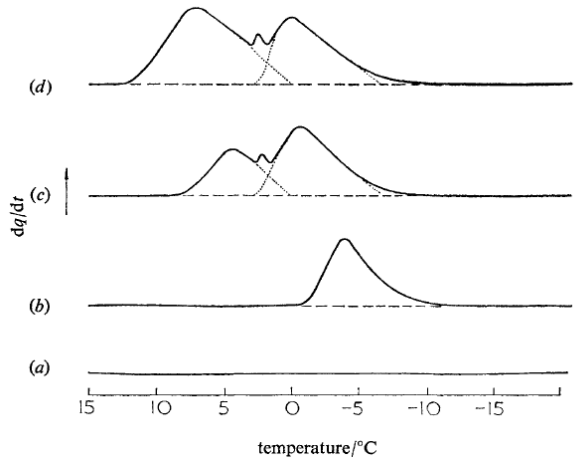

Figure 4. DSC traces of the melting of water in nanoporous silica[8]

Further evidence of the bound water theory is given by ^{17}O-NMR results which indicate that fructose releases bound water from the particle surface. This is seen in the up-

field shift of the peak corresponding to the suspension with fructose with respect to the suspension without fructose.

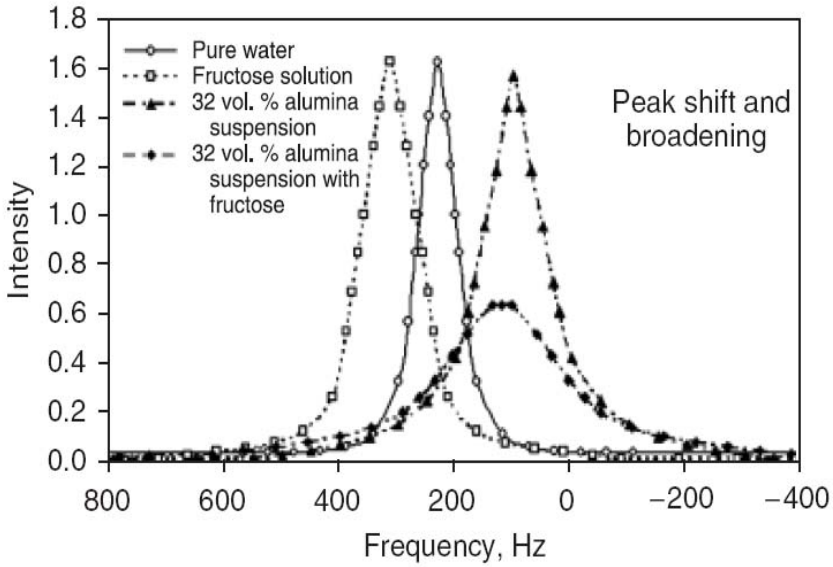

Figure 5. NMR relaxation behavior of suspensions showing that fructose modifies aqueous suspensions of alumina nanoparticles[9]

The literature describing the viscosity of cyanate ester/alumina nanocomposites is not as well developed as the literature for aqueous alumina suspensions. There are reports of suspensions made with fumed silica[10,11], polyhedral oligomeric silsesquioxane[12], layered silicate[13], and zirconium tungstate[14] filler particles. There is information about these ceramic fillers, which have been added to modify the rheology and mechanical properties of cyanate ester resins, but work on alumina fillers is currently limited. There is a patent describing a high temperature adhesive which incorporates tough, low thermal expansion materials which include alumina[15], but it does not provide any information on the detailed description of the system. Recently, our group explored the properties of BECy/alumina nanocomposites at low alumina loadings,[16] but no work has been done so far to characterize more highly loaded suspensions. Goertzen et al. studied highly loaded suspensions of BECy and silica nanoparticles[17] . It was found that at low loadings, the viscosity of the suspension remained Newtonian. Suspensions below 10 vol% were shear thinning and the shear thinning behavior

increases with particle loading. The shear thinning behavior was attributed to hydrogen bonding between silica aggregates in the suspension. This can be seen in Figure 6, below.

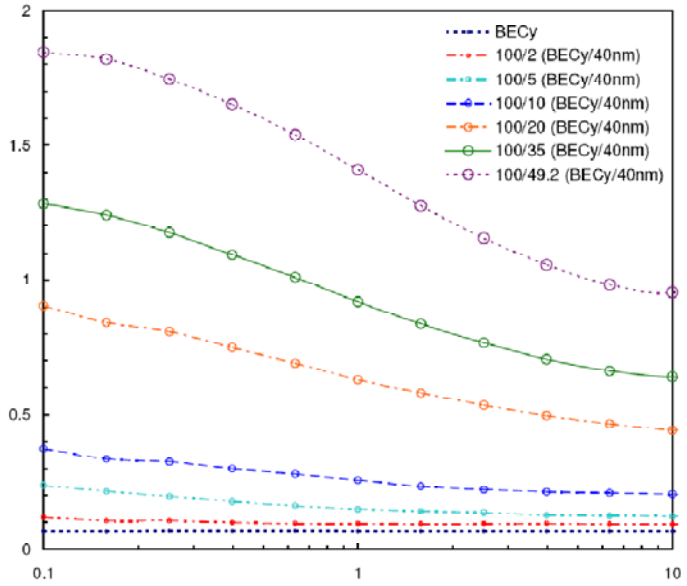

Figure 6. Viscosity of BECy/silica nanoparticle suspensions. Note that 49.2phr corresponds to 20.7vol% silica loading[18]

Raghavan[11] studied silica dispersions in other organic liquids, such as glycols. These suspensions showed shear thinning and shear thickening at high shear rates for 10 vol% solids and also exhibited higher relative viscosities than predicted with the Einstein Equation.

In another study of ceramic particles in BECy, Wooster[19] studied the viscosity of layered silicates. The particles, which did not dissociate in BECy, resulted in a slight viscosity increase, and the particles which exfoliated and allowed BECy to intercalate between the silicate sheets resulted in increased viscosity.

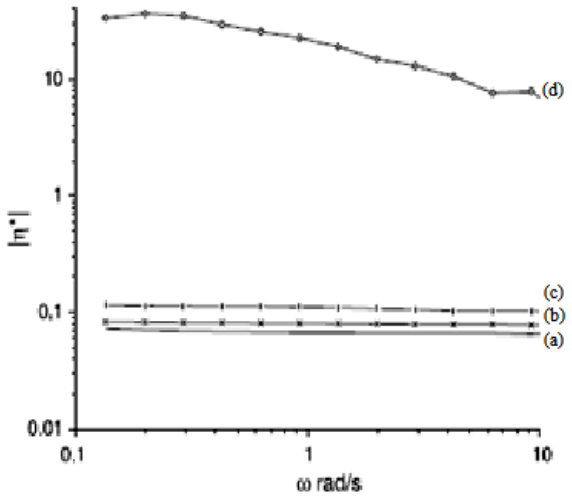

Figure 7. Viscosity of several BECy/layered silicate suspensions at 5wt% montmorillonite[20]. The solid line is BECy (a), sodium montmorillonite (b), methyltallow-bis-2-hydroxyethyl quaternary ammonium cation exchanged montmorillonite (c), and phenylated ammonium cation montmorillonite (d). These appear in the order of increasing viscosity.

A conclusion that was drawn from this study is that the viscosity is dependent on the amount of silicate exposed to the monomer. In samples a-c, the particles remained coherent but in sample d, the clay layers were separated which allowed BECy to enter between the silicate sheets and have more contact with the monomer. Also, Newtonian behavior is seen in the suspensions where the particles remained intact, and shear thinning is seen in the case of the nanocomposite with increased particle exposure to suspending liquid.

Sheng measured the viscosity of BECy/alumina nanoparticle suspensions up to 3 vol% and found the relative viscosity was higher than predicted by the theoretical Einstein equation for dilute suspensions of spherical particles[20].

Experimental Details

Viscosity

Viscosity, η, quantifies the ease of flow of a material. In the case of particle containing suspensions, this property is extremely relevant, since it will provide information about how easily a material can flow through processing equipment. Viscosity is a

fundamental parameter of a material and can be found by the ratio of shear stress to strain rate.

$$\eta = \frac{\tau}{\dot{\gamma}}$$

Equation 1.2

In the equation above, τ is shear stress, $\dot{\gamma}$ is shear strain rate, and η is dynamic viscosity.

Shear stress is a measure of the force that is exerted on an area in a direction parallel to the flow direction, and shear rate describes how fast a fluid layer moves with respect to another fluid layer in a laminar flow. In a laminar flow, the direction of flow at each point in the fluid is constant. The following equations further describe stress and strain rate.

$$\tau = \frac{F}{A}$$

Equation 1.3

$$\dot{\gamma} = \frac{\Delta v}{\Delta h}$$

Equation 1.4

In these equations, F is force, A is the area parallel to the flow direction, Δv is the velocity difference between layers and Δh is the distance between layers. These equations exactly define shear stress and strain rate, but they are not very practical. To find stress and strain rate experimentally, other equations, based on instrument geometry, are used. Also, it is important to note that these equations only applicable to laminar flow conditions such as those found in the experimental setups employed for this work.

Examples of different fluid flow properties are shown in Figure 8, below. A fluid is called “Newtonian”, which is behavior (i), when the viscosity value is constant through all values of strain rate (it is strain rate independent). Also, the shear stress is proportional to the strain rate. The viscosity of BECy, and low solids content suspensions of BECy show this behavior. Aqueous suspensions encountered in this work are primarily non-Newtonian, and

are shear thinning or shear thinning with a yield stress, which are behaviors illustrated in plots (iii) and (iv).

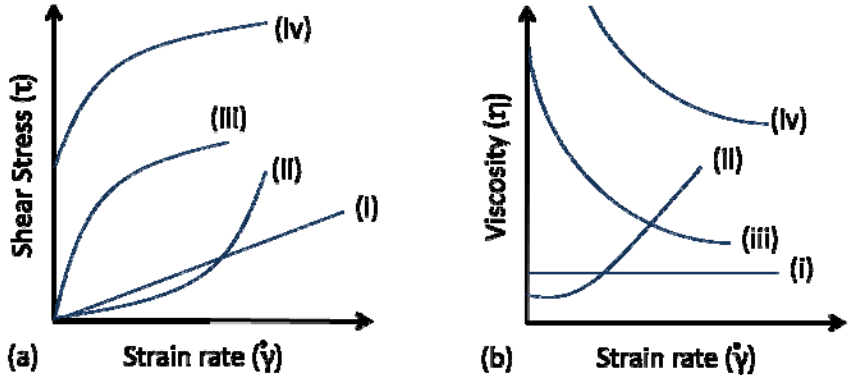

Figure 8. i) Newtonian, ii) shear thickening, iii) shear thinning, iv) shear thinning with a yield stress. Adapted from reference[21].

Measurement systems used to perform the viscosity measurements include a coaxial cylinder system and a cone and plate system. In a coaxial cylinder system, the sample is placed into a cup and then a cylinder is immersed in the sample. A Searle-type system was used where the inner cylinder is rotated and the torque opposing its motion is measured. When there is a narrow gap between the cup and cylinder, the shear stress is nearly constant throughout the gap, so these systems can measure the viscosity of a liquid precisely. The equations, below, describe the shear stress and shear rate in a standard ISO coaxial cylinder system.[22]

$$\tau_{21} = \frac{0.0446 * M}{R_i^3}$$

Equation 1.5

$$\dot{\gamma} = 1.291 * n$$

Equation 1.6

In these equations, n is the rotational frequency and M is a correction factor. R_i is the radius of the inner cylinder, which can be seen in Figure 9, below.

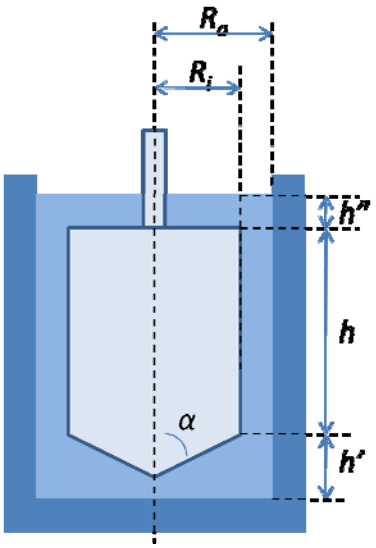

Figure 9. Coaxial cylinder, ISO system, (Searle type). Adapted from reference[23]

The cone and plate geometry offers a high accuracy viscosity determination with a small amount of sample. This was found to be a great advantage because samples of 10-20mL would be sufficient for viscosity measurements instead of 100mL samples required for the cup and cylinder configuration.

The cone sensor shape is defined by the cone radius, R, and angle, α. A cone of $\alpha = 1^{o}$ was used, and this shallow angle is recommended to ensure a uniform shear rate through the sample[23]. Equations for determining the shear stress and shear rate, which can be used to find viscosity, are listed below:

$$\tau_{21} = \frac{3M}{2\pi R^3}$$

Equation 1.7

$$\dot{\gamma} = \frac{\omega}{\tan \alpha}$$

Equation 1.8

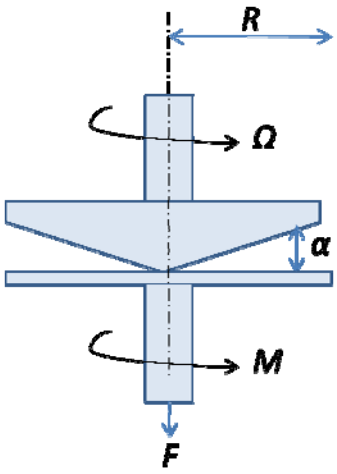

Figure 10. Cone and plate configuration. Adapted from reference[23]

The limitation of the cone and plate configuration is that at high angular velocities, centrifugal forces will throw the fluid out of the gap. Also, another downfall of the technique is that there is high level of error if the sample is loaded incorrectly. It was found that a micropipette was an easy way to ensure that the gap was filled consistently with the same amount of sample.

During the transition period between measuring with the cylinder system and cone and plate system, identical samples were measured with both systems and it was found that the viscosity was the same no matter which measuring system employed. Therefore, data was directly comparable between the two measurement configurations and no distinction will be made when reporting data for the various samples.

Aqueous suspensions

Aqueous suspensions of nanoparticles were studied in order to gain more insight on the viscosity reduction that is observed when saccharides are added. Much work has already been done on this topic, and it is well established that some mono-saccharides[5], di-saccharides[2], polysaccharides[1] and sugar alcohols[4] do reduce the viscosity of these suspensions. Some saccharides, however, are more effective than others. It was found in this work that the viscosity reduction ability of mono- and di- saccharides occurs in this order: fructose > glucose > sucrose. Also, other saccharide and saccharide derivative molecules including myoinositol, d-mannitol, methyl glucopyranoside, and raffinose pentahydrate were

studied and are reported in the manuscript. Lactose monohydrate was studied as well and is shown in Figure 11.

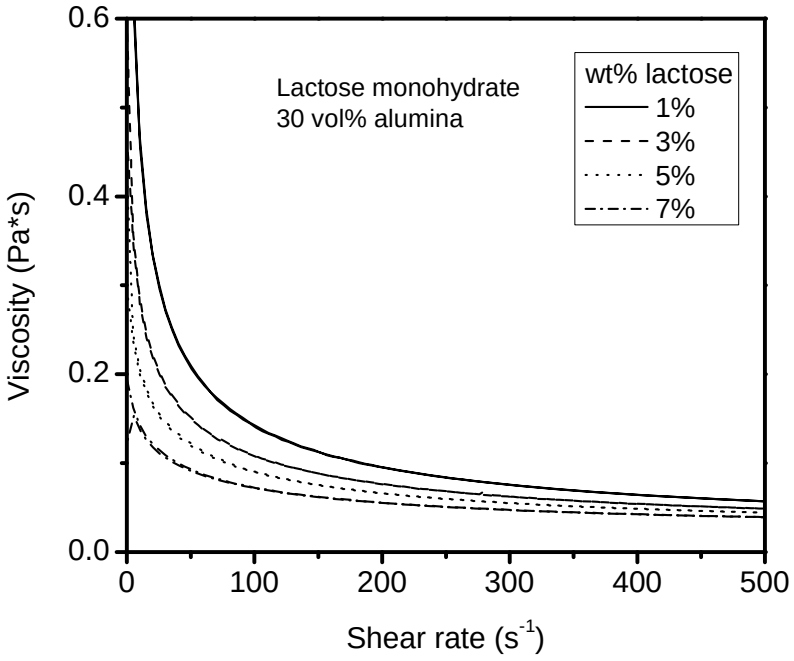

Figure 11. Viscosity of suspensions with 30 vol% alumina nanoparticles and various amounts of lactose monohydrate based on the weight of alumina.

Figure 11 illustrates the typical behavior of the aqueous alumina nanoparticle suspensions. The viscosity becomes less with increasing shear rate (shear thinning) and the viscosity is dependent on the amount of saccharide added. There are two curves shown for each sample: one is the viscosity measured with increasing shear rate from 0 – 500 s^{-1} and the other is the viscosity measured with decreasing shear rate from 500 s^{-1} back to 0 s^{-1}. The curves coincide because there is a unique equilibrium viscosity value at each shear rate.

When performing shear rate dependent tests for these shear thinning suspensions, it is important to consider the time dependent effects. If the measurement is done too quickly, there may be error introduced in the measurement. It may take some time for equilibrium to be achieved throughout the measurement at each shear rate.

As the shear rate increases during a measurement period, flocculated particles in a suspension may be broken up by the shear forces imposed on the sample. The shear thinning phenomenon has been attributed to the release of liquid from flocculated particle structures that are broken at high shear rates. At low shear rates the liquid is immobilized inside the flocs, but at high shear rates the released liquid allows the suspension to flow with a lower viscosity.[24-27]

During the decreasing shear step and after the sample has experienced high shear rates (500 - $0s^{-1}$), samples must be given enough time to return to the initial, flocculated condition. Especially at lower shear rates, the viscosity of the sample can appear to be less than the equilibrium value. Likewise, during the increasing shear step the viscosity can appear to be greater than the equilibrium value. This behavior is illustrated in Figure 12, below. So, if the samples are given enough time to equilibrate so that the flocs are broken and reformed between shear rate steps, the viscosity data for both the increasing and decreasing shear portions will coincide.

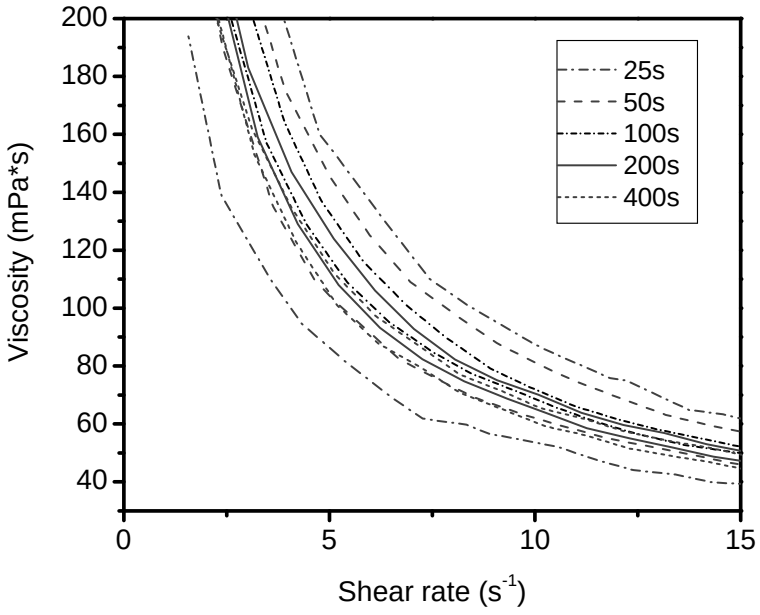

Figure 12. Speed of shear rate increase on viscosity for a 3.0 μm sample with no additive. The legend indicates the time to reach 100 s^{-1} from the stationary state.

It can be seen that as the time spent at each shear rate increases, the curve becomes more reproducible. This is expected, since the optimum measurement time increases as the shear rate becomes closer to zero.[28] The "25 s" and "400 s" runs show significant difference in viscosity for comparable shear rates. On the other hand, the 200 s and 400 s data are very reproducible.

In order to record the equilibrium viscosity value, in subsequent runs the measurement time was set so that the difference between the advancing and decreasing branches is insignificant. This was found to be at least 10 s at each measurement point. An example set of curves is shown in Figure 13. For viscosity values recorded with the TA2000EX rheometer (TA instruments, New Castle, DE), at each measurement point, the 10s interval was performed consecutively for 3 measurements and the average viscosity value was reported. Since the viscosity curves for these samples are reproducible throughout the three consecutive measurements, the suspension must have an equilibrium state at each shear rate.

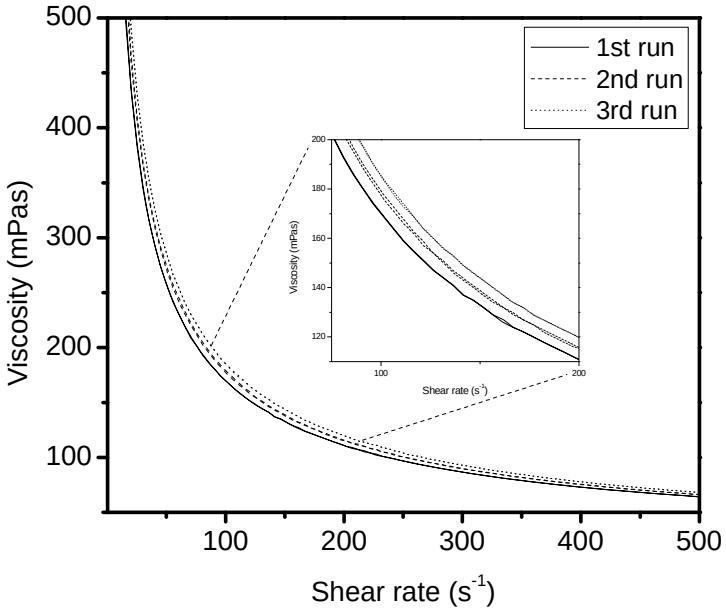

Figure 13. Three consecutive runs of the same sample (30 vol% 40 nm particles with 1% fructose) show that the curves for each run are coincident. The small viscosity increase with each run is attributed to water evaporation over time.

Suspensions with BECy as liquid

Early experiments with BECy included the addition of saccharides to the monomer which resulted in an increased viscosity as seen in Figure 14. This behavior was not unreasonable because saccharides added to water also increase the viscosity of the solution.

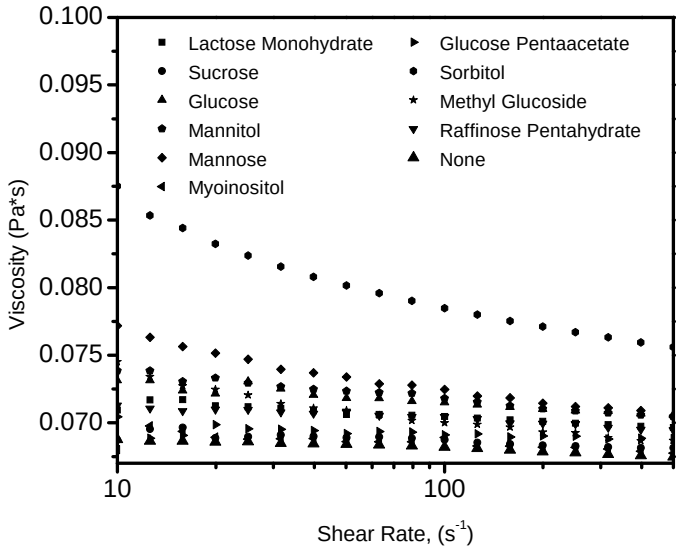

Figure 14. Addition of saccharides to BECy increases the viscosity

It was thought that the addition of saccharides would reduce the viscosity of highly loaded suspensions of alumina in BECy similar to the way that the viscosity was reduced in aqueous suspensions. BECy/alumina suspensions with saccharide additions proved that this was not the case. It is believed that the limited solubility of saccharide in BECy in contrast to water is the probable cause of viscosity increase. Only glucose pentaacetate and myoinositol appeared to dissolve completely, but these molecules did not reduce the viscosity of a 5 vol% alumina suspension either.

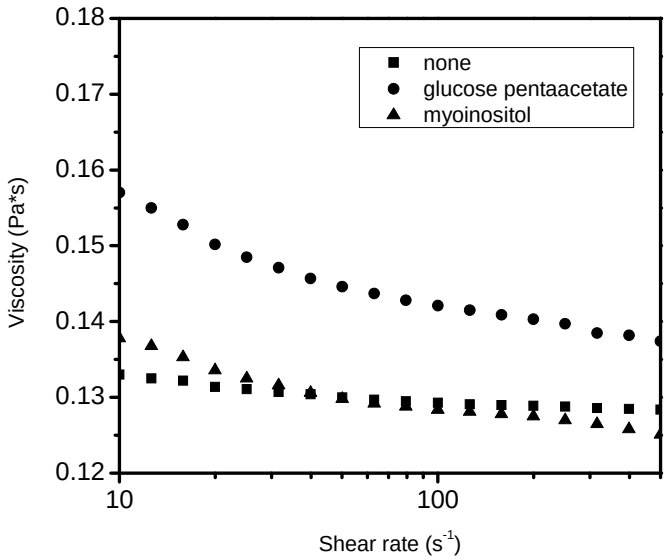

Figure 15. Addition of glucose pentaacetate and myoinositol at 2wt% based on alumina does not reduce the viscosity of a 5 vol% suspension.

Next we searched for a molecule that was similar to a monosaccharide that would be attracted to the alumina surface and compatible with BECy. It was found that the carboxylic acids such as benzoic and cinnamic acid dissolved in the monomer and reduced the viscosity of the suspension. Benzoic acid was pursued due to its simpler structure. Further experiments with nuclear magnetic resonance (H-NMR) spectroscopy were performed to understand the possible mechanism of the viscosity reduction by determining the interactions between BECy, alumina and benzoic acid.

Through these studies, the viscosity reduction of aqueous and organic liquid-based suspensions of alumina nanoparticles with the addition of various additives has been explored and quantified. These studies have also helped elucidate the plausible mechanisms for the viscosity reduction, by studying the flow behavior of the suspensions. The roles of these additives are discussed in more detail in the following chapters.

References

[1] Schilling, C. H., C. Li, et al. (2002). "The rheology of alumina suspensions: influence of polysaccharides." J. Eur. Ceram. Soc. **22**(6): 923-931.

[2] Kim, J. C., C. H. Schilling, et al. (2000). "Plasticizing dense alumina slurries with mono- and di-saccharides." Mater. Lett. **42**(4): 221-224.

[3] Sikora, M., C. H. Schilling, et al. (2002). "Dextrin plasticizers for aqueous colloidal processing of alumina." J. Eur. Ceram. Soc. **22**(5): 625-628.

[4] Schilling, C. H., M. Sikora, et al. (2002). "Rheology of alumina-nanoparticle suspensions: effects of lower saccharides and sugar alcohols." J. Eur. Ceram. Soc. **22**(6): 917-921.

[5] Li, C. and M. Akinc (2005). "Role of bound water on the viscosity of nanometric alumina suspensions." J. Am. Ceram. Soc. Society **88**(6): 1448-1454

[6] Levy, E., A. I. Kolesnikov, et al. (2009). "Structure of water in mesoporous organosilica by calorimetry and inelastic neutron scattering." Surf. Sci. **603**(1): 71-77.

[7] Johari, G. P. (2005). "Water's size-dependent freezing to cubic ice." J. Chem. Phys. **122**(19): 194504/1-194504/5.

[8] Rennie, G. K. and J. Clifford (1977). "Melting of ice in porous solids." J. Chem. Soc., Faraday Trans. 1 **73**(4): 680-9.

[9] Li, C., M. Akinc, et al. (2005). "Relationship between water mobility and viscosity of nanometric alumina suspensions." J. Am. Ceram. Soc. **88**(10): 2762-2768

[10] Goertzen, W. K., X. Sheng, et al. (2008). "Rheology and curing kinetics of fumed silica/cyanate ester nanocomposites." Polym. Eng. Sci. **48**(5): 875-883.

[11] Raghavan, S. R., H. J. Walls, et al. (2000). "Rheology of Silica Dispersions in Organic Liquids: New Evidence for Solvation Forces Dictated by Hydrogen Bonding." Langmuir **16**(21): 7920-7930.

[12] Liang, K., G. Li, et al. (2006). "Cyanate ester/polyhedral oligomeric silsesquioxane (POSS) nanocomposites: synthesis and characterization." Chem. Mater. **18**(2): 301-312.

[13] Wooster, T. J., S. Abrol, et al. (2005). "Rheological and mechanical properties of percolated cyanate ester nanocomposites." Polymer **46**(19): 8011-8017.

[14] Haman, K., P. Badrinarayanan, et al. (2009). "Effect of a Zirconium Tungstate Filler on the Cure Behavior of a Cyanate Ester Resin." ACS Appl. Mater.

[15] Andersson, C. A. and P. J. Roach (2002). Cyanate ester-based composite adhesive. PCT Int. Wo, (M Cubed Technologies, Inc., USA). 19 pp.

[16] Sheng, X. (2008). Polymer nanocomposites for high-temperature composite repair. MSE. Ames, Iowa State University**:** 145.

[17] Goertzen, W. K., X. Sheng, et al. (2008). "Rheology and curing kinetics of fumed silica/cyanate ester nanocomposites." Polym. Eng. Sci. **48**(5): 875-883.

[18] W. K. Goertzen, X. Sheng, M. Akinc, and M. R. Kessler, Polymer Engineering and Science; 2008; 48, 875-883.

[19] Wooster, T. J., S. Abrol, et al. (2005). "Rheological and mechanical properties of percolated cyanate ester nanocomposites." Polymer **46**(19): 8011-8017.

[20] Sheng, X. (2008). Polymer nanocomposites for high-temperature composite repair. MSE. Ames, Iowa State University**:** 145.

[21] Rahaman, M. N. (2003). Ceramic Processing and Sintering. New York, Marcel Dekker, Inc.

[22] Clasen, C. and W.-M. Kulicke (2004). Viscosimetry of Polymers and Polyelectrolytes. New York, Springer-Verlag.

[23] White, J. L. (1990). Principles of Polymer Engineering Rheology. United States of America, John Wiley and Sons, Inc.

[24] Tari, G., J. M. F. Ferreira, et al. (1998). "Influence of particle size distribution on colloidal processing of alumina." J. Eur. Ceram. Soc. **18**(3): 249-253.

[25] Studart, A. R., E. Amstad, et al. (2006). "Rheology of concentrated suspensions containing weakly attractive alumina nanoparticles." J. Am. Ceram. Soc. **89**(8): 2418-2425.

[26] Derooij, R. A. A. P., D. Vandenende, J. Mellema (1993). "Steady Shear Viscosity of Weakly aggregating Polystyrene Latex Dispersions." Journal of Chemical Physics **99**(11): 9213-9223.

[27] Potanin, A. A., R. Derooij, D. Vandenende, J. Mellema (1995). "Microrheological Modeling of Weakly Aggregating Polystyrene Latex Dispersions." Journal of Chemical Physics **102**(14): 5845-5853.

[28] Mezger, T. G. (2006). The Rheology Handbook: For users of rotational and oscillatory rheometers. . Hannover, Germany, Vincentz Network GmbH & Co.

Chapter 2

Behavior of shear thinning aqueous alumina nanoparticle suspensions with saccharides: experiment and model

A paper to be submitted to *Journal of the American Ceramic Society*

Katherine Lawler, Michael R. Kessler, Mufit Akinc

Department of Materials Science and Engineering
Iowa State University, Ames, IA 50011, U.S.A

Abstract

Concentrated aqueous alumina nanoparticle suspensions with additions of saccharides such as fructose, glucose, sucrose, and others were studied by rheometry and low temperature differential scanning calorimetry. The viscosity of the suspensions and melting behaviors of the frozen suspensions were used to develop a model based on fractal-type agglomeration which describes the viscosity decrease seen with the addition of these saccharides. It appears that characteristics of particle flocculation are dependent on the saccharide concentration and type. The proposed model is in qualitative agreement with the observed behavior and earlier bound water hypothesis.

1. Introduction

Aqueous suspensions of ceramic nanoparticles are frequently used in the production of slip cast, gel cast, and tape cast ceramic components. The non-hazardous nature of water makes it an ideal solvent for ceramic suspensions. Likewise, saccharide molecules are environmentally friendly and biorenewable which is attractive as industry is transitioning toward sustainable technologies.

γ-phase alumina is a metastable transition alumina which is created during the dehydration of precursor aluminum hydroxides. The surface of nanosized γ-phase powders is highly hydroxylated due to exposure to water vapor. It was postulated by Franks[1] that the OH^- surface groups are primarily singly coordinated due to the presence of many defects, such as plane edges, steps and vacancies, on the powder surface. The advantages of γ-phase nanosized alumina include a lower sintering temperature than α-phase powders and the potential ability to form ultra fine grain size ceramics and nanocomposites.

Aqueous processing of nanosized ceramic particle suspensions poses significant scientific and technological challenges. Due to the decrease in particle size, the specific surface area of these powders is much higher than that of sub-micron sized particles. This provides greater possible contact area for each particle, and consequently interactions with the solvent and other particles and dispersants become more prominent. The interactions within a ceramic particle suspension are complex. There are solvent-particle, particle-particle, solvent-dispersant, and dispersant-particle interactions possible. Many variables may factor including: pH and ionic strength of the solution, reduction of conformational entropy, solubility and structure of the dispersant, and temperature to name a few.[2]

According to the Derjaguin, Landau, Verwey and Overbeek (DVLO) theory, the rheology of a suspension can be controlled by electrical double layer interactionwhich is controlled by adjustment of both the attractive and repulsive forces between particles in suspension.[3] Adsorption of additives, such as saccharides, on the surfaces of particles may promote steric stabilization. Tomasik found that the polysaccharide maltodextrin, a partially hydrolyzed starch, does adsorb onto sub-micron α-alumina and reduces the shear stress at various shear rates.[3] Kim also studied the effect of saccharides on the rheological characteristics of slurries of sub-micron particles and determined that mono- and di-saccharides also adsorb onto alumina with similar results[4]. The research done by Li, Schilling, and Akinc showed that the addition of fructose, sucrose and other polysaccharides to aqueous suspensions produces suspensions of more favorable rheology.[5,6]

The primary purpose of this work is to study the complex behavior of dispersant-particle and solvent-particle interactions through viscosity and DSC measurements of concentrated suspensions. By measuring the bulk properties of the suspensions, it is possible to gain insight about the particle interactions. Water and adsorbed additives at the particle-solvent interface have effects on viscosity[1]. It has been shown previously that saccharides reduce the viscosity of aqueous alumina nanoparticle suspensions, but the shear thinning character of these has not been examined in detail. Low temperature DSC measurements have also been performed, but the effect of different saccharides on the suspension behavior has not been studied.

2. Experimental

2.1. Materials

For this investigation, nanosized γ-phase alumina powder with an average particle size of 48 nm (Nanophase Technology Corporation, Burr Ridge, IL) LOT# AAGE1607 was used. The specific surface area of this powder was taken to be 34 m^2/g, as stated by the manufacturer, and the density of γ-alumina was taken to be 3.6 g/cm^3. The alumina powders were dried for 2 hours at 110^oC before use. Typical TEM micrographs of as received alumina powders are shown in Figure 1.

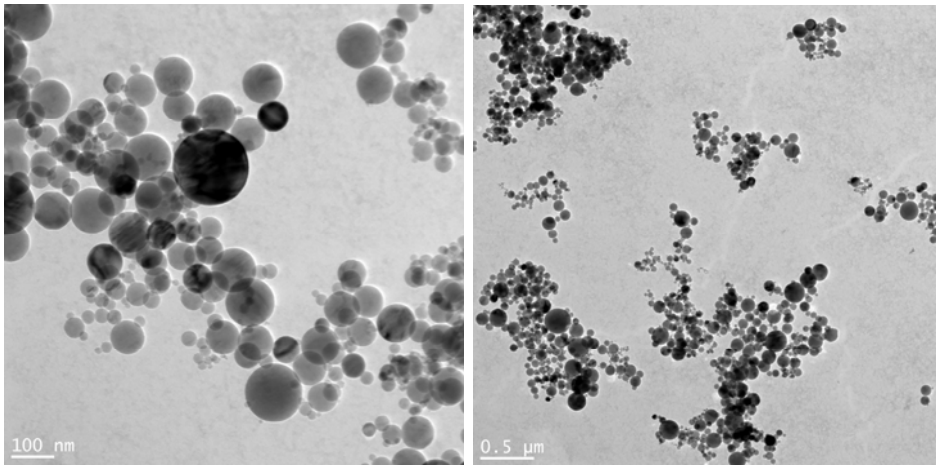

Figure 1. TEM micrographs of nanosized alumina powder. Nano particles are spherical and show significant variation in size.

Saccharides used in this study were obtained from Sigma-Aldrich (St. Louis, MO) except Methyl α-D glucopyranoside and sucrose which were obtained from Fluka (Distributed by Sigma-Aldrich, St. Louis, MO) and Fisher (Pittsburg, PA) respectively. The saccharides were used as received, and suspensions were prepared in deionized water.

2.2. Sample preparation and viscosity measurements

Samples were prepared by adding the desired amount of saccharide to deionized water, then adding the desired amount of alumina powder to the water/sugar solution. For example, in a 30 vol% suspension with 10% fructose, first 100 g of water was measured into a Nalgene brand bottle, then 10.8 g of saccharide was added to the water. To this solution, 108 g of alumina powder (3.6 g/cm^3*30 cm^3 = 108 g) was added. All samples were shaken

with a rocking platform for 24 hours to ensure homogeneity before proceeding with rheological measurements.

A Haake RS75 rheometer (Gebrueder Haake GmbH, Karlsruhe, Germany) with a Z40 type cylinder sensor was used for the first set of experiments. The remainder of the experiments was carried out with a TA instruments 2000EX rheometer (New Castle, DE) with a 1^{o} cone and plate sensor and solvent trap. The difference between the data obtained from the two instruments was negligible; hence it is deemed no distinction is necessary in reporting the data. Experiments were carried out at $25^{o}C$ and the sample temperature was maintained with a circulating bath or a peltier plate. Unless otherwise noted, the shear stress was measured while increasing the shear rate continuously from 0.5 to 500 s^{-1} and back to 0.5 s^{-1} with ten measurement points in each decade. At each measurement point, unless otherwise noted, three consecutive measurements were made in 10 s intervals at the specified shear rate and the average viscosity value was reported.

2.3 Differential Scanning Calorimetry (DSC)

A TA Instruments (New Castle, DE) Q2000 differential scanning calorimeter was used to study the melting behavior of aqueous suspensions in order to gain a better understanding of the solvent/particle and saccharide/particle interactions. Suspensions from 20-70vol% alumina with no saccharide and suspensions of 40vol% alumina with various saccharides were prepared and approximately 12 mg of each sample was sealed hermetically in an aluminum sample pan. Samples were cooled to $-20^{o}C$, held for 1 minute and then the temperature was increased at $1^{o}C$/min up to $10^{o}C$.

3. Results and Discussion

3.1. Viscosity of alumina suspensions with no additive

As the volume percent solids is increased in suspensions of 48 nm particles, the viscosity increases. Figure 2 shows viscosity as a function of shear rate for suspensions of 20-70 vol%. It can be seen that all suspensions are shear thinning. Figure 3 shows the viscosity of each suspension at $100s^{-1}$. This figure illustrates how the viscosity increases

greatly as the solids content is increased beyond 30 vol%. This is in good agreement with the behavior seen in previous work by Li et al.[7]

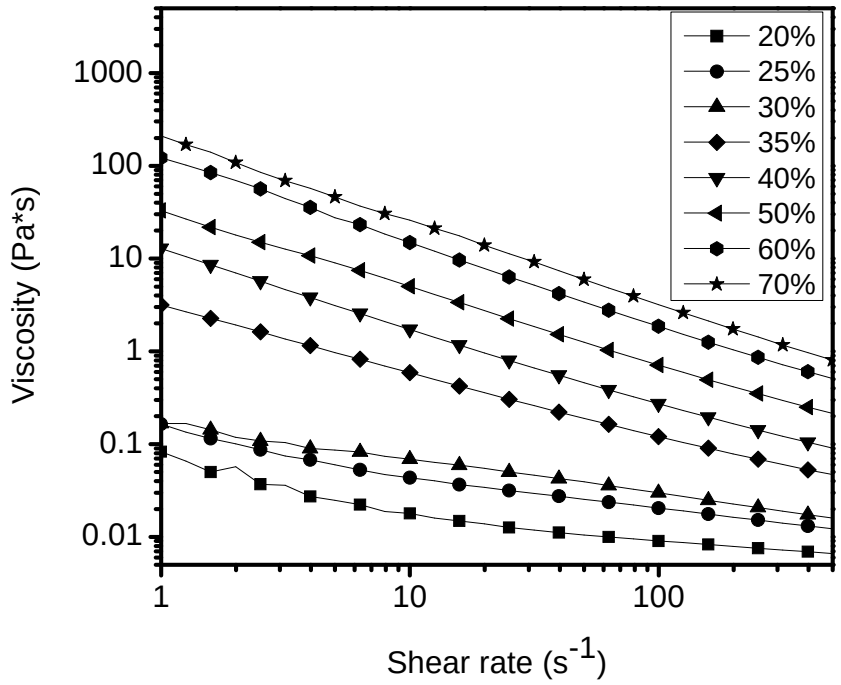

Figure 2. Viscosity as a function of shear rate for alumina suspensions of various volume percent solids. Data points are taken from the decreasing shear rate branch of the cycle (500 - 0.5s^{-1} curve).

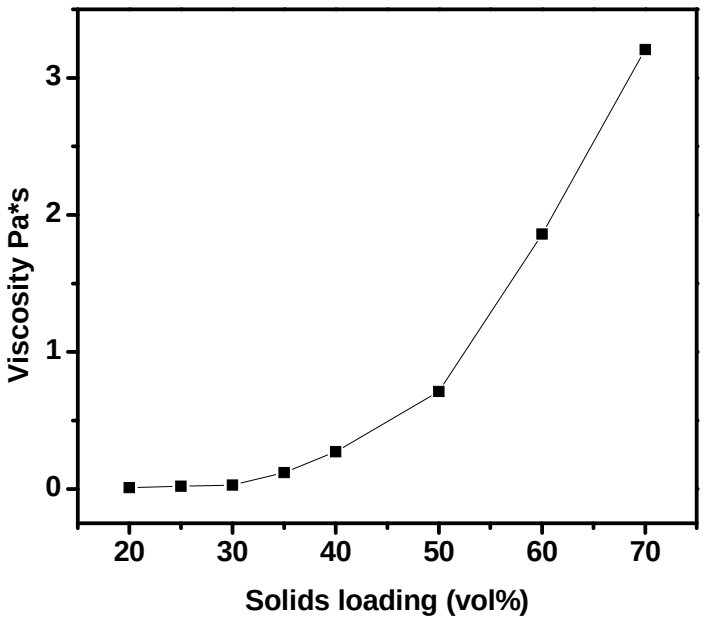

Figure 3. Viscosity at $100s^{-1}$ for each suspension of alumina particles

Figure 3 clearly demonstrates that the viscosity of the aqueous alumina nanoparticle suspensions increases with increased solids content. From 20-35 vol% there is a modest increase in viscosity, then the viscosity increases almost exponentially from 40% to 70%. By 50 vol% alumina, the mixture loses fluidity and becomes a paste that can still be mixed by shaking.

3.2. Role of low molecular weight saccharides on alumina nanoparticle suspension viscosity

For this set of experiments the solids content of the suspensions was kept constant at 30 vol% and saccharide concentration of 18% by weight of alumina. It was known from previous work of Li's[8] that 18% fructose would lower the viscosity of the suspension dramatically, but it was not known how glucose and sucrose would compare. It was shown through NMR experiments that, for 20vol% suspensions, the maximum amount of fructose adsorbed on the particles was about 0.12g/g Al_2O_3 which is close to 18wt% (0.18g/g Al_2O_3)

[7]. So, it is expected that these samples will demonstrate the minimum viscosity attainable by the addition of these saccharides.

Figure 4 clearly shows that all suspensions with or without the additives exhibit shear thinning as expected for concentrated particle suspensions. Also, each of the additives lowers the viscosity of the suspension, as was reported for fructose previously[8]. Fructose has the greatest effect, followed by glucose, and sucrose. The viscosity measurements for each of these samples consisted of three consecutive trials with excellent reproducibility (not shown). A slight difference between viscosity values on increasing and decreasing shear rates may be attributed to the speed of shear rate change and indicative of non-equilibrium state. These measurements were performed at 2 s per measurement point which is less than the ideal measurement time of 10 s stated in the experimental section.

Table 1 shows the shear rate-dependent viscosity ratio, VR, expressed as $\eta(\dot{\gamma}_1)/\eta(\dot{\gamma}_2)$ where $\dot{\gamma}_2 = 10\dot{\gamma}_1$ [9]. The control sample (no saccharide) is most sensitive to shear rate while the sample with fructose is the least affected. This is a manifestation of effectiveness of saccharide as viscosity modifier through the shear rates compared (50 and 500s^{-1}).

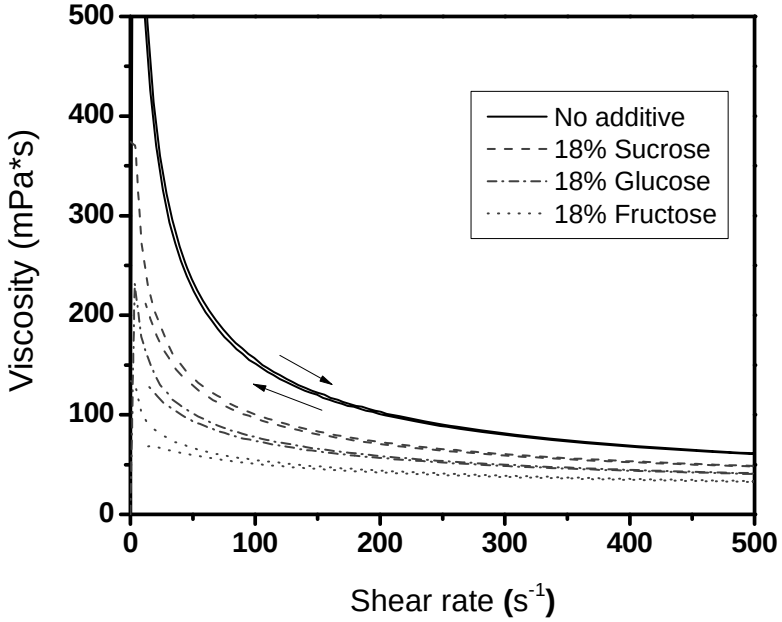

Figure 4. The effect of 18 wt % fructose, glucose, and sucrose on the viscosity of 30 vol% alumina nanoparticle suspensions. (Arrows indicate increasing and decreasing shear rate)

Table 1. Viscosity at selected shear rates and shear rate dependent viscosity ratio (VR) for fructose, glucose, and sucrose containing suspensions at 30 vol% alumina.

	Viscosity (mPa*s)			
Saccharide	**50s^{-1}**	**100s^{-1}**	**500s^{-1}**	**VR***
None	236	157	61	3.87
Sucrose	121	100	48	2.51
Glucose	93	78	40	2.32
Fructose	62	55	33	1.88

*the viscosity ratio at 50s^{-1} to 500s^{-1} shear rate.

3.3 Influence of saccharide concentration in alumina nanoparticle suspensions

Influence of saccharide concentration on the viscosity of 30 vol% alumina suspensions was studied by varying the fructose or glucose concentration from 1% to 18% by weight of dry alumina. Three repetitions of each measurement were made as before, and the data in consecutive runs were reproducible. The results for fructose and glucose are shown in Figures 5a and 5b, respectively.

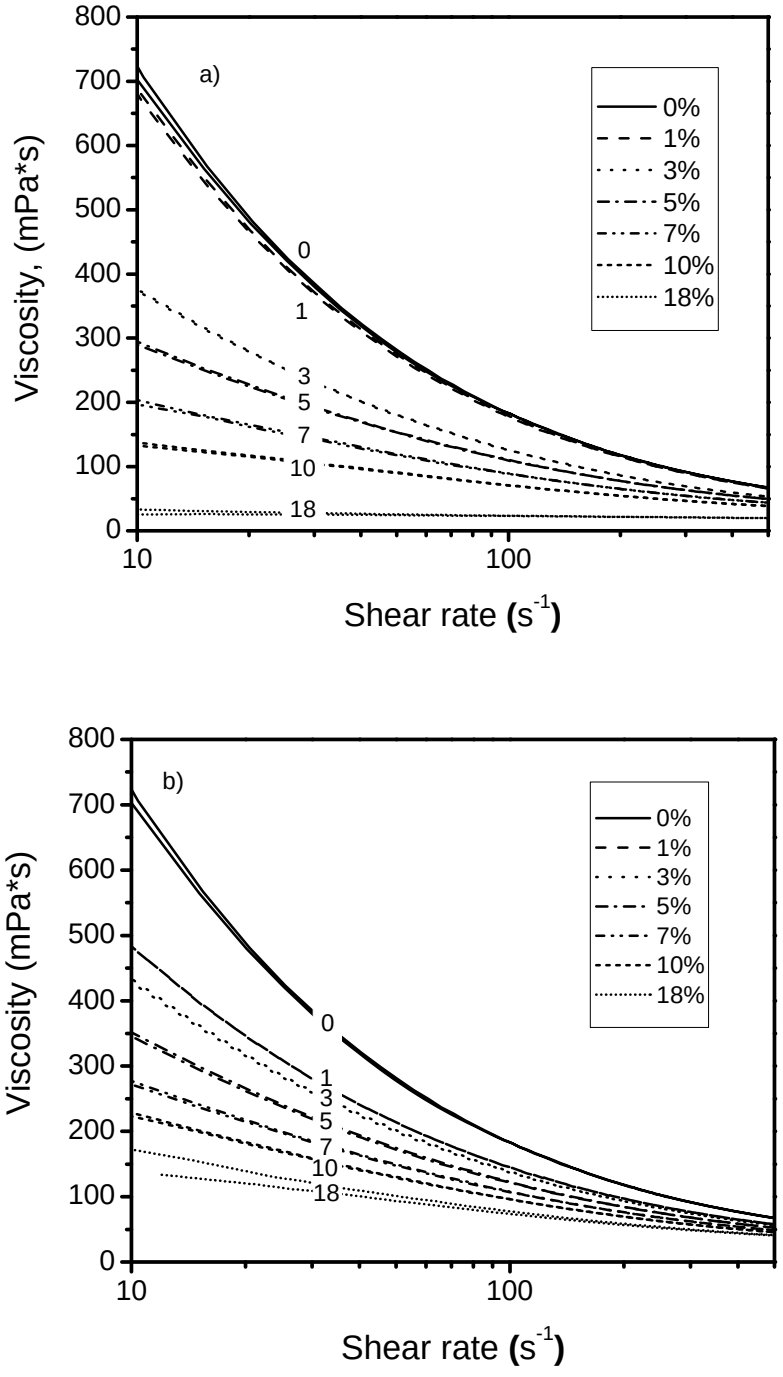

Figure 5. Variation of viscosity with shear rate for 30 vol% alumina suspensions as a function of a) fructose, and b) glucose concentration. The pair of curves for each concentration represents advancing (higher) and decreasing (lower) branches of the shear rate.

In Figures 5a and b, the hysteresis between advancing and decreasing shear rate is negligible. Secondly, as the concentration of the saccharide increases the suspension viscosity decreases. However, the effect at 1% is almost negligible for fructose but significant for glucose, while at 3% the viscosity decreases by nearly two-fold for both saccharides in the low shear rate regime. Also, the behavior of suspension gradually changes from shear thinning towards Newtonian as the saccharide concentration increases, as indicated by the viscosity ratio in Table 2. With the exception of 1%, fructose is more effective in reducing the viscosity than glucose. Figure 5a also indicates that the viscosity nearly reaches a limiting value at 18% fructose. Any additional increase in fructose concentration is expected to have little or no reduction in viscosity.

Figure 6, below, compares the effectiveness of fructose and glucose as a function of saccharide concentration. At 500 s^{-1}, both saccharides perform similarly over the whole concentration range. But, there is a greater discrepancy in the low shear range. At high shear rates, a limiting viscosity is approached, which may account for the uniformity between fructose and glucose.

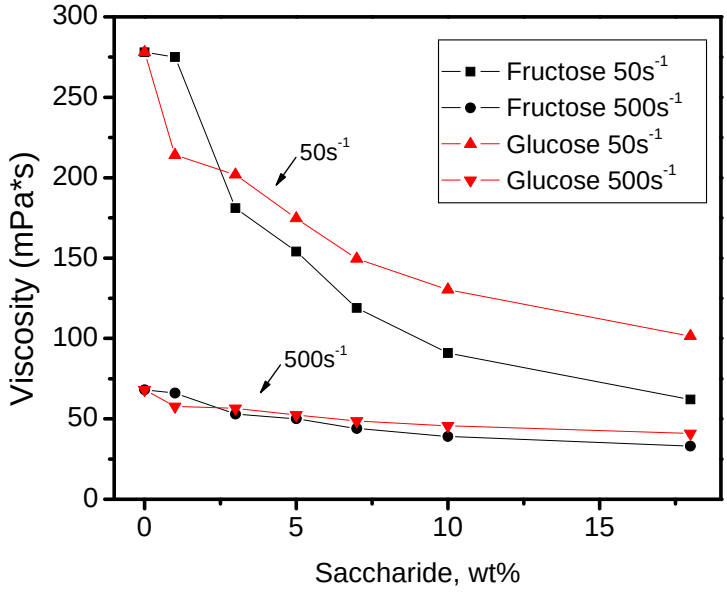

Figure 6. Variation of viscosity as a function of fructose or glucose concentration at 50 and 500 s^{-1}. Values for glucose and fructose at 500s^{-1} are very similar for every saccharide loading.

Table 2. Viscosity at 50 and 500 s^{-1} and viscosity ratio as a function of fructose concentration

Alumina nanoparticle suspension viscosities (mPa*s)							
% Fructose	50s^{-1}	500s^{-1}	VR	% Sucrose	50s^{-1}	500s^{-1}	VR
0	278	68	4.12	0	278	68	4.12
1	275	66	4.16	1	214	58	3.70
3	181	53	3.39	3	202	57	3.57
5	154	50	3.22	5	175	53	3.32
7	119	44	2.73	7	150	49	3.07
10	91	39	2.36	10	130	46	2.85
18	62	33	1.88	18	101	41	2.47

Suspensions of 40 vol% alumina nanoparticle with varying amounts of saccharides were prepared and the viscosity of these was measured as with the 30vol% samples shown above. The viscosity of these suspensions decreases as the saccharide loading increases for

both glucose and sucrose as in the 30 vol% samples. Figure 7 compares the two additives at selected wt%.

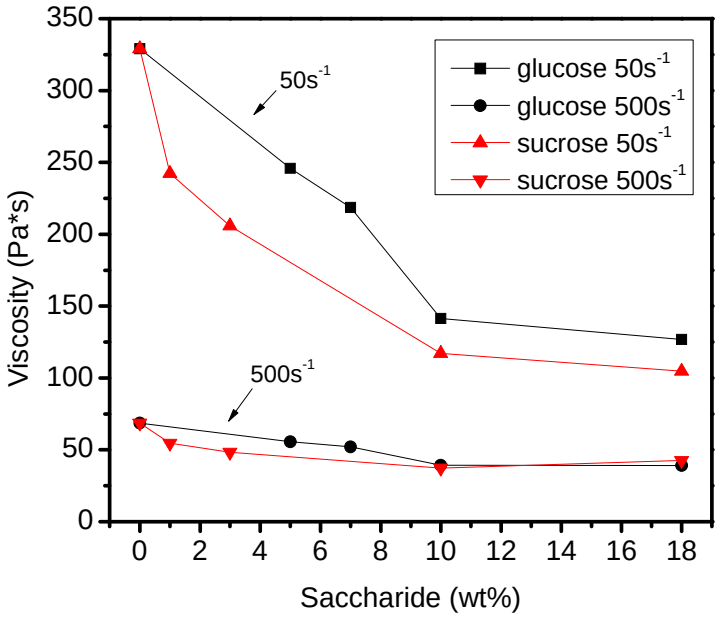

Figure 7. Variation of viscosity as a function of glucose or sucrose concentration at 50 and 500 s^{-1} for 40% alumina suspensions.

Sucrose, glucose and fructose are highly hydrated molecules which do not dissociate in solution. As the concentration of these sugars increases in an aqueous solution, the viscosity increases[10], but as the concentration of sugar in an alumina nanoparticle suspension increases, the viscosity decreases. Nearly every figure in this paper describing suspensions of alumina nanoparticles shows experimental proof that the greater the concentration of saccharide, the lower the viscosity of the suspension. It appears that up to 18 wt% there is no optimum saccharide concentration because the viscosity is consistently lowered with each saccharide addition.

To investigate this system further, 60 vol% alumina nanoparticle suspensions were prepared to see if saccharides reduced the viscosity of suspensions at higher solids loadings as well. In these suspensions, as the wt% glucose is increased, the viscosity of the suspension decreases. The 3 and 5% curves are similar, but 5% does lower the viscosity more than 3% glucose. These samples show greater thixotropy, which is the difference between the

increasing and decreasing shear curves, most likely due to the high solids content. Interestingly, in addition to lowering the viscosity, saccharides also reduce the magnitude of thixotropy at 100 s^{-1}. This is shown in Figures 8 and 9. With the addition of 10 wt% glucose, the thixotropy magnitude is reduced to 40 mPa*s. Zupanicic[11] also reported that the degree of thixotropy is reduced as the suspension is stabilized.

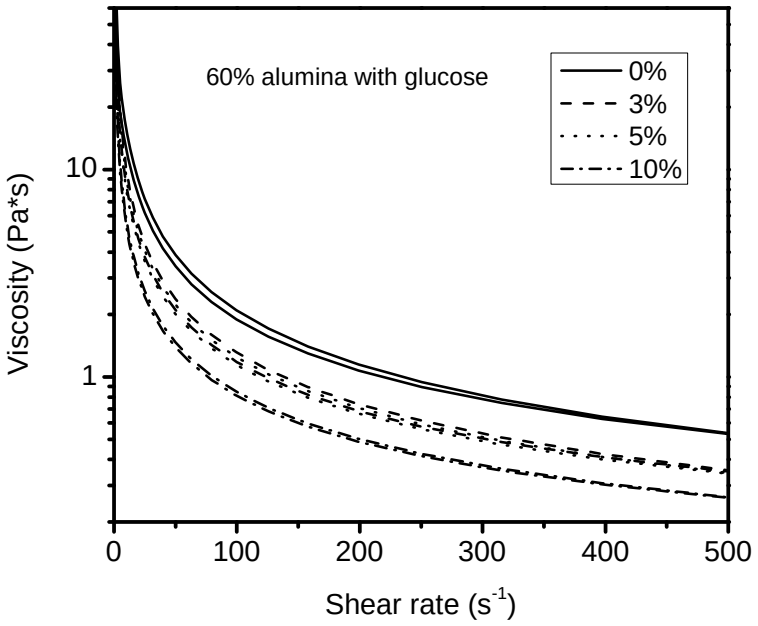

Figure 8. Viscosity of 60% alumina suspension as a function of shear rate with varied glucose concentration

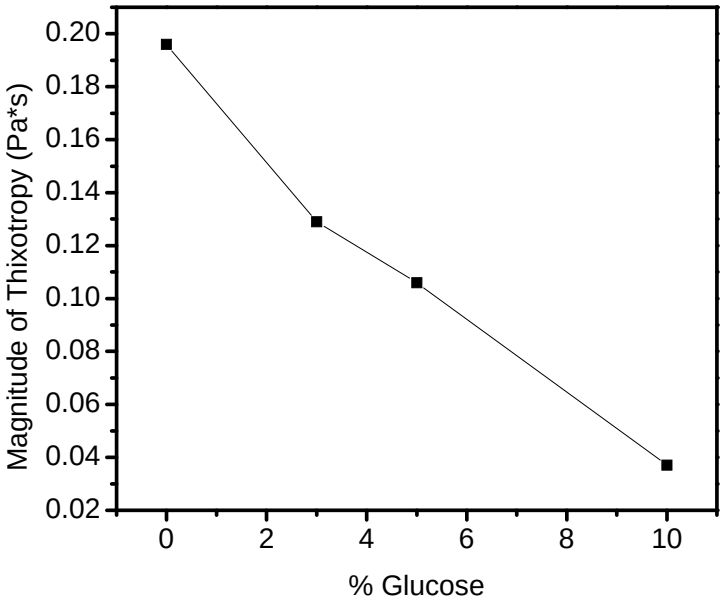

Figure 9. Magnitude of thixotropy at $100s^{-1}$ for 60 vol % alumina nanoparticle suspensions with the addition of glucose

Table 3. Viscosity at 50, 100 and 500 s^{-1} and viscosity ratio as a function of glucose concentration for 60 vol% alumina suspensions. Viscosity values are taken from the 500-$0.5s^{-1}$ branch of the viscosity curve. The high viscosity ratio (VR) indicates shear thinning behavior which decreases with the concentration of glucose.

% glucose	**$50s^{-1}$ (Pa*s)**	**$100s^{-1}$ (Pa*s)**	**$500s^{-1}$ (Pa*s)**	**VR***
0	3.42	1.90	0.54	6.33
3	2.11	1.18	0.35	6.03
5	2.01	1.14	0.34	5.91
10	1.39	0.81	0.26	5.35

*the viscosity ratio at $50s^{-1}$ to $500s^{-1}$ shear rate.

Kim et.al [12] and Schilling[6] concluded that fructose and sucrose had the greatest effect in viscosity reduction, while glucose was claimed to be not effective. As shown in Figures 4 - 8 our data clearly indicates that glucose is indeed effective in lowering the viscosity of the suspension over the whole shear rate range. The only significant difference between the

suspensions employed by Kim et.al and ours is the fact that the former added NH_4Cl to maintain a constant ionic strength. Nevertheless, since saccharides hardly ionize in aqueous solutions, it is not necessary to add NH_4Cl to the suspension to keep the ionic strength constant. Furthermore, since the sample with no saccharide is used as a reference to determine the viscosity reduction, the addition of NH_4Cl only complicates the system by adding another variable and is unnecessary.

The viscosity ratio shows that the addition of saccharides also reduces the dependence of viscosity on shear rate (i.e. shear thinning). This ratio can only be used as a comparison to show the relative degree of shear thinning within a given set of similar suspensions. In the case of 30vol% alumina nanoparticle suspensions, the VR indicates that the shear thinning character with addition of saccharides increases in the order: fructose<glucose<sucrose. In the case of 30 vol% alumina nanoparticle suspensions with various loadings of glucose and sucrose, the VR decreases as the saccharide wt% increases. This is a manifestation of lesser shear thinning behavior with increased concentrations of saccharide in the suspension.

In the 60 vol% suspension, a glucose addition of 10 wt% creates a fluid suspension. A fluid suspension is characterized as one with a viscosity of less than 1Pa*s at a shear rate of $100s^{-1}$.[13] It is expected that a higher glucose concentration will lower the suspension viscosity even further.

Rheological modeling of shear stress

The shear stress as a function of shear rate for 0 - $100s^{-1}$ for suspensions of 20 - 70 vol% with no saccharide addition and 40vol% with saccharide additions was analyzed using the Windhab rheological model[14] which is recommended by the IOCCC (International Office of Cocoa, Chocolate and Sugar Confectionary) for the analysis of chocolate melts[15]:

$$\tau = \tau_0 + (\tau_1 - \tau_0)\left[(1 - \exp\left(\frac{-\dot{\gamma}}{\dot{\gamma}^*}\right))\right] + \eta_\infty * \dot{\gamma}$$

Equation 1

This model incorporates the yield point, τ_o, and the shear stress at the y-axis crossover point, τ_1. The difference between τ_1 and the yield stress τ_o, i.e. (τ_1 - τ_o), is considered to represent the "shear induced structural change" and η_∞ is the slope value of the flow curve at high

shear rates. These parameters are all extrapolated from the data. The value of $\dot{\gamma}^*$ is assigned to achieve the best fit. This parameter corresponds to the shear thinning character of the flow curve at low shear rates. This is a modification from the original model, which uses another formula to calculate this value. τ_o was taken to be the shear stress at the shear rate of $0.5s^{-1}$. An example for fitting the model for the 40 vol% sample is shown in Figure 10. Fitting parameters are given in Table 4.

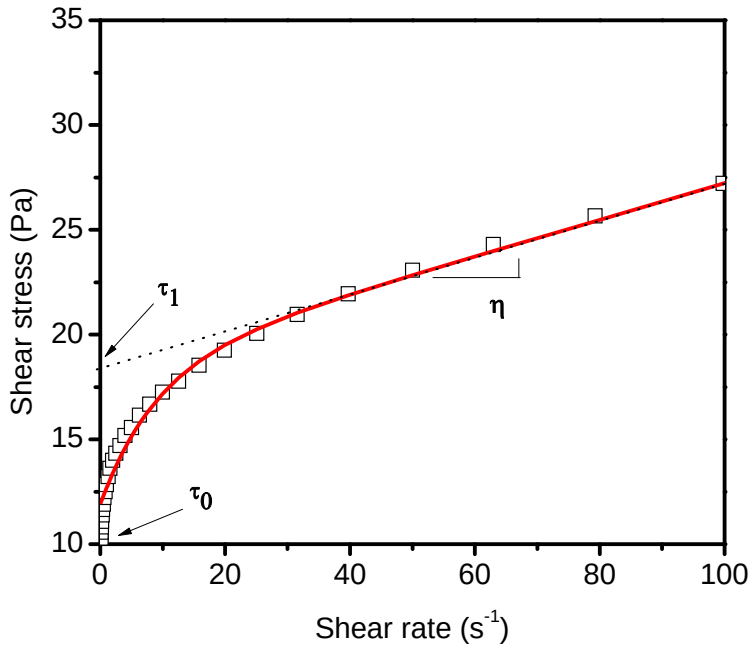

Figure 10. Illustration of application of the Windhab model on 40 vol% alumina nanoparticle suspension. The symbols represent the experimental data and the solid line is the best fit Windhab model. The fit with only one adjustable parameter is excellent with the exception of a slight deviation in the very low shear rate region.

Table 4. Parameters for Windhab model analysis of alumina nanoparticle suspensions and 40 vol% suspensions with 5% saccharide.

Saccharide	Vol % alumina	τ_0 (Pa)	τ_1 (Pa)	$\tau_1 - \tau_0$ (Pa)	γ^* (s^{-1})	η_∞ (Pa*s)
none	20	0.075	0.139	0.0636	14	0.0077
none	25	0.151	0.458	0.307	14.5	0.0159
none	30	0.114	0.835	0.722	14	0.0215
none	35	2.62	6.701	4.081	8.5	0.0534
none	40	11.9	18.47	6.57	9	0.0876
none	50	32.07	53.52	21.45	7	0.1755
none	60	128.3	153.7	25.4	8	0.3198
none	70	207.4	277.8	70.46	10	0.4213
glucose	40	2.392	6.532	4.140	10	0.0618
sucrose	40	2.224	6.713	4.489	10	0.0693
myoinositol	40	3.176	7.263	4.087	9	0.0694
raffinose	40	0.968	4.477	3.509	10	0.0583
mannitol	40	2.214	6.914	4.70	13	0.5986
glucopyranoside	40	2.109	6.049	3.941	10	0.05864

Suspensions of 20, 25, and 30% alumina have a very low yield point, or none at all. At 35% the yield point increases moderately, and suspensions greater than 40% by vol. have a significantly large yield point which can be seen physically in the paste-like behavior of these suspensions, especially at 60 and 70% alumina. The yield point of all suspensions with 5% saccharide additions is consistently lower than the sample with 40vol% alumina and no saccharide additions.

The value for shear induced structural change increases in a nearly exponential manner with increasing alumina. Similarly, the yield point and y-axis crossover point increase near-exponentially. The value of $\dot{\gamma}^*$ seems to roughly correlate with the yield point. For suspensions with low yield point the value of $\dot{\gamma}^*$ is about 14 s^{-1} and for suspensions with a measurable yield point the value is less than or equal to 10 s^{-1}. Lower values of $\dot{\gamma}^*$ indicate suspensions which are more strongly shear thinning at low shear values. The minimum value of $\dot{\gamma}^*$ at 50vol% may be significant since this suspension marks the transition from a fluid suspension to a paste.

Similarly, suspensions of 30vol% with fructose additions was analyzed with the Windhab model. Shear stress as a function of shear rate is pictured in Figure 11.

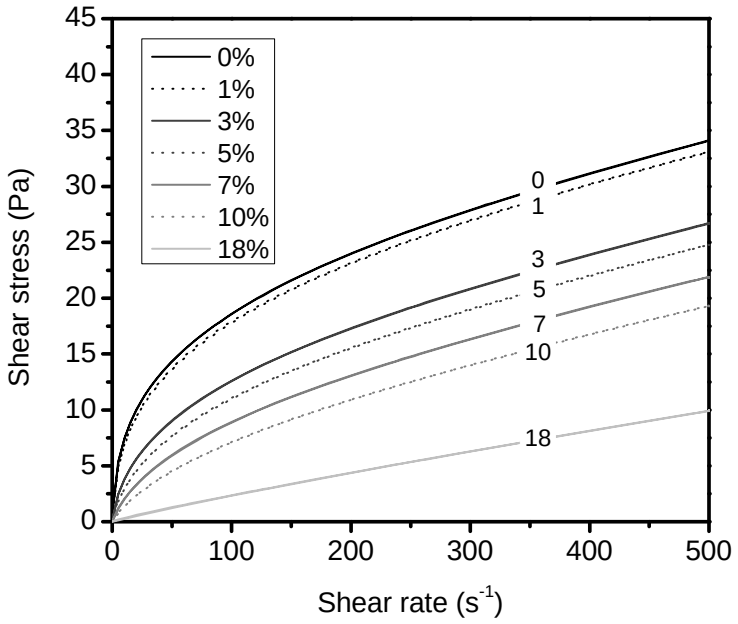

Figure 11. Experimental data for shear stress vs. shear rate for 30 vol% suspensions with added fructose

Table 5. Fitting parameters for 30vol% alumina suspensions with fructose

fructose, wt %	τ_0 (Pa)	τ_1 (Pa)	$\tau_1 - \tau_0$ (Pa)	γ^* (s^{-1})	η_∞ (Pa*s)
0	0.394	8.646	8.252	9	0.0957
1	0.417	9.182	8.765	10	0.0915
3	0.123	5.414	5.291	11	0.0763
5	0.464	3.935	3.471	14	0.0719
7	0.3834	2.741	2.357	15	0.0625
10	0.2764	1.748	1.471	17	0.0540
18	0.0194	0.209	0.189	20	0.0215

The parameter γ^* increases with the concentration of fructose. In this case, the higher the value of gamma, the less curvature and the more Newtonian the suspension. This matches well with the conclusion gathered by the VR for this set of suspensions. The values for the yield point, y-axis crossover point and shear induced structural change decrease with the

addition of fructose. The value for η_∞ also decreases with fructose concentration which is indicative of the viscosity reduction with this saccharide but not a direct measure of the viscosity at a particular shear rate.

The shear induced structural change value decays exponentially with fructose addition. As fructose is added to the water/nanoparticle suspension, the suspension structure is more easily broken with shear stress. It appears that 18% saccharide reduces this value to practically zero. This indicates that the interaction between the particle flocs diminishes with the addition of 18wt% fructose.

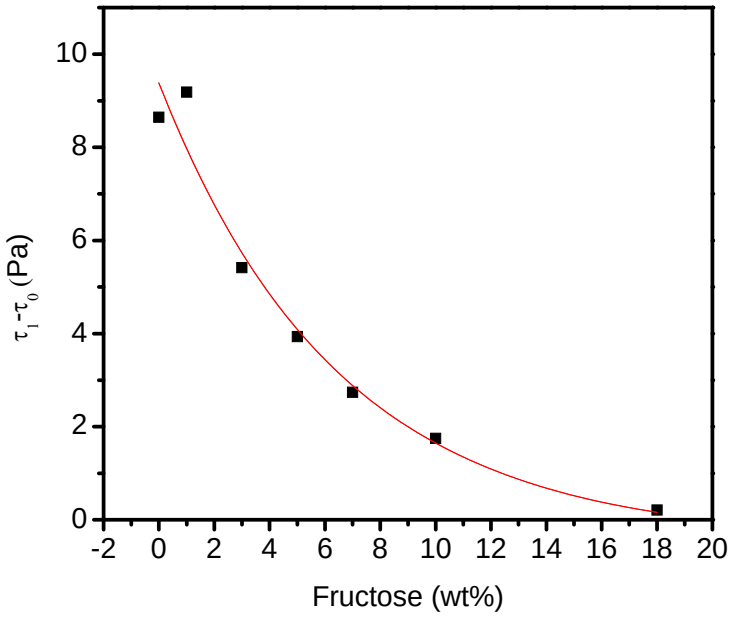

Figure 12. Variation of shear induced structural change with fructose concentration for 30vol% alumina nanoparticle suspensions.

3.4 Influence of saccharide type on the viscosity of alumina nanoparticle suspension

The viscosity of 40 vol% alumina suspensions containing several saccharides at a level of 5 wt% was also measured using TA Instruments 2000EX rheometer with a 1^o cone-plate configuration and solvent trap to ensure there was no significant evaporation of water. Saccharide amounts were normalized to be equimolar to 5% glucose by weight.

Different saccharides and derivatives were used to see if the type of sugar had a significant influence on the degree of viscosity reduction. We were interested to see, also, if there was any correlation between the materials or molecular characteristics of the sugars and the observed viscosity reduction. Of the select saccharides used for this part, glucose is a mono-saccharide hexose, myoinositol and methyl glucopyransoide are derivatives of mono-saccharide, sucrose is a di-saccharide, mannitol is a linear chain sugar alcohol, and raffinose pentahydrate is a tri-saccharide (contains 3 rings). The molecular structures of these molecules are shown in Table 6.

It can be seen in Figure 13 and Table 7 that all saccharides reduce the viscosity of 40% alumina suspensions. Raffinose pentahydrate with a 43.6% reduction compared to the control at $100s^{-1}$, reduces the viscosity most, the monosaccharides and derivatives have a similar effect, and myoinositol reduces the viscosity slightly less than the rest with a 22.4% reduction at $100s^{-1}$.

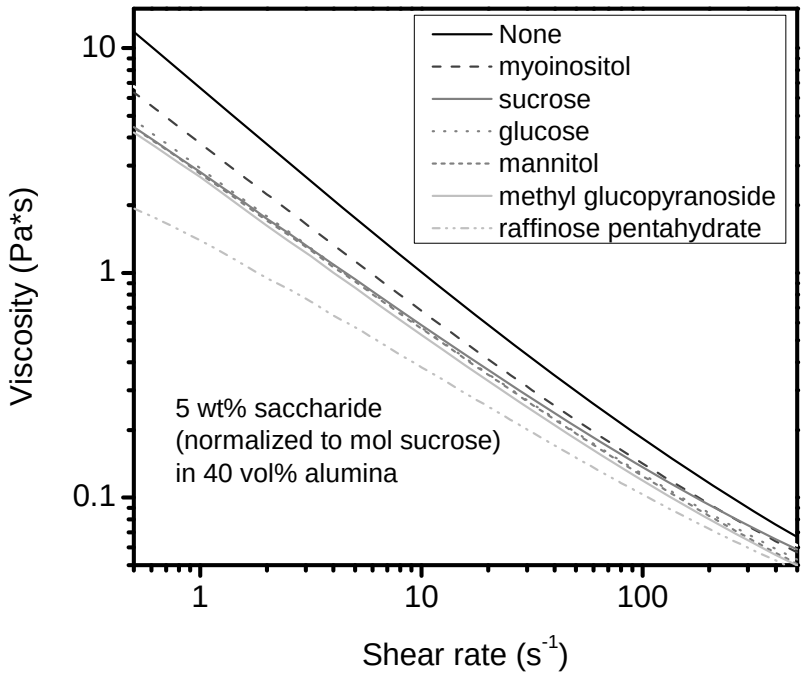

Figure 13. Magnitude of viscosity reduction with the addition of 5 wt% saccharide to 40vol% alumina nanoparticle suspensions. The retrace curve from $500\text{-}0.5s^{-1}$ is plotted so that each curve can be easily distinguished.

Table 6. Molecular Structure of select saccharides

Saccharide	Molecular Structure
fructose	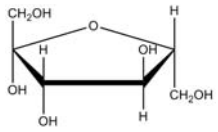
glucose	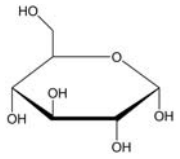
sucrose	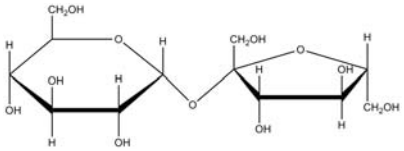
mannitol	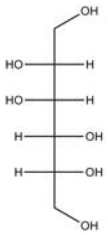
myoinositol	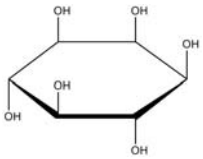
raffinose pentahydrate	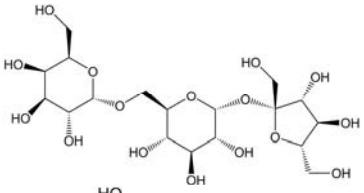
methyl-α glucopyranoside	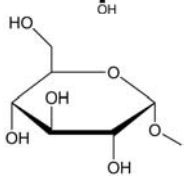

Table 7. Viscosity reduction by various saccharides at 5 % wt addition to 40 vol% alumina nanoparticle suspension. Viscosity reduction is relative to viscosity of suspension with no saccharide addition

Saccharide	% Viscosity
None	--
Myoinositol	22.4
Sucrose	25.4
Glucose	30.5
Mannitol	31.7
Methyl glucopyranoside	34.9
Raffinose pentahydrate	43.6

There are many variables such as: length, hydrophobicity, solubility, polarizabilty, steric accessibility of bonds, etc. that may be related to the viscosity reduction with different saccharides. The value for the largest dimension (size) was estimated by minimizing the energy for each molecule[16] and finding the largest diameter across the molecule.

Table 8. Selected characteristics of saccharide molecules

Saccharide	Formula Weight	Formula	T_m, (^oC)	Density g/cm^3	OH groups	Size Å	Ring/ chain
myoinositol	180.16	$C_6H_{12}O_6$	224.5	1.75	6	6.4	ring
sucrose	342.3	$C_{12}H_{22}O_{11}$	185	1.58	8	10.1	ring
glucose	180.16	$C_6H_{12}O_6$	149-152	1.56	5	7.3	ring
d-mannitol	182.17	$C_6H_{14}O_6$	168	1.49	6	7.2	chain
methyl glucopyranoside	194.18	$C_7H_{14}O_6$	169-171	1.46	4	7.0	ring
raffinose pentahydrate	594.51	$C_{18}H_{32}O_{16} \cdot 5H_2O$	78-80.5	1.46	11	14.4	ring
fructose	180.2	$C_6H_{12}O_6$	104	1.6	5	7.5	ring

From Table 8, it appears that generally as the melting point decreases and the density of the crystalline sugar decreases, the saccharide becomes more effective at reducing the viscosity. This suggests that as the cohesive energy of the molecule with itself becomes lower, its ability to modify the viscosity of the suspension increases. This trend also

generally fits fructose, glucose and sucrose although the density of each monosaccharide is similar.

The structure of raffinose pentahydrate incorporates five water molecules, which could reduce the viscosity of the suspension by reducing the solids content if all were dissociated from the molecule. Assuming all five water molecules contribute to the amount of water in the suspension, the solids content would be reduced to 38.6 vol%. This has the potential to reduce the suspension viscosity by 16% assuming that the behavior is similar to that seen in Figure 3. If this is the case, the magnitude of viscosity reduction due to only the saccharide would be similar to that of sucrose. This does not change the melting point trend described above because the melting point, also, may be affected by the presence of hydration of this molecule.

3.5 Differential Scanning Calorimetry

In order to study the melting behavior of water as it is altered by the interactions with the alumina surface and the saccharides, a series of melting experiments with DSC were carried out. DSC curves for aqueous alumina nanoparticle suspensions with solids contents ranging from 20 to 70 vol% are shown in Figure 14. The two peaks, free water and bound water, as attributed by Li[7] for each curve were fit with a non-linear curve fit tool[17] to find the area, A, under each. To calculate the relative amounts of free and bound water the heat of fusion, ΔH, for each type is needed. It was determined by Li that the heat of fusion for bound water is approximately half that of bulk water. The total water, W_{total}, is related to the enthalpies of both water types by the following equation[7]:

$$W_{total} = W_{free} + W_{bound} = \frac{A_{bound}}{\Delta H_{bound}} + \frac{A_{free}}{\Delta H_{free}}$$

Equation 2

The relative fractions of free and bulk water were calculated and are shown in Figure 15. It can be seen in both Figures 14 and 15 that as the solids content increases, the relative fraction of free water decreases and the fraction of bound water increases. At 20 vol% solids, the water is mostly free. At this solids content it can be assumed that the free water is filling

in the space between particles and the bound fraction, surrounding the particles, melts at a lower temperature than the free water. As the solids content is increased beyond 20%, the bound water peak becomes larger and dominates at solids contents greater than 40 vol% alumina.

Also, as the solids content increases, the bound and free water peaks converge toward the creation of a single peak spanning across the entire melting range. This indicates that the water bonding environment is becoming more uniform with the addition of very high vol% alumina. Since the particles are expected to have the same influence on the surrounding water molecules, no matter the concentration, the free water must be tending towards the bound water state.

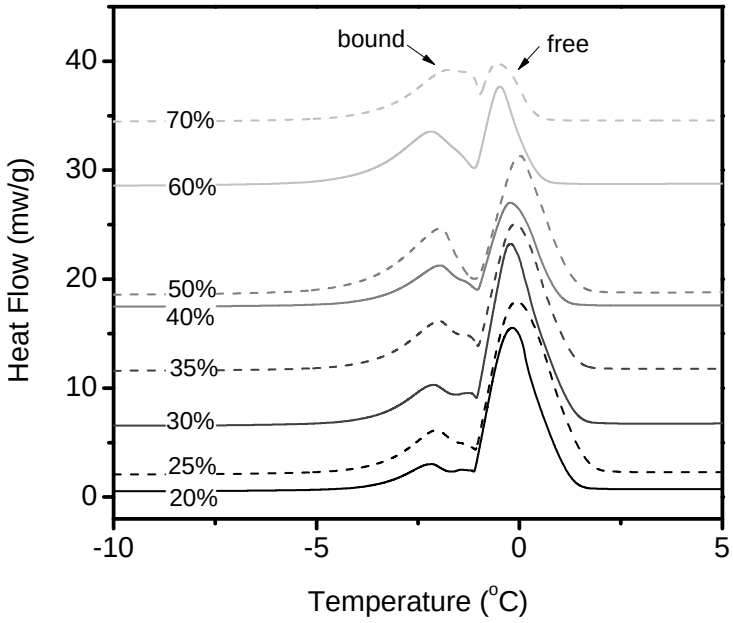

Figure 14. DSC curves of aqueous alumina nanoparticle suspensions. Samples were heated at a rate of 1°C/min. The area under each curve is related to the amount of water present. The curves were shifted vertically for illustration purposes.

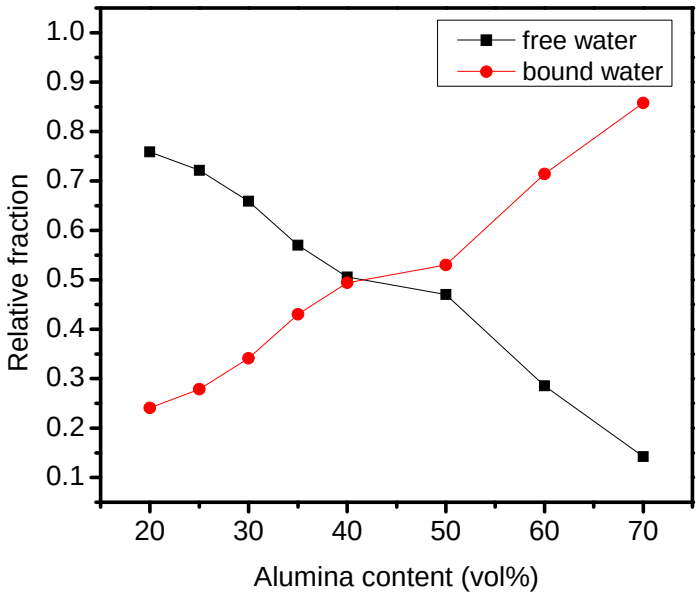

Figure 15. Fitting the normalized area under the free water peak shows a monotonic increase in bound water with alumina content.

When water freezes, each molecule will hydrogen bond to form a solid network of ice. During a freezing event in the presence of a surface, the solidification of the hydrogen bond network of ice can be modified from its bulk form. Studies of the structure of water in confined environments of nanometer dimensions show that the properties of water are changed at this scale[18]. Previous DSC studies[18,19,20,21] show that the melting of water entrapped in silica pores occurs at a lower temperature than the bulk water. It is thought that interface ice melting is favored at lower temperatures due to the lower interfacial energy between water and the pore wall than ice and the pore wall[19]. Since both the alumina and silica surfaces are highly hydroxylated, it is assumed that the cause of interfacial ice melting in alumina suspensions is similar to the mechanism offered for the nanoporous silica/water system.

The melting point depression for water in the presence of nanometer-scale pores for silica was calculated by Rennie[20] by employing the Kelvin equation. For a 36 nm pore radius, a depression of 1.4^{o}C was predicted, and for a 20 nm pore radius a depression of 2.5^{o}C was predicted. As the pore radius decreases, the melting point depression becomes larger. For 20-

60 vol% alumina suspension, the average temperature shift in the bound water peak is 2.34 ± 0.14°C which corresponds well to a pore radius slightly greater than 20 nm. Since the average particle size for the alumina is 48 nm, an average radius slightly greater than 20 nm is reasonable. The fact that the temperature decrease is similar for all samples suggests that the alumina particles in suspension are similar in size distribution. Another possibility is that the particles are flocculated with pore channels of similar size separating them.

The melting behavior of suspensions with 40% by vol alumina and 5% by weight saccharide, normalized to be equimolar with glucose, was also investigated. DSC curves in Figure 16 were also shifted vertically for clarity. It is evident that there are changes in the peak positions, peak shapes, and onset points for the melting of the suspensions with saccharides compared to the reference. The peak positions and shift from the 40% alumina suspension reference peak are recorded in Table 9.

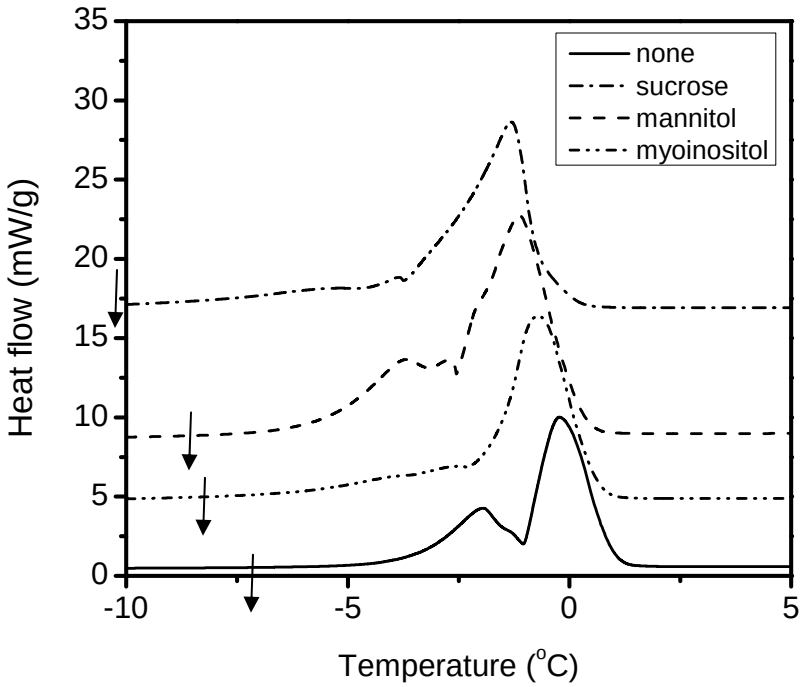

Figure 16. Melting behavior of 40 vol% alumina nanoparticle suspensions with 5wt% saccharide. Arrows indicate the onset of the bound water peak. The onset was found by extrapolating the zero signal value, found above 2.5°C, for each curve, and finding its intersection with the heat flow signal.

Table 9. Peak temperatures and shifts for 40 vol% alumina nanoparticle suspensions with 5wt% saccharide

	Free water		Bound water	
Saccharide	**Peak temp, ^{o}C**	**Shift, ΔT_m C^o**	**Peak temp ^{o}C**	**Shift, ΔT_m C^o**
None	-0.33	-	-1.84	-
Myoinositol	-0.88	-0.55	-2.76	-0.91
Mannitol	-1.22	-0.89	-3.88	-2.04
Sucrose	-1.45	-1.12	-3.99	-2.14

The shift of the free water peak to lower temperatures can be explained by freezing point depression (equation 3) caused by the solubility of saccharide molecules in water.

$$\Delta T_f = K_f * m_B$$

Equation 3

where ΔT_f is the freezing point depression of the solution relative to the pure solvent, K_f of water is 1.86 ^{o}C/m and m_B of sugar is 0.407mol/kg for 5 wt% saccharide. Assuming that the saccharide molecules do not dissociate to form ions, freezing point depression predicts as shift of -0.76^{o} C. The free water peak in each 40 vol% suspension follows the freezing point depression rule within ± 0.4^{o}C. Mannitol is the saccharide that most closely fits the prediction with -0.89^{o}C.

Since the bound water is in a different environment than free water its peak position is not expected to follow the same freezing point depression rule. The bound water peaks in samples containing saccharide show a greater negative deviation from the bound water peaks in the reference sample. The shift for mannitol and sucrose is approximately -2.0^{o}C. This temperature shift is significant and an indication that the bound water is being affected by the presence of the saccharide molecules as well. Furthermore, the bound water is interacting in a more complicated way than the simple solution thermodynamics can predict.

In addition to shifting the peak position to a lower value, the addition of saccharides broadens the bound water peak. This could be explained by the modification of the bound water network to create lower energy bonds. The interfacial energy between ice and

saccharides near the surface of the alumina particles may be lower than the interfacial energy between ice and the particle surface.

This broadening of the bound water peak was also seen in the work of Li[22]. He studied the addition of various wt% fructose in 30vol% alumina by DSC. In the paper, he mentions that the bound water peak is reduced with the addition of fructose. But, it appears that the area under the bound water peak was not actually reduced, but the peak was broadened. Due to poor peak shape definition, curve fitting software could not be used to determine the area under the curve. Instead, in order to get a rough estimate of the bound water content, the area was integrated using a cut and weigh approach. An average of 3 measurements for each curve was found. For 0% fructose, the bound water region had a weight of 0.0213g, and for 3, 5, 7, and 15% fructose the bound water region had weights of 0.0125, 0.0217, 0.231, and 0.280 g respectively. This corresponds to good agreement with the 5 and 7% samples with a % wt change of 1.8 and 8.5%, respectively. The 3 and 15% fructose samples showed more deviation from the 0% fructose value due to poor peak shape definition arising from peak overlap in the original figure. Even though the error in these samples is larger, clearly, the bound water peak has not disappeared with the addition of fructose. Also, the onset of melting of the bound water is shifted to lower temperatures with each addition. Further explanation of this phenomenon will be found later in the discussion.

Further evidence of peak broadening and shifting is seen in suspensions of 30vol% alumina with 5% of the various saccharides (see Figure 17). The peak shape for corresponding saccharides is similar to those seen in Figure 16. This indicates that the bound water peak shape is characteristic of the saccharide. It may be due to the various characteristics of the OH groups on each saccharide or other properties.

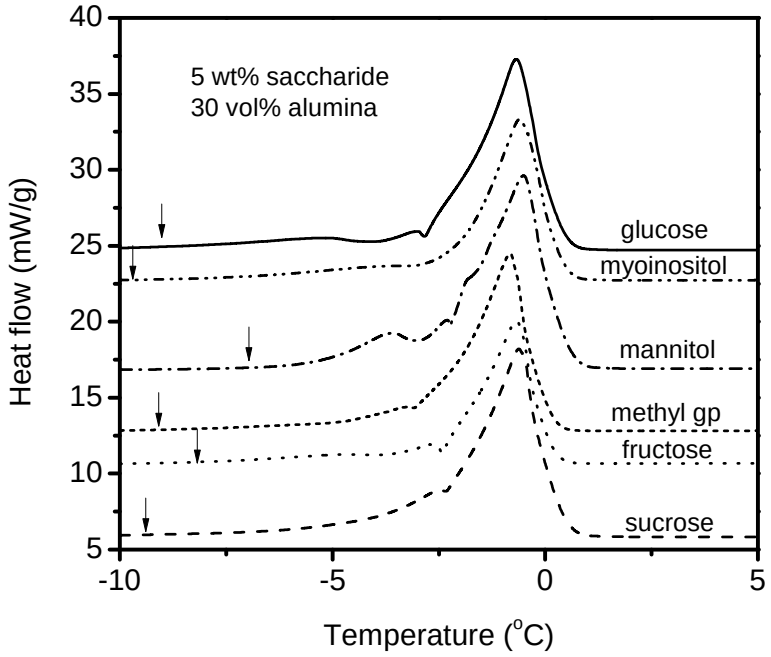

Figure 17. Melting of suspensions with 30vol% alumina and 5% by weight saccharides normalized to glucose. Arrows, again, represent the onset temperature of melting.

3.6 Model

Unlike the previous study by Li, the bulk water peak (in Figure 14) did not disappear completely at 60 vol% solids content. Instead it was observed that 85% of the water was bound and the remainder was free. Possible reasons for the discrepancy include the method of sample preparation such as the procedure for powder addition or differences in the batches of alumina particles. Therefore, the "effective particle packing model" based on the interaction of bound water layers cannot be supported by the experiments in this study. Instead, a fractal percolation limit may explain the greater increase in viscosity at 35 vol% alumina.

Fractal models of colloidal particles are common, and generally well accepted[23]. A simplified hypothetical model can be described as such: beginning with a sphere as a primary particle with a volume of $4/3\pi r^3$, and additional monosize particles which are not justified for this system, the space occupied, $V_{occupied}$, by 9 spheres (body centered packing) within the next coordination ring of radius = 3r becomes 9/27, or 33%. This is illustrated in Figure 18.

Assuming that the colloidal structure can be modeled by repetitions of this cell, each connected to one another, the percolation limit would be reached at 33 vol% solids. This could also be calculated with simple cubic (shown in the illustration) or face centered cubic packing inside each second coordination sphere to achieve a percolation limit at 26 vol% and 44 vol%, respectively.

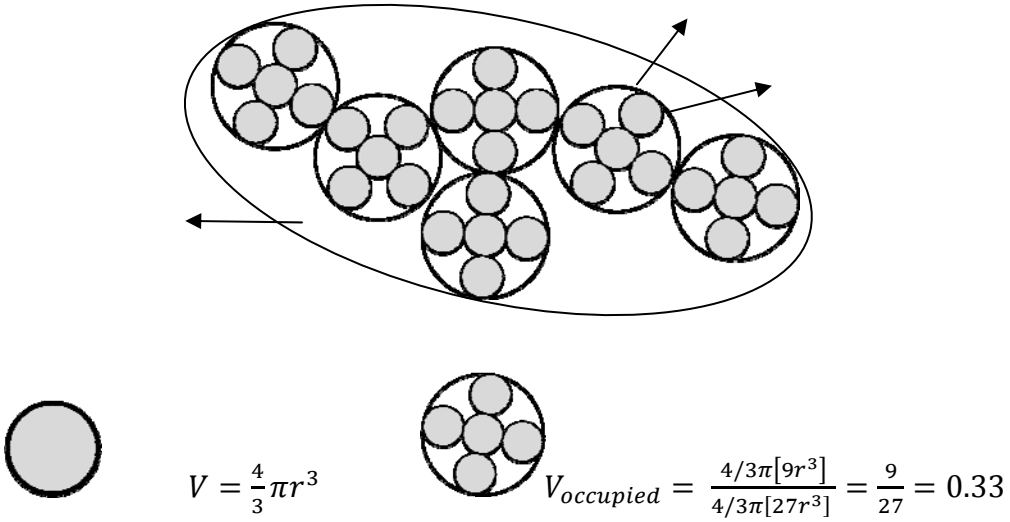

Figure 18. Schematic illustration of fractal-type clustering of monosize particles

It is possible that at 33 vol% solids (or 26%, or 44%) the clusters form a network. This would result in increased interaction force (friction) between the alumina particles, and therefore a higher viscosity. As the solids loading is increased, clusters will become more constrained and entangled, thus increasing the viscosity. In Figure 3 it is evident that the viscosity is increased greatly after 40 vol% is reached. Any further additions of alumina (50-70%) would over constrain the clusters and the viscosity will increase sharply. The TEM image of alumina nanoparticles in Figure 1, seems to show a fractal-type clustering of particles which may lend additional support for the proposed model. Although the suspension used to produce the TEM image was dilute, and not representative of a concentrated suspension, it may provide a snapshot of how the particles tend to group together in clusters as the solids concentration is increased, as was the case during drying of the TEM sample on the grid.

The problem with this simple model is that it is an overgeneralization of a more complicated phenomenon. There are interaction forces present between particles, and flocs in real systems consist of branched structures that are not consistent with the classical fractal picture[24] shown above.

The fractal theory can provide a means of expressing the degree to which primary particles fill the space within an aggregate[24]. The fractal dimension, *f*, can have the range of values[25] $1.6 < f < 3$ where 3 corresponds to a uniformly formed collection of particles, much like the illustration above, and 1.6 is a more loosely bound aggregate. The fractal dimension is related to the number of particles per aggregate by:

$$n = N_o \left(\frac{R}{a}\right)^f$$

Equation 4

Where *n* is the number of particles per fractal aggregate, *a* is the primary particle size and *R* is the radius of the aggregate. For polystyrene latex spheres, when shear is applied, *f* increases to 2.5 and remains constant[25]. For this system, the aggregates becomes more compact as shear is applied until there is no further densification possible, which is indicated by the constant value of *f*. The densification is accompanied by an aggregate size decrease due to fewer low-density branches.

The maximum aggregate radius depends on shear rate, which has been extensively studied for latex spheres. The general form of shear dependence of the aggregate size is:

$$\frac{R}{a} = (\mu\dot{\gamma})^{-m}$$

Equation 5

where μ is a numerical coefficient, $\dot{\gamma}$ is the shear rate, and *m* is a constant.

The viscosity as a function of shear rate for 30vol% alumina with fructose and glucose in Figure 5 were fit to a power law similar to Equation 5 and fitting parameters are shown in Table 10. The equation describing the viscosity of these suspensions is:

$$\eta = (\mu_\eta \dot{\gamma})^{-m_\eta}$$

Equation 6

where μ_η is the pre-exponential factor, and m_η is the exponential factor. It may not be a coincidence that the forms of Equations 5 and 6 are similar. It has been shown that the application of stresses will disrupt flocs and this is shear rate dependent[24,26]. By equations 5 and 6, the reduction in viscosity is proportional to the reduction in floc size. An important observation is that the addition of saccharides at any amount does not change the fundamental shear thinning property of these suspensions. The power law relationship holds for all, so the suspensions do not enter into a new state with different rheological characteristics and must keep the fractal character. Saccharides must be modifying the suspension environment, but not changing its fundamental nature.

Table 10. Fitting parameters for 30 vol% suspensions with additions of fructose and glucose

	Fructose		Glucose	
Wt%	$\boldsymbol{\mu_\eta}$	$\boldsymbol{m_\eta}$	$\boldsymbol{\mu_\eta}$	$\boldsymbol{m_\eta}$
0	2540.9	0.578	2404.1	0.571
1	2322.5	0.569	1415.4	0.510
3	973.68	0.462	1123.9	0.475
5	824.43	0.449	898.91	0.452
7	420.54	0.358	748.18	0.436
10	260.08	0.301	491.27	0.376
18	54.889	0.169	400.39	0.367

There are several characteristics of the viscosity curve that are modified by the addition of saccharides. The pre-exponential factor, μ_η, decreases with increased saccharide. This is shown in Figure 19. Mathematically, the pre-exponential is the initial value that decays as a function of the independent variable. Therefore, it is reasonable to assume that μ_η reflects the yield value of each suspension.

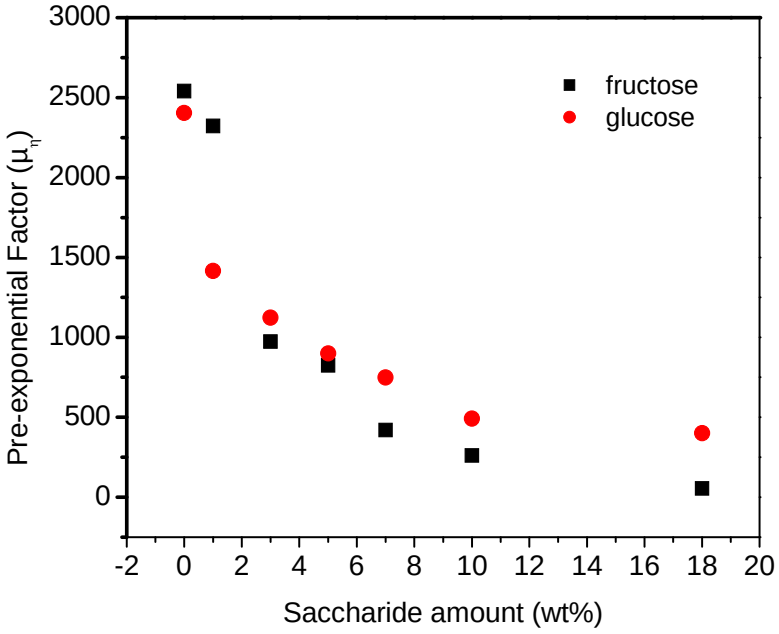

Figure 19. Pre-exponential factor, $\mu_{\eta,}$ for 30 vol% suspensions with fructose and glucose

The value of the exponential factor, m_η, decreases almost linearly with the addition of saccharides as shown in Figure 20. This constant corresponds to the rate of decay, or the amount of shear thinning experienced by each suspension. This was also reflected in the VR value in Table 2. The value of *m* for the ripening of $Mg(OH)_2$ and $Fe(OH)_2$ nanoparticles (~22 nm, and ~43 nm, respectively) was found to be 0.58 ±0.01[25], which is very close to the value for the alumina suspension with no saccharide where m = 0.57.

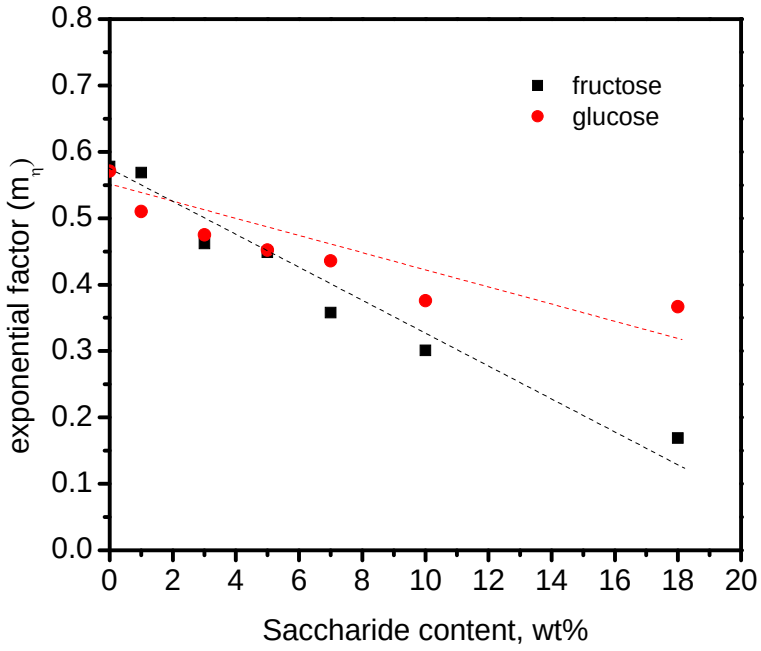

Figure 20. Variation of exponential factor for 30vol% suspensions with fructose and glucose concentration (data from Table 10)

Strong non-Newtonian behavior, especially the existence of yield stress, can be considered an indication of aggregation processes[25]. There are two important factors in the breakup of aggregates in shear flow: kinetic breakup due to shear induced collisions between flocs and instantaneous breakup due to fluid stresses[27]. Kinetic breakup is reflected in the shear thinning with application of shear stress during the measurement process. In this study, shear thinning has been demonstrated in all instances of suspensions with and without saccharides. Also, this process has been shown to be reversible, but time dependent, indicative of a kinetic process.

The other instantaneous breakup process due to fluid stresses is not reversible. This is possibly how saccharides lower the viscosity of the suspensions independent of the effects of shear stress. If the saccharides minimize floc size and weaken interactions between flocs, then the suspensions will have a lower viscosity before the application of shear. Also, the yield stress would be decreased, which was demonstrated.

Due to the initial reduced size of the flocs, it is expected that the suspensions will have lesser shear thinning character since shear stresses will not be able to to break up flocs further once the limiting size is reached. This was demonstrated to be true by the VR. Also, if the flocs are smaller and denser to begin, there will be a greater amount of free water in the suspension due to fewer, and smaller, interstitial spaces between particles. This corresponds to the bound water theory presented by Li[7]. Also, if the interstitial spaces are becoming smaller with increased saccharide, the melting point depression for bound water will decrease. This was demonstrated by the DSC experiments as the onset of the bound water peak was shifted to lower temperatures but did not disappear. The bound water will not disappear because it is modified by the alumina surface, which is constant for a given vol% alumina even if the floc size changes.

To confirm this hypothesis, it is necessary to determine the size of alumina nanoparticle flocs in suspension to see if the size decreases with the addition of saccharides and the application of shear. Small angle x-ray Scattering (SAXS) may be a useful technique to study this based on previous studies.[28,29,30] It would also be useful to study different saccharides to see if the floc breakup correlates to the type of sugar. Acoustophoretic zeta potential measurements also may be useful to study the particle interactions.

4. Conclusion

It was shown that the addition of saccharides reduces the viscosity of aqueous alumina nanoparticle suspensions. The viscosity decrease is related to the type of saccharide, and is dependent on the concentration.

The DSC measurements show that saccharides influence the water environment of the suspensions by modifying both the bound and free water, and the melting behavior is dependent on the structure of the saccharide. Analysis of the viscosity as a function of shear rate for different saccharide concentrations in a 30vol% alumina suspension by the fractal model indicates that the addition of saccharides affects the floc size and/or formation which leads to the resultant reduced viscosity.

Many observed phenomena are supported by the proposed fractal floc theory. The presence of flocs with pore channels is supported by the freezing point depression found in the bound water peaks. If flocs are similar in fractal dimension, this can explain the similar

melting temperature of the bound water peak in suspensions of 20-60vol% alumina. It was found that the addition of saccharides lowered the melting point of the bound water which would correspond to the decreased size of pore channels in more closely associated flocs.

The addition of saccharides lowers the viscosity of the suspensions, which was attributed to smaller floc sizes and less interaction between flocs both initially and with increasing shear rate caused by increased fractal dimension. An illustration of this is given in Figure 21.

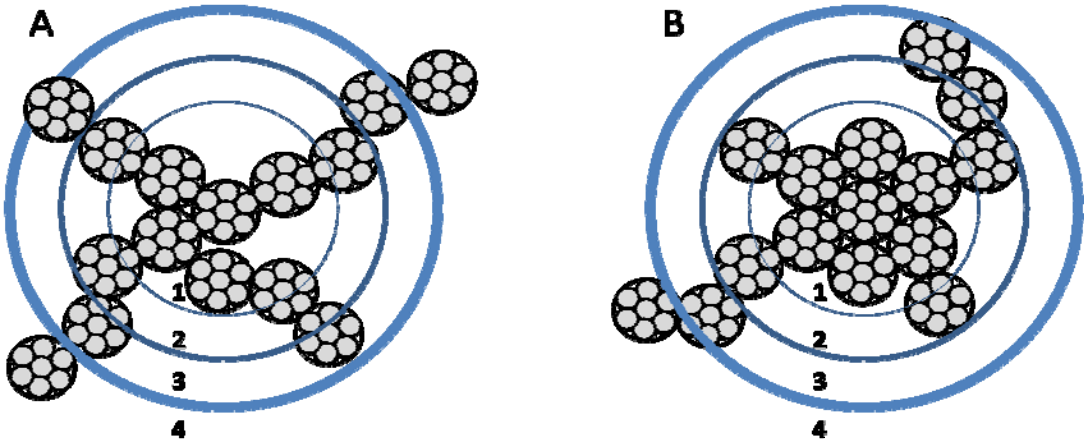

Figure 21. Illustration of model behavior of alumina nanoparticles in suspension A) without saccharides B) with saccharides

The gray circles in Figure 21 represent the same primary particles as in Figure 18 which are arranged in idealized close packed spheres. Scheme A in Figure 21 represents a floc in a suspension without saccharides and scheme B represents a floc in a suspension with saccharides. The circumscribed circles represent the coordination of the close packed spheres from the center of the floc. A and B represent flocs at rest in a suspension. The floc in B is more closely associated than A, which would result in fewer interactions between neighboring flocs because the low density branches (in coordination circles 2-4) are fewer. It can be imagined that during applied shear, in the case of B, some of the low density branches will be broken which would leave the closely associated center to have few interactions with other flocs in a similar state. This situation contrasts with A where the center is not closely associated and there may be more interactions, and therefore a higher viscosity at a given

shear rate after the low density branches are broken. Further support for this is the exponential yield point decrease with saccharide addition, which is good evidence that flocs are initially less interactive with the addition of saccharides.

It has been shown previously that saccharides will adsorb onto the alumina particle surface and alter the interactions between alumina nanoparticles[7,31]. This is likely to change the way the particles interact to form flocs. The altered flocculation behavior may be the cause of reduced viscosity of suspensions with added saccharides.

References

[1] Franks, G. V. and Y. Gan (2007). "Charging behavior at the alumina-water interface and implications for ceramic processing." J. Am. Ceram. Soc. **90**(11): 3373-3388.

[2] Hidber, P. C., T. J. Graule, et al. (1997). "Influence of the dispersant structure on properties of electrostatically stabilized aqueous alumina suspensions." J. Eur. Ceram. Soc. **17**(2-3): 239-249.

[3] Tomasik, P., Christopher H. Schilling, Ryszard Jankowiak, Jong-Cheol Kim (2003). "The role of organic dispersants in aqueous alumina suspensions." Journal of the European Ceramic Society **23**: 913-919.

[4] Kim, J. C., C. H. Schilling, et al. (2000). "Plasticizing dense alumina slurries with mono- and di-saccharides." Mater. Lett. **42**(4): 221-224.

[5] Schilling, C. H., C. Li, et al. (2002). "The rheology of alumina suspensions: influence of polysaccharides." J. Eur. Ceram. Soc. **22**(6): 923-931.

[6] Schilling, C. H., M. Sikora, et al. (2002). "Rheology of alumina-nanoparticle suspensions: effects of lower saccharides and sugar alcohols." J. Eur. Ceram. Soc. **22**(6): 917-921.

[7] Li, C. and M. Akinc (2005). "Role of bound water on the viscosity of nanometric alumina suspensions." J. Am. Ceram. Soc. Society **88**(6): 1448-1454.

[8] Li, C., M. Akinc, et al. (2005). "Relationship between water mobility and viscosity of nanometric alumina suspensions." J. Am. Ceram. Soc. **88**(10): 2762-2768.

[9] Mezger, T. G. (2006). The Rheology Handbook: For users of rotational and oscillatory rheometers. . Hannover, Germany, Vincentz Network GmbH & Co.

[10] Mazurkiewicz, J., P. Tomasik, et al. (2001). "Relationships between water activity and viscosity of solutions." Food Hydrocolloids **15**(1): 43-46.

[11] Zupancic, A., R. Lapasin, et al. (1999). "Rheological properties of aqueous alpha -Al2O3 suspensions: influence of dispersant concentration." Can. J. Chem. Eng. **77**(4): 627-636.

[12] Kim, J. C., C. H. Schilling, et al. (2000). "Plasticizing dense alumina slurries with mono- and di-saccharides." Mater. Lett.**42**(4): 21-224.

[13] Studart, A. R., Esther Amstad, Ludwig J. Gauckler (2007). "Colloidal Stabilization of Nanoparticles in Concentrated Suspensions." Langmuir **23**: 1081-1090.

[14] Beckett, S. T., Ed. (1995). Physico-Chemical Aspects of Food Processing. Bishopbriggs, Glasgow, Blackie Academic and Professional.

[15] Association, I. C. (2000). Viscosity of Cocoa and Chocolate Products. Analytical Method 46.

[16] (2007). ChemBioDraw Ultra. Cambridge, MA, CambridgeSoft.

[17] (2008). Origin Pro 8. Northhampton, MA, OriginLab Corporation.

[18] Bellissent-Funel, M. C., J. Lal, et al. (1993). "Structural study of water confined in porous glass by neutron scattering." J. Chem. Phys. **98**(5): 4246-52.

[19] Levy, E., A. I. Kolesnikov, et al. (2009). "Structure of water in mesoporous organosilica by calorimetry and inelastic neutron scattering." Surf. Sci. **603**(1): 71-77.

[20] Rennie, G. K. and J. Clifford (1977). "Melting of ice in porous solids." J. Chem. Soc., Faraday Trans. 1 **73**(4): 680-9.

[21] Johari, G. P. (2005). "Water's size-dependent freezing to cubic ice." J. Chem. Phys. **122**(19): 194504/1-194504/5.

[22] Li, C. and M. Akinc (2005). "Role of bound water on the viscosity of nanometric alumina suspensions." J. Am. Ceram. Soc. Society **88**(6): 1448-1454.

[23] Krall, A. H. and D. A. Weitz (1998). "Internal Dynamics and Elasticity of Fractal Colloidal Gels." Phys. Rev. Lett. **80**(4): 778-781.

[24] Chakraborti, R. K., K. H. Gardner, et al. (2003). "Changes in fractal dimension during aggregation." Water Research **37**(4): 873-883

[25] Potanin, A. A. (1991). "On the mechanism of aggregation in the shear flow of suspensions." J. Colloid Interface Sci. **145**(1): 140-57.

[26] Sonntag, R. C. and W. B. Russel (1986). "Structure and breakup of flocs subjected to fluid stresses. I. Shear experiments." J. Colloid Interface Sci. **113**(2): 399-413.

[27] Sonntag, R. C. and W. B. Russel (1987). "Structure and breakup of flocs subjected to fluid stresses. II. Theory." J. Colloid Interface Sci. **115**(2): 378-89.

[28] Li, L., s. Kuwamoto, et al. (2008). "SAXS studies on agglomerative silica suspension under shear." AIP Conf. Proc. 1027(Pt. 1, 15th International Congress on Rheology, 2008): 779-781.

[29] Kawaguti, C. A., S. H. Pulcinelli, et al. (2006). "Small angle X-ray scattering study of surface modified tin oxide nanoparticles prepared by sol-gel route." Journal of Sol-Gel Science and Technology **37**(3): 213-217.

[30] Blau, W., T. Gerber, et al. (1988). "Measurements of particle-size distributions and agglomerate structures by small angle x-ray scattering and light scattering." Freiberg. Forschungsh 778: 168-180.

[31] Li, C. (2004). Rheological properties of aqueous nanometric alumina suspensions. MSE. Ames, ISU.

Chapter 3

Cyanate ester-alumina nanoparticle suspensions: effect of alumina concentration on viscosity and cure behavior

A paper to be submitted to *Polymer Engineering and Science*

Katherine Lawler, Michael R. Kessler, Mufit Akinc

Department of Materials Science and Engineering
Iowa State University, Ames, IA 50011, U.S.A

Abstract

The effect of alumina nanoparticles on the viscosity and curing behavior of a bisphenol E cyanate ester monomer (BECy) suspension was investigated by rheometry and differential scanning calorimetry. The viscosity was found to increase with solids content and was fit well by the Mooney equation. Cure experiments indicate that alumina particles catalyze the curing of the suspensions. The viscosity reduction achieved at high particle loadings by the addition of benzoic acid was also investigated by NMR.

1. Introduction

Bisphenol E Cyanate ester (bis(4-cyanatophenyl)-1,1 –ethane) or BECy, is a low viscosity monomer with a reported viscosity of 0.09-0.12Pas [1]. It is frequently used in circuit board and aerospace composites due to its high glass transition temperature (T_g), low dielectric loss properties, and resistance to fluids encountered in the operation of aircraft[2]. Other desirable qualities of this resin are low volatility, with less than 1% volatile content before curing[3], and low toxicity[4] which are important attributes for the safety of those who work with BECy resins.

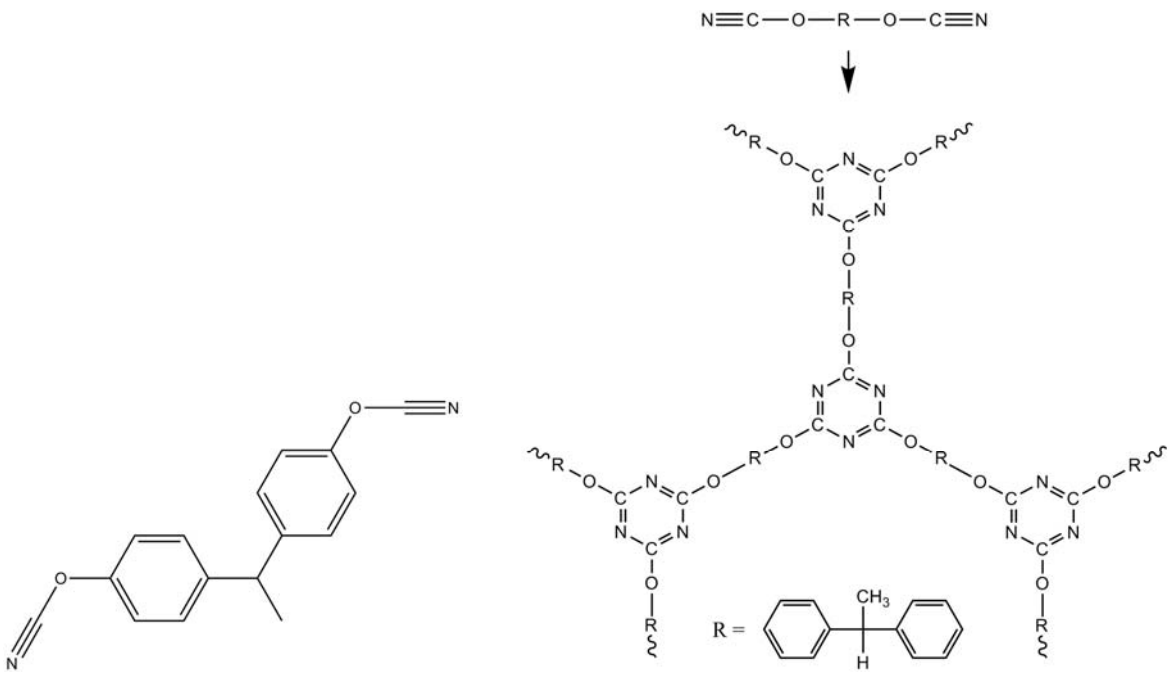

Figure 1. Formation of BECy molecule and scheme for polymer network (triazine ring) formation[1,5].

Cyanate esters and other thermosetting polymers have been modified by adding nano-scale additives, such as fumed silica[1], layered silica clay particles[6], carbon nanotubes and fibers to achieve desired processing characteristics and mechanical properties. The addition of alumina nanoparticles has not been extensively studied.

Polymer matrix composites are prone to suffer delaminations over time which can occur due to operating conditions and mechanical impacts. To repair these defects, scarf patch repair or resin injection methods can be used. The resin repair method has been limited due to the low T_g of available adhesives. The resin currently being studied, BECy, is unique due to its low viscosity and high T_g which may make it suitable for an injectable repair resin[3].

In an injectable repair system, the repair resin will need to be taken up into the cracks of a damaged composite panel to achieve a complete fill and recovery of strength. Shimp investigated the transport of resin in filament bundles and found that viscosity is the dominant parameter for percolation rate and capillary flow[2]. It is expected that these properties will be important in the process of crack filling during damage repair. The use of BECy is advantageous because of its low viscosity at room temperature before curing. It is expected that alumina nanoparticles may be used to optimize desired flow and post–cure

mechanical properties for a repair resin. Furthermore, a resin containing nanosized alumina particles could be injected readily through a small aperture making the addition of nanoparticles to BECy ideal for this application.

In the present study, the viscosity and dynamic cure of BECy monomer/alumina nanoparticle suspensions were studied to investigate the effect of adding alumina nanoparticles to the BECy resin on the processing behavior. Addition of benzoic acid was also investigated to lower the viscosity of highly loaded suspensions.

2. Experimental

2.1. Materials

For this investigation, nanosized γ-phase alumina powders with an average particle size of 48 nm (Nanophase Technology Corporation, Burr Ridge, IL) LOT#AAGE1607 were used. The specific surface area of the γ-alumina powder was 34 m^2/g, and the density was taken to be 3.6 g/cm^3. A TEM image of the powders can be seen in Figure 2. The BECy monomer, EX-1510, and polymerization catalyst (EX-1510-B) were obtained from Bryte Technologies (Morgan Hill, CA) and used as received. Benzoic acid (C_6H_5COOH) powder of A.C.S grade was supplied by Fisher (Pittsburg, PA).

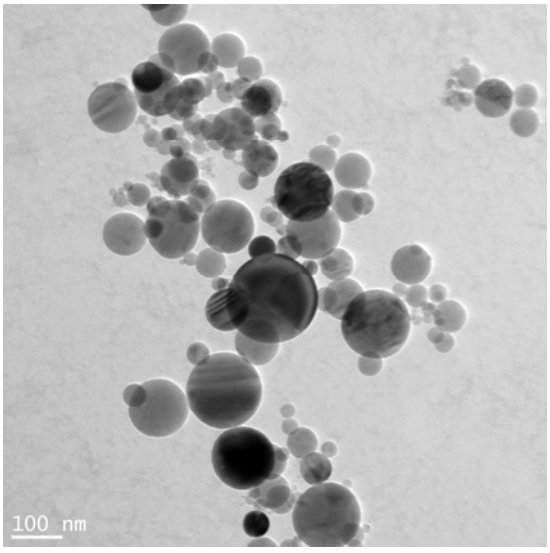

Figure 2. TEM micrograph of alumina nanoparticles. Particles are spherical and show significant variation in size.

2.2. Sample preparation

Alumina powders were dried at 110°C for 2 hours before mixing with cyanate ester. BECy and benzoic acid were used as received with no pre-treatment. The BECy monomer/alumina suspensions were prepared by transferring the desired amount of monomer, usually 5 g, into a glass vial then adding the desired amount of alumina powder to the vial. The vial was then sealed and suspended in an ultrasonic bath until visually homogeneous for a minimum of 30 minutes. Samples with low vol% alumina were mixed easily, but the high vol% samples (15 and 20%) took more than one hour. BECy/alumina/benzoic acid samples were made by the same method as above, but the benzoic acid was first dissolved in BECy before the addition of alumina.

Cured samples for TEM imaging were prepared by mixing BECy and alumina as described above. The portion of the suspension which was to be cured was mixed with catalyst at 3phr (parts per hundred resin) with a stir bar then degassed for 60 minutes to remove trapped air. The samples were cured in silicone rubber molds at 150°C for 2 hours. A post-cure step was not used because the samples were rigid enough for handling after the first cure step.

2.3 Characterization

A TA Instruments 2000EX rheometer (New Castle, DE) with a 1° cone and peltier plate to maintain a temperature of 25°C was used. A 300μL sample was loaded using a micro pipette and pre-sheared at $28s^{-1}$ (0.5 rad/s) for 30s to ensure that the gap was filled and a uniform shear history was established for all measurements. The pre-shear step was followed by a no-shear period of one minute before collecting data. Viscosity as a function of shear rate was measured from 0.1 to $500s^{-1}$ and back to $0.1s^{-1}$. Ten points were measured per decade with 3 periods of 10s at each shear point.

A TA Instruments DSC Q2000 differential scanning calorimeter was used to study the curing behavior of alumina containing samples. Suspensions from 0.5-20 vol% alumina were prepared and approximately 12 mg of each sample was sealed hermetically in an aluminum sample pan. Samples were ramped from 25 to 350°C at 6°C/min in helium to obtain a dynamic cure scan. For each alumina loading, the same sample was cooled back to

25°C and heated again at 10°C/min to 350°C to obtain the glass transition temperature (T_g) of the cured sample.

A JEOL 2100 transmission electron microscope (TEM) was used to capture images of the cured nanocomposites. An accelerating voltage of 200kV was used. Samples were sliced to 50-60nm thickness using an ultramicrotome and placed on formvar film grids for imaging.

A Nuclear Magnetic Resonance (NMR) spectrometer Varian VXR-300 (Palo Alto, CA) was used to study the interactions of benzoic acid with BECy and alumina. The machine operated at 300 MHz. Samples of about 0.5mL were dissolved in 2.5mL deuterated chloroform prior to measurement.

3. Results and Discussion

3.1. TEM images of cured nanocomposite samples

TEM images show that the alumina particles are well dispersed in the BECy polymer matrix (see Figure 3). From these images, it appears that the particles have a tendency to agglomerate in small clusters, but large clusters are absent. Increasing alumina particle concentration is well illustrated in the micrographs again indicative of good dispersion and uniform distribution of the particles throughout the polymer matrix. The white spots are due to particle pull out from the resin during sectioning the sample for TEM.

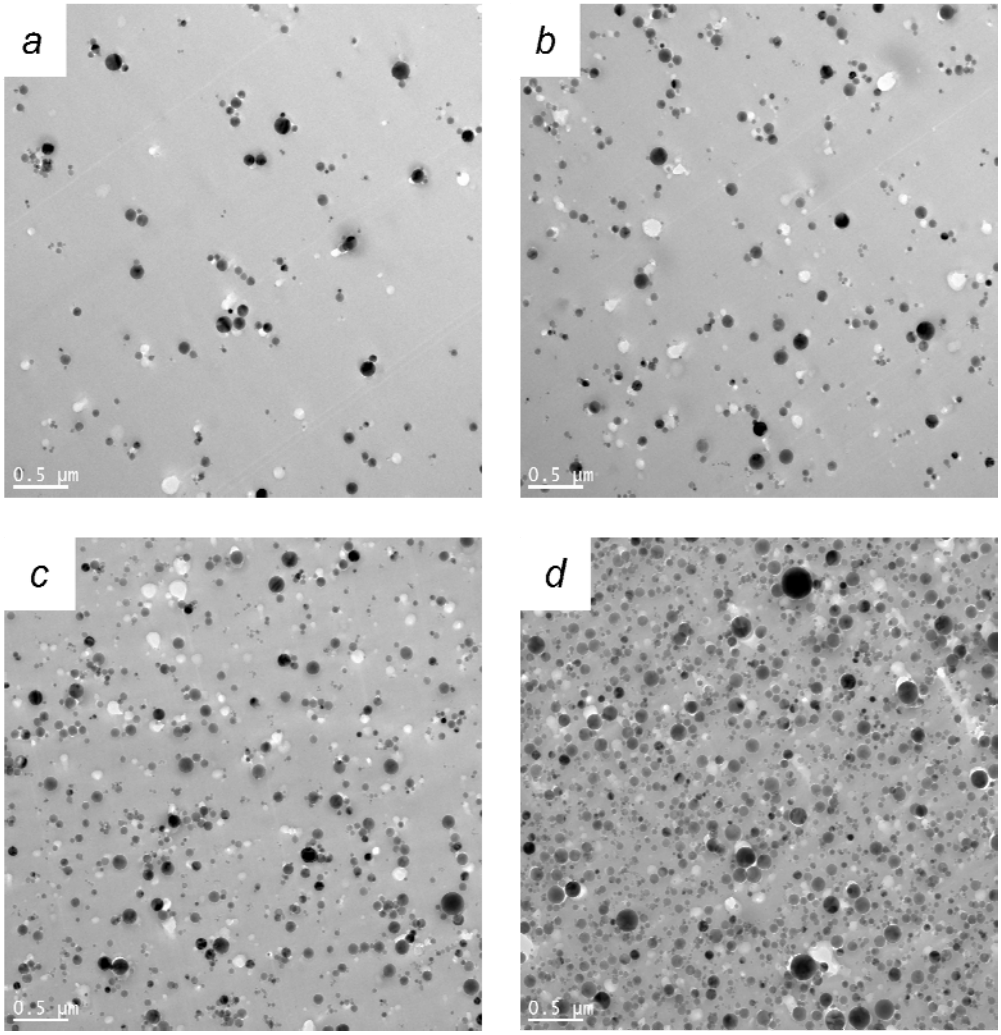

Figure 3. TEM images of the BECy/alumina nanoparticle composite samples with a) 2.5%, b) 5%, c) 10%, d) 20% alumina by volume

3.2. Viscosity of BECy/alumina nanoparticle suspensions

The viscosity of suspensions as a function of shear rate for suspensions with 1-20 vol% alumina nanoparticles is shown in Figure 4.

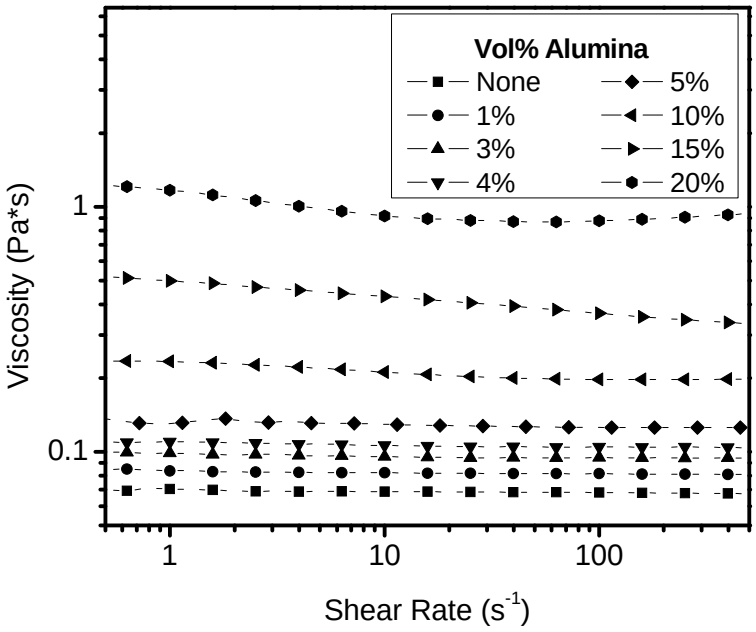

Figure 4. Viscosity of BECy/alumina nanoparticle suspensions

Figure 4 illustrates the effect of nanoparticle concentration on the viscosity of the suspensions. The behavior of samples up to and including 5% is nearly Newtonian with a slight increase in suspension viscosity with alumina concentration. As the concentration of particles increases beyond 5%, some shear thinning is seen, and at 20 vol%, shear thinning as well as shear thickening above $60s^{-1}$ is observed.

In a similar study[1] of the rheology of 40nm silica nanoparticle/BECy suspensions, shear thickening was found in a 20.7 vol% suspension above $20s^{-1}$. The magnitude of shear thickening in suspensions of silica is much more pronounced than alumina. This could be due to the spherical shape of the alumina versus the physically agglomerated shape of the fumed silica particles. The TEM images of cured suspensions in Figure 3 show that alumina particles are spherical and well dispersed.

The near-Newtonian behavior of suspensions up to and including 5 vol% alumina indicates that the particles are not interacting with each other. The increase in viscosity with volume fraction at these low solids loadings is anticipated as predicted by the well known Einstein, and Krieger-Doughery expressions[7]. In addition, the increased interaction with monomer and the surface of particles might contribute to higher suspension viscosity. A

similar conclusion was reached by Wooster[6] in the study of layered silicates and BECy. He stated that the rheology of suspensions with layered silicates was dependent on the amount of silicate exposed to the monomer.

The nearly linear viscosity increase at low loadings is shown in Figure 5. This behavior suggests that the increased viscosity due to particle/monomer interaction is a reasonable explanation because the total surface area of alumina in the suspension is also increasing linearly.

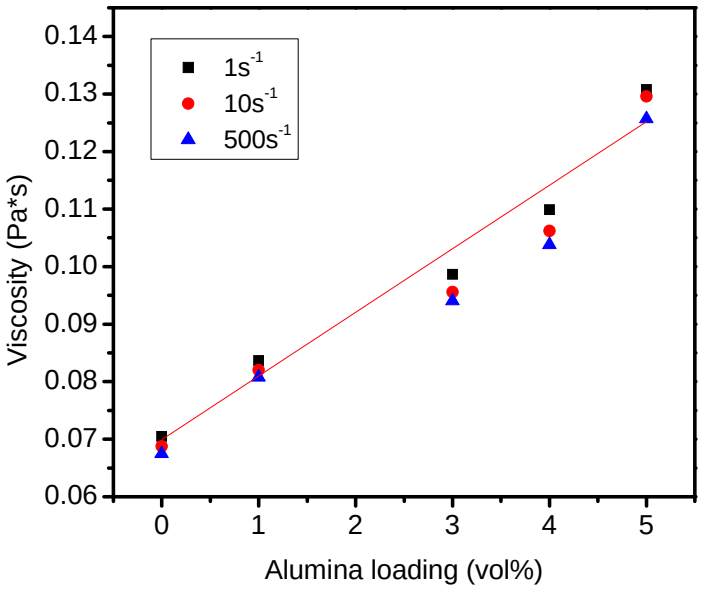

Figure 5. Linear increase in viscosity of BECy/alumina nanoparticle suspensions at low alumina loadings

The behavior of suspensions greater than 5vol% alumina is non-Newtonian. This type of behavior is indicative of particle interactions which contribute to the shear thinning and shear thickening rheologies[8].

In addition to viscosity that is dependent on shear rate above 5 vol% alumina, the viscosity at a given shear rate increases exponentially with solids loading. This is shown in Figure 6. Particle-particle interactions are also the likely reason for the exponential increase in viscosity at a given shear rate beyond 5 vol%. As particles are brought more closely

together in suspensions with higher solids contents, there is a greater chance of interaction. This can be seen in the TEM images of sample at selected vol% in Figure 3. At 20vol% the particles are in close proximity but still well dispersed. Also seen in Figure 6 is the degree of shear thinning at lower shear rates. As the solids content increases, the magnitude of shear thinning also increases.

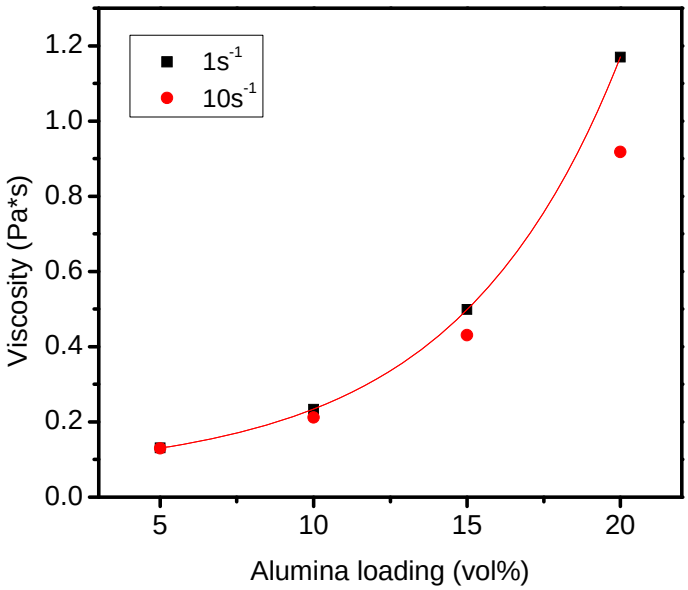

Figure 6. Exponential increase in viscosity of BECy/alumina nanoparticle suspensions at higher alumina loadings

The relative viscosity (η/η_s), where η_s is the viscosity of neat BECy resin, of suspensions was compared to the viscosity predicted by existing models. The Einstein (Equation 1) and Krieger-Dougherty (Equation 2) relationships were found to greatly underestimate the viscosity at any solids loading. K_e is the Einstein coefficient, typically 2.5, ϕ_m is the maximum packing fraction, which ranges from 0.37 for agglomerated random close packing to 0.74 for hexagonal close packing[9], and ϕ is the solids content. These models assume that the suspensions are dilute and the particles are non-interacting. Typically, suspensions of 0 – 30 vol% are considered dilute, so this criteria is met by all suspensions. Also, the Newtonian behavior of suspensions with 1-5 vol% alumina suggests that these suspensions contain non-interacting particles. But, it can be seen in Figure 7, that the

experimental viscosity increases with solids content at a much greater rate than the prediction by the both the Einstein and Krieger-Dougherty equations[7] where Ke was assumed to be 2.5 and ϕ_m was assumed to be 0.74. The greater viscosity may be due to the greater surface area of the nanoparticles, or a stronger interaction with the solvent, BECy, than expected by these models.

$$\eta/\eta_s = 1 + K_e\phi$$

Equation 1

$$\eta/\eta_s = \left(1 - \frac{\phi}{\phi_m}\right)^{-[\eta_s]\phi_m}$$

Equation 2

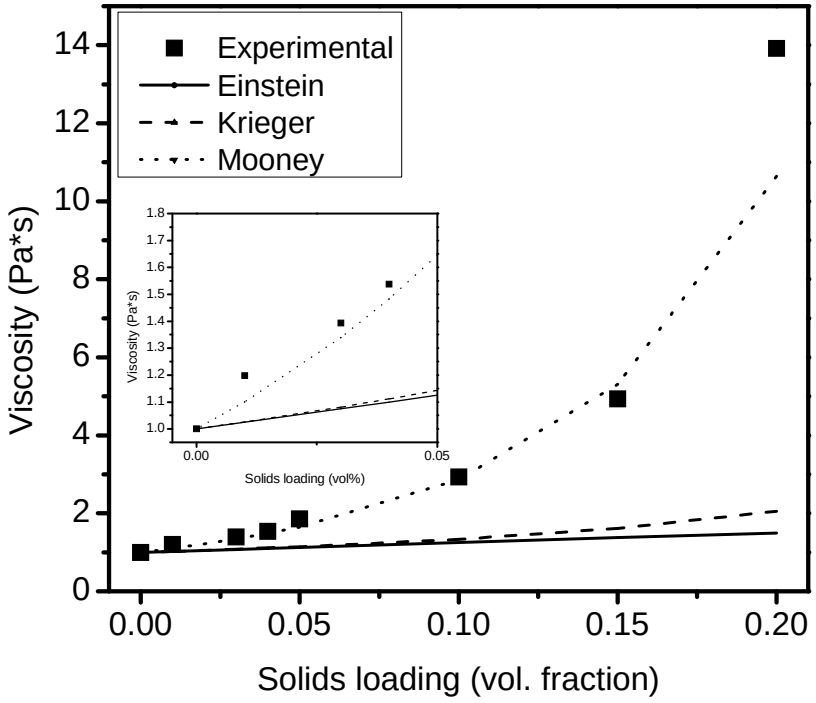

Figure 7. Comparison of suspension viscosity at 500 s^{-1} with existing Einstein, Krieger-Dougherty, and Mooney viscosity models

Another equation by Mooney (Equation 3) was recently found to describe the viscosity of BECy suspensions with 0 - 3 vol%[10]. This equation has been shown to fit suspensions containing polydisperse particles and suspensions with agglomeration[11]. It was developed to describe the viscosity of polydisperse particle suspensions and particle-particle interactions are accounted for. Furthermore, this model assumes that small particles are crowded into the space unoccupied by the larger particles[12].

The Einstein coefficient, K_e, was varied by Equation 4 to get the best fit. This parameter is related to the level of agglomeration. V_S refers to the volume of spheres in a typical agglomerate, and V_L is the volume of solvent that is entrapped or on the surface of the agglomerate. The larger the coefficient the larger the amount of agglomeration present in the suspension.

$$\eta/\eta_s = \exp\left(\frac{K_e\,\phi}{1-(\phi/\phi_m)}\right)$$

Equation 3

$$K_e = 2.5 + \frac{V_L}{V_S}$$

Equation 4

The fit above used values of $\frac{V_L}{V_S} = 1$ and $\phi_m = 0.37$ which are reasonable values from a structural standpoint. The maximum solids content was taken to be the value for random close packing of agglomerated particles, and the low value of K_e indicates that the level of agglomeration is low. The value for maximum solids content seems reasonable from experiment; samples with 20 vol% alumina seemed to reach the practical limit for sample preparation.

3.3 Influence of alumina on DSC dynamic cure of nanocomposites

No catalyst was used in the preparation of samples used for dynamic cure experiments. Figures 8a and b show the dynamic cure behavior of the alumina nanoparticle/BECy composite samples in the form of DSC scans. The neat BECy peak temperature of 301°C is consistent with a previous study[13]. At 0.5 vol% alumina the single

peak splits into two showing a shoulder around 230°C which grows gradually and shifts to lower temperatures as more alumina is added. The original peak at 301°C also shifts to lower temperatures, but its intensity remains relatively constant from 0.5 – 3 vol%. At 4 vol%, the high temperature peak disappears completely leaving the low temperature as the single thermal effect which persists up to 20 vol% alumina, the highest solids contents tested.

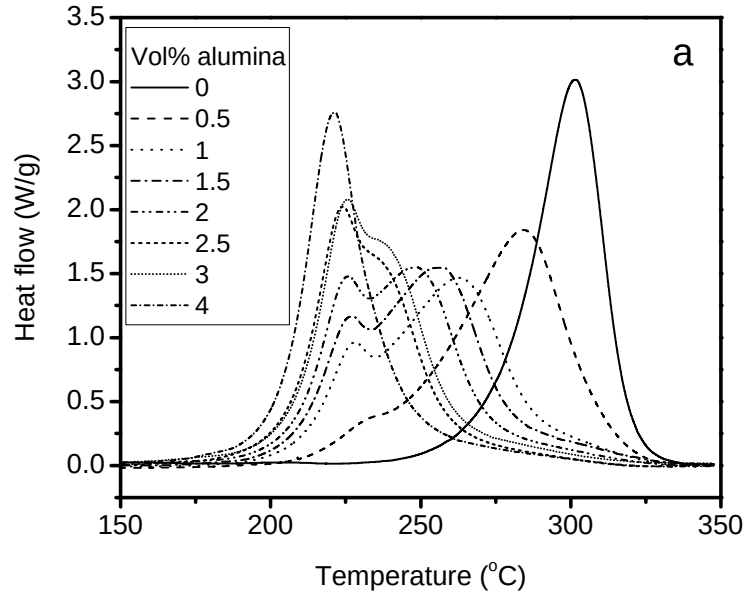

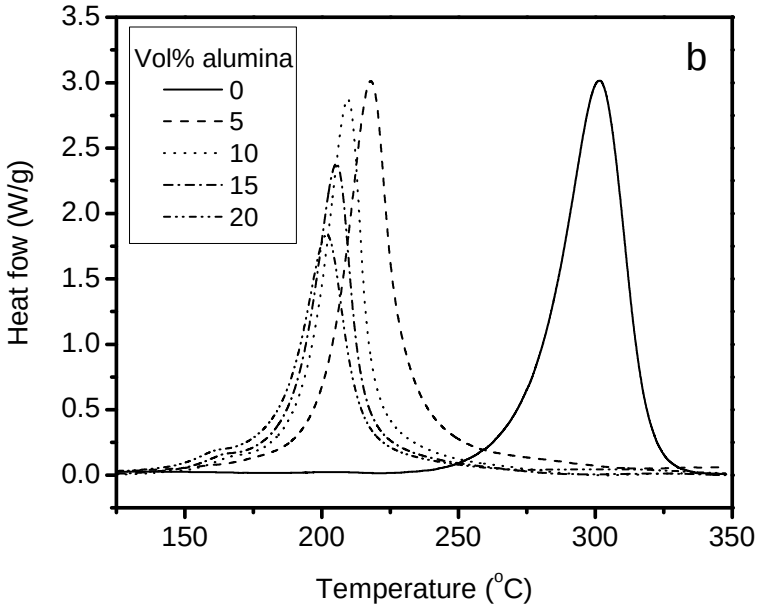

Figure 8. DSC plot of BECy/alumina nanocomposite curing with a) 0 to 4 vol% alumina nanopowder loading which illustrates peak splitting with even lowest alumina addition and b) 5 to 20 vol% showing a single cure peak.

The presence of two peaks indicates that there are two resin environments which are undergoing polymerization simultaneously but with different cure kinetics. The lower temperature peak is due to the presence of alumina which is presumably providing a catalytic effect. Upon the addition of 0.5 vol% alumina, appearance of second cure peak at 230 ^{o}C, about 70 ^{o}C below the cure temperature of neat BECy is a strong indication for the catalytic effect of alumina particles. As more alumina is added, the lower temperature peak decreases further by 10^{o}C until the original higher cure temperature peak disappears. It seems that when the alumina loading is ≥4 vol% the curing is entirely catalyzed by the alumina surface. Figure 9 shows the variation of alumina catalyzed peak temperature as a function of alumina loading. A similar effect of alumina nanoparticles on the cure of BECy was reported previously in our group and it has been attributed to the Lewis acidity of the alumina surface[10].

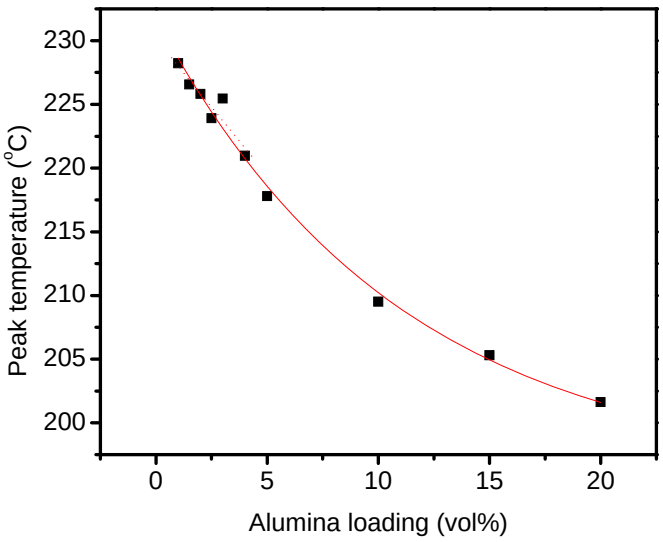

Figure 9. The variation of the alumina catalyzed peak temperature as a function of alumina loading. Peak curing temperature decreases exponentially with alumina loading.

The manufacturer's catalyst is prescribed to be used at 3phr (0.03g catalyst/1g resin), which is also a small fraction of the total sample. The OH- sites present on the surface of bare alumina powder can be estimated by a TGA measurement which is shown in Figure 10. The mass loss between 200 and 800°C may be attributed to the loss of surface hydroxyl groups[14]. The calculated hydroxyl concentration is 41μmol/m^2 and corresponds to 0.0244 OH/OCN in the case of 4% alumina. Assuming the catalyst recommended by the manufacturer is composed primarily of nonylphenol, the OH/OCN ratio is 0.0125, which is approximately half of the hydroxyl concentration on the alumina surface.

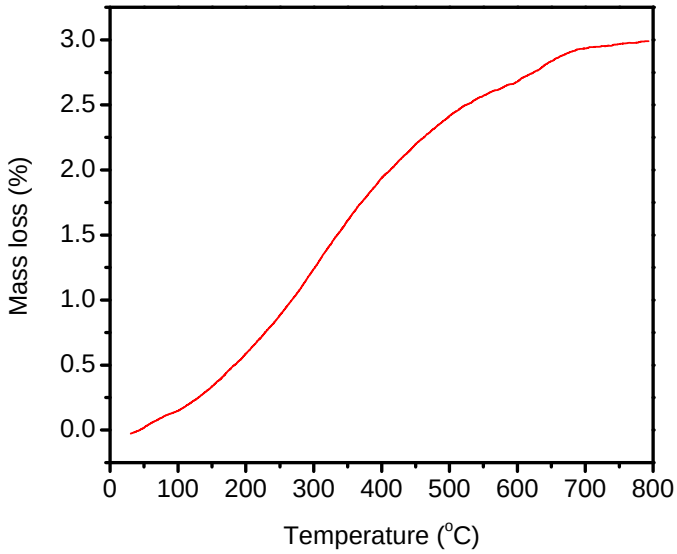

Figure 10. TGA plot of alumina powder between room temperature and 800 °C. Note the gradual and continuous mass loss from room temperature up to 700 °C. It was assumed that the mass loss up to 200 °C can be attributed to physically adsorbed or hydrogen bonded water while above 200 °C all the mass loss may be attributed to dehydroxlation of the surface, although some mass loss from the bulk may not be completely excluded.

Hamerton explains that a key product during cyclotrimerization of BECy without a catalyst is an intermediate iminocarbonate that is formed by a reaction of BECy with a phenolic hydroxyl group. In fact, the cyclotrimerization reaction will not take place without a small amount of impurity to form this complex[15]. Since the neat BECy cured without an

added catalyst, there must be a small amount of impurity present in the resin which was not removed after synthesis. It is probable that it is necessary to add 4% alumina to achieve a reaction completely catalyzed by the hydroxyl groups on the alumina surface instead of the resin impurity.

If this is the case, it is likely that the T_g should be greatly reduced with ≥4 vol% alumina additions due to the presence of excess hydroxyls that will cause the termination of the growing polymer network at a lower molecular weight. To see whether the T_g was affected by the alumina addition, T_g of polymer at various alumina loadings was determined at 10 °C/min heating rate. As illustrated in Figure 11, the T_g decreases with the addition of alumina in a linear fashion with an approximate decrease of 3°C for every 1 vol% alumina added. With up to 5 vol% alumina additions the T_g is lowered only ~ 15°C from the neat BECy T_g of ~278°C. The addition of 20 vol% alumina has a drastic effect on the T_g, lowering it by ~65°C.

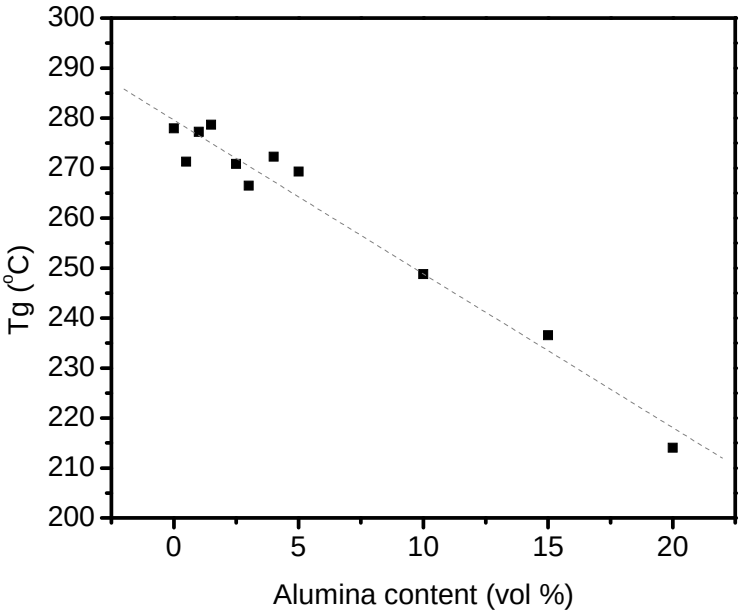

Figure 11. T_g of cured polymers as a function of alumina concentration. The T_g of the polymers was measured by DSC at a rate of 10 °C/min.

3.4 Benzoic acid addition as a dispersant

A significant increase in viscosity is seen in suspensions with ≥10vol% alumina especially at low shear rates (See Figures 4 and 6). This was attributed to increased particle-particle interactions as discussed above. In aqueous and organic solvent-based suspensions of nanoparticles, a lower viscosity has been achieved by the addition of an appropriate dispersant. It has been shown that the dispersant molecules adsorb onto the particle surfaces and reduce interactions either sterically (steric stabilization) or by modifying the surface charge (electrostatic stabilization) or both (electrosteric)[16,17].

To check if the viscosity of the alumina nano powder/BECy suspensions may be reduced by the addition of appropriate dispersants, cinnamic or benzoic acid was added to highly loaded suspensions (15 and 20%). It was found that both acids were effective. But, benzoic acid was chosen for use in further experiments due to its simpler and similar structure to the suspending medium of BECy.

The viscosity of 15 and 20vol% alumina suspensions with additions of benzoic acid at various wt% based on alumina are shown in Figure 12. Reduction in viscosity relative to suspension without any benzoic acid addition at 10 and 100 s^{-1} is summarized in Table 1.

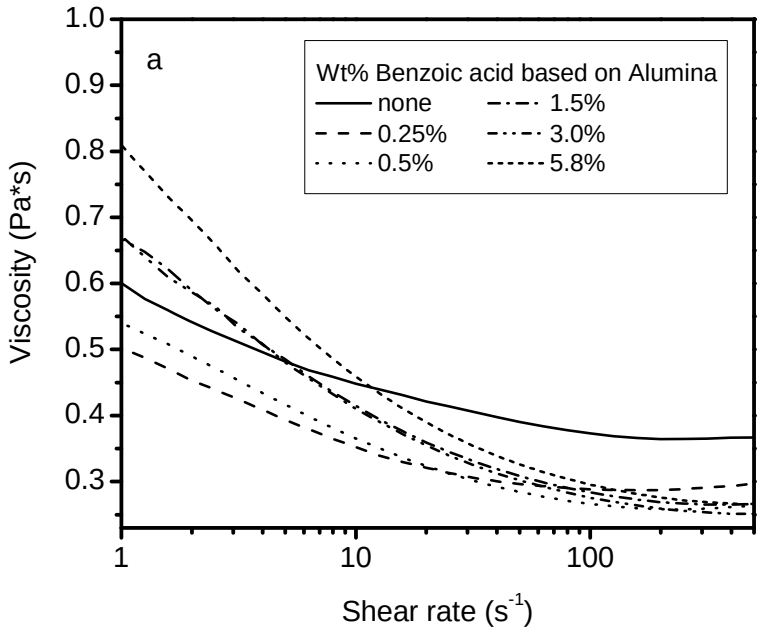

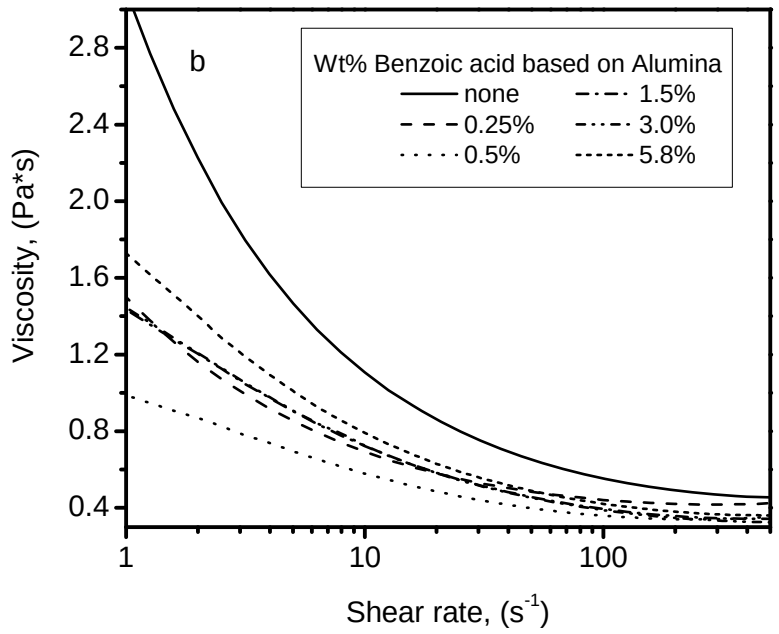

Figure 12. Viscosity of suspensions as a function of shear rate at several levels of benzoic acid addition, at a) 15vol% and b) 20vol% alumina nano particle loadings

Table 1. Viscosity reduction for each benzoic acid loading with respect to the sample with no benzoic acid

	% reduction at $10s^{-1}$		% reduction at $100s^{-1}$	
Amount acid (wt%)	**15%**	**20%**	**15%**	**20%**
0.25	21.4	37.3	22.6	19.8
0.5	18.5	47.7	28.5	34.6
1.5	7.4	35.7	23.7	28.4
3.0	8.5	34.6	26.1	29.5
5.8	-	28.6	21.0	23.7

It can be seen that the viscosity of each suspension is reduced with the addition of benzoic acid up to 3wt%. The greatest viscosity reduction at $100s^{-1}$ is achieved at a level of 0.5wt% benzoic acid based on the weight of alumina powder.

Proton NMR provides a tool to analyze the interaction of hydrogen atoms in BECy and benzoic acid. Proton NMR for the BECy shows the hydrogen atoms associated with the benzene ring between 7.2 and 7.3 ppm, the $–CH_3$ group at 1.63 and 1.66 ppm, and the quartet

associated with the lone hydrogen opposite the $–CH_3$ group is centered at 4.22ppm. The structure of BECy is shown in Figure 1 for reference.

On the other hand, benzoic acid peaks are seen as a doublet at 8.13, a triplet of triplets at 7.63, a triplet at 7.5 and a singlet at 7.26 ppm. Sodium benzoate was measured to see the deprotonated version of the molecule and peaks were found as a doublet centered at 8.18, a collection of peaks at 7.5 and a singlet at 7.27 ppm and 1.56 ppm. Sodium benzoate did not completely dissolve in the solvent, so the peaks around 7.5 were not easily distinguished.

The comparison of doublets centered near 8.13 and 8.18 ppm can be used to determine the state of benzoic acid added, whether it is in the protonated or deprotonated state. Figure 13 shows a schematic of these molecules.

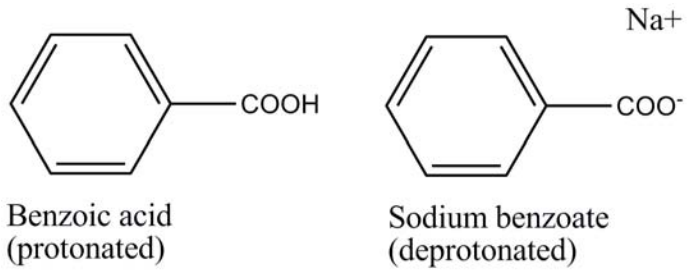

Figure 13. Structures of benzoic acid and sodium benzoate

In the mixture of BECy/Benzoic acid, both COOH and COO^- shifts are seen. It appears that the deprotonated peak grows with time and the protonated peak diminishes over time. So, it appears that the interaction of benzoic acid with BECy results in a deprotonation of benzoic acid. The peak area ratio of benzoic acid-to-BECy was calculated at several time intervals after preparation. The ratio is reduced from 0.79 to 0.16 with time from 4 to 20 hours. This can be seen in Figure 14.

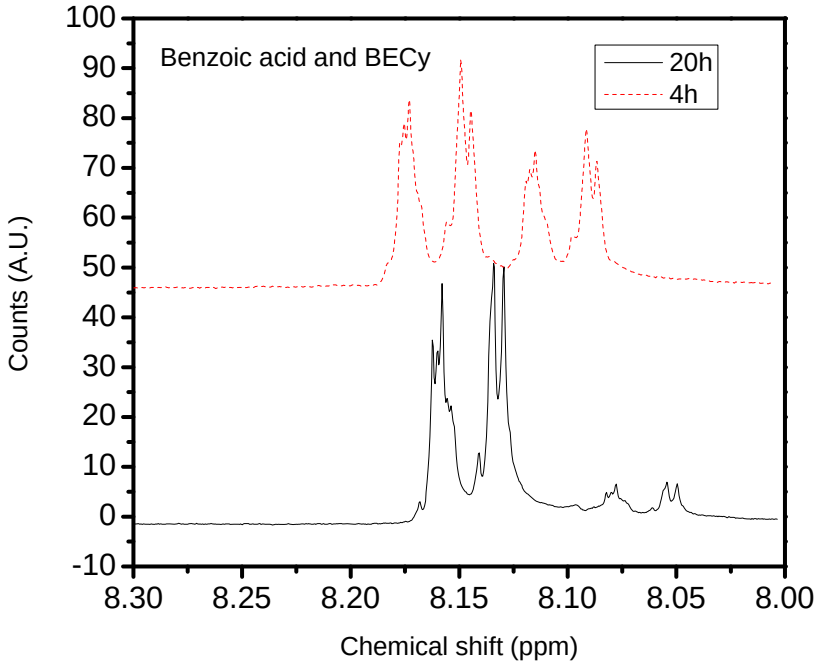

Figure 14. H-NMR spectra of BECy/benzoic acid mixture over time

The deprotonation of benzoic acid was also seen in the benzoic acid/BECy/alumina samples. One spectrum was measured immediately after sample preparation, another was measured 4 h later (with a fresh sample), and another 8 h from the first measurement The spectra are shown in Figure 14. The ratio of peak areas of the doublets was compared for each sample relative to deprotonated sample. The peak ratio again goes from 0.84 at the time of preparation to 0.28 and 0.17 after 4 and 8 hours, respectively. The addition of alumina to BECy and benzoic acid was found to broaden the remaining COOH peak. This is an indication of hydrogen bonding between benzoic acid and alumina in the presence of BECy.

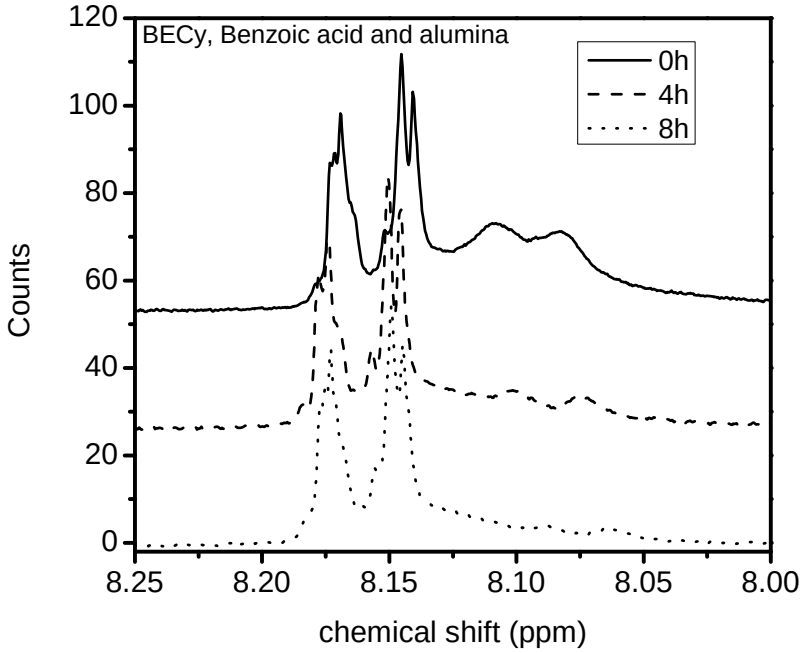

Figure 15. H-NMR spectra of BECy/benzoic acid/alumina suspension over time

Samples of BECy and alumina, and BECy and benzoic acid both show a peak at 5.1 ppm. The broadened peak at 5.1 ppm arises due to alumina or benzoic acid in the presence of BECy. Since it is a singlet, it is most likely due to interactions with the single hydrogen in the BECy monomer. The introduction of the 5.1 ppm peak does appear with an increase in the asymmetric nature of the quartet, which is also attributed to that hydrogen. The peak is broadened which indicates hydrogen bonding, so alumina or benzoic acid must be associating with it. Furthermore, since the number of molecules of benzoic acid or alumina that is added is less than the number of molecules of BECy present, the quartet will not disappear.

So, NMR studies show that BECy and alumina interact by hydrogen bonding and BECy and benzoic acid are interacting by hydrogen bonds as well. It is not the interaction of BECy and benzoic acid that lowers the viscosity. The addition of benzoic acid to BECy actually increases the viscosity to 0.13 Pa*s from the original BECy viscosity of 0.07 Pa*s while maintaining Newtonian behavior on the 2nd and 3rd steps as seen in Figure 15.

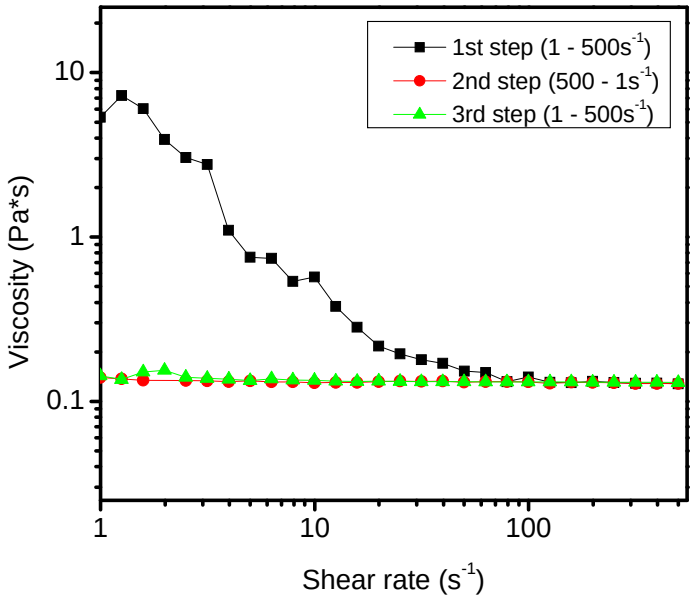

Figure 15. Viscosity of BECy/benzoic acid suspension. The reason for the shear thinning in the first step and Newtonian behavior after is not known.

Since the viscosity reduction is observed in the presence of alumina particles, the interaction of benzoic acid with the alumina, as confirmed by the NMR results, must be responsible for the reduction of suspension viscosity. There is previous evidence from Secondary Ion Mass Spectroscopy that benzoic acid, in the benzoate form, will adsorb onto an alumina surface[18]. If benzoic acid could be grafted onto the alumina particle surface and the resultant suspension made from these particles possessed a lower viscosity than a suspension of bare particles, this would be good evidence for the proposed mechanism.

4. Conclusion

The addition of alumina nanoparticles increases the viscosity of the suspensions greater than predicted by the Einstein and Krieger-Dougherty models, but the Mooney equation provides a reasonable fit. Above 5vol% alumina additions, shear thinning and dramatic viscosity increases (exponentially) were observed presumably due to strong particle-particle interactions. Considering rheological behavior only, an alumina content of

up to 10% would be appropriate for an injectable composite repair assuming the ideal viscosity for resin transfer molding 0.1-0.3 Pa*s[2] is an appropriate basis.

The viscosity of highly loaded suspensions (15 and 20%) was reduced with the addition of benzoic acid. Evidence of hydrogen bonding was shown through NMR, and it is likely that the viscosity decrease is due to benzoic acid interacting with the alumina particle surface.

DSC measurements suggest that the hydroxyl groups on the alumina particles catalyze the polymerization reaction, and at 4vol% alumina addition, the polymerization is initiated entirely by the alumina particles. Due to excess hydroxyl groups afforded by the alumina particle surface, the T_g decreases monotonically which is considered detrimental to the function of thermosetting polymers, such as cyanate esters, developed for high temperature applications. So, taking into account the polymer structure upon curing, the recommended amount of alumina should be less than 5%, or alternatively dehydroxylated alumina may be employed.

The catalysis of the polymerization reaction by alumina particles which lowers the cure temperature may be seen as a benefit. Lower cure temperatures are favorable for composite repair applications[3] because the repair of the damage part may be achieved at lower cure temperatures. Therefore, an optimum alumina loading must be established to achieve lower curing temperature, while maintaining acceptable T_g and mechanical properties of BECy/alumina nanocomposite system.

Acknowledgements

Thanks to Tracey Pepper at Iowa State University for assistance with TEM images. This work was partially funded by the Ames Laboratory Seed Grant Program and supported by a grant from the Strategic Environmental Research and Development Program (SERDP), under the “Environmentally Benign Repair of Composites Using High Temperature Cyanate Ester Nanocomposites” project (Project Number WP-1580).

References

[1] Goertzen, W. K., X. Sheng, et al. (2008). "Rheology and curing kinetics of fumed silica/cyanate ester nanocomposites." Polym. Eng. Sci. **48**(5): 875-883.

[2] Shimp, D. A. and W. M. Craig, Jr. (1989). "New liquid dicyanate monomer for rapid impregnation of reinforcing fibers." Int. SAMPE Symp. Exhib. **34**(Tomorrow's Mater.: Today, Book 2): 1336-46.

[3] Sheng, X., M. Akinc, et al. (2008). "Cure kinetics of thermosetting bisphenol E cyanate ester." J. Therm. Anal. Calorim. **93**(1): 77-85.

[4] BECy Toxicity white paper. 2008.

[5] (2007). ChemBioDraw Ultra. Cambridge, MA, CambridgeSoft.

[6] Wooster, T. J., S. Abrol, et al. (2005). "Rheological and mechanical properties of percolated cyanate ester nanocomposites." Polymer **46**(19): 8011-8017.

[7] Rahaman, M. N. (2003). Ceramic Processing and Sintering. New York, Marcel Dekker, Inc.

[8] Dinger, D. R. (2002). Rheology for Ceramists. Clemson, SC, Dinger Ceramic Consulting Services.

[9] Nielsen, L. E. and R. F. Landel (1994). Mechanical Properties of Polymers and Composites. New York, Marcel Dekker, Inc.

[10] Sheng, X., M. Akinc, M. R. Kessler: "The Rheology and Dynamic Mechanical Analysis of Bisphenol E Cyanate Ester/Alumina nanocomposites", Polymer Engineering and Science; 03/30/2009 submitted.

[11] Nielsen, L. E. and R. F. Landel (1994). Mechanical Properties of Polymers and Composites. New York, Marcel Dekker, Inc.

[12] Mooney, M. (1951). "The viscosity of a concentrated suspension of spherical particles." J. Colloid Sci. **6: 162-70.**

[13] Haman, K., P. Badrinarayanan, et al. (2009). "Effect of a Zirconium Tungstate Filler on the Cure Behavior of a Cyanate Ester Resin." ACS Appl. Mater. Interfaces ACS ASAP.

[14] Abboud, M., M. Turner, et al. (1997). "PMMA-based composite materials with reactive ceramic fillers. Part 1.-Chemical modification and characterization of ceramic particles." J. Mater. Chem. **7**(8): 1527-1532.

[15] Hamerton, I., Ed. (1994). Chemistry and Technology of Cyanate Ester Resins. Bury St Edmunds, Suffolk, UK, Chapman and Hall.

[16] Tomasik, P., Christopher H. Schilling, Ryszard Jankowiak, Jong-Cheol Kim (2003). "The role of organic dispersants in aqueous alumina suspensions." Journal of the European Ceramic Society **23**: 913-919.

[17] Schilling, C. H., C. Li, et al. (2002). "The rheology of alumina suspensions: influence of polysaccharides." J. Eur. Ceram. Soc. **22**(6): 923-931.

[18] Affrossman, S., J. M. R. MacAllister, et al. (1987). "SIMS study of adsorbates. I. Benzaldehyde and benzoic acid on aluminum." Surf. Sci. (2-3): 633-46.

General Conclusions

The viscosities of both aqueous and cyanate ester monomer (BECy) based suspensions of alumina nanoparticle were studied. The applications for these suspensions are different: aqueous suspensions of alumina nanoparticles are used in the production of technical ceramics made by slip casting or tape casting, and the BECy based suspensions are being developed for use in an injection-type composite repair resin.

In the case of aqueous suspensions, it is advantageous to achieve a high solids content with low viscosity in order to produce a high quality product. The addition of a dispersant is useful so that higher solids content suspensions can be used with lower viscosities. For BECy suspensions, the addition of nanoparticles to the BECy resin is expected to enhance the mechanical properties of the cured composite.

The addition of saccharides to aqueous suspensions leads to viscosity reduction. Through DSC measurements it was found that the saccharide molecules formed a solution with water and this resulted in lowering the melting temperature of the free water according to classic freezing point depression. Saccharides also lowered the melting temperature of the bound water, but this followed a different rule. The shear thinning and melting behaviors of the suspensions were used to develop a model based on fractal-type agglomeration. It is believed that the structure of the particle flocs in these suspensions changes with the addition of saccharides which leads to the resultant viscosity decrease.

The viscosity of the BECy suspensions increased with solids content, and the viscosity increase was greater than predicted by the classical Einstein equation for dilute suspensions. Instead, the Mooney equation fits the viscosity behavior well from 0-20 vol% solids. The viscosity reduction achieved at high particle loadings by the addition of benzoic acid was also investigated by NMR. It appears that the benzoic acid interacts with the surface of the alumina particle which may be the cause of the viscosity reduction.

The flow behavior of alumina particles in water and BECy is markedly different. Aqueous alumina suspensions are shear thinning at all alumina loadings and capable of 50 vol% loading before losing fluidity whereas BECy/alumina suspensions show Newtonian behavior up to 5 vol%, and above 5 vol% show shear thinning at all shear rates. Highly

loaded suspensions (i.e. 20vol% alumina) exhibit shear thinning at low and moderate shear rates and shear thickening at higher shear rates. The maximum particle loading for a fluid suspension, in this case, appears to be about 20 vol%.

The difference in the viscosity of these suspensions must be related to the solvent-particle interactions for each system. The reason is not exactly known, but there are some notable differences between BECy and water. Water molecules are ~0.28 nm in length and highly hydrogen bonded with a low viscosity (1 mPa*s) whereas in the cyanate ester (BECy) system, the solvent molecule is about 1.2 nm, in the largest dimension, with surfaces of varied charge distribution throughout the molecule. The viscosity of the monomer is also reasonably low for organic polymer prescursor, about 7 mPa*s.

Nanoparticles in water tend to agglomerate and form flocs which are broken with the shear force applied during viscosity measurement. The particle-particle interaction is very important in this system. In BECy, the particles appear to be well dispersed and not as interactive. The solvent-particle interaction appears to be most important. It is not known exactly how the alumina particles interact with the monomer, but NMR suggests hydrogen bonding. These hydrogen bonds between the particle and monomer could very well affect the viscosity.

A conclusion that can be reached in this work is that the presence of hydroxyl groups on the surface of the alumina particles is significant and seems to affect the interactions between other particles and the solvent. Thus, the hydrogen bonding between particles, particle/additive and/or particle/solvent dictates the behavior of nanosized alumina particle suspensions. The addition of dispersants can change the particle interactions and hence reduce the suspension viscosity. This was demonstrated with saccharides in the aqueous system and with benzoic acid in suspensions with BECy.

Appendix A

Toxicity of Cyanate Ester/Nanocomposite Resins for Composite Repair

A white paper submitted to SERDP

Michael R. Kessler, Mufit Akinc, Xia Sheng, Katherine Lawler, and Wilber Lio
Department of Materials Science and Engineering, Iowa State University,
and Ames Laboratory, Ames, Iowa

1. Introduction

Interlaminar fracture, or delamination, is a common failure mode which often occurs in composites as a result of low energy impact or manufacturing defects. Localized delaminations are repaired by scarf removal of material and subsequent rebuilding (which requires cleaning and paint removal with hazardous VOC containing solvents) or by resin infusion which involves injecting low viscosity resin via an access hole into the failed area. In some cases the repair resin is diluted with volatile organic solvents or reactive diluents to achieve low viscosity. Once the resin solution is infiltrated, volatile solvents evaporate or remain until the resin is cured (typically at elevated temperatures). Additionally, these low viscosity resins usually have lower glass transition temperatures than the matrices in many military grade composites, limiting their application for elevated temperature service. For very high temperature composites, such as bismaleimides (BMIs), field repairs are not even attempted with current repair resins because of the low glass transition temperature of the cured adhesives.

In an ongoing SERDP research project, we are investigating a new class of extremely low viscosity adhesives based on bisphenol E cyanate ester (BECY) which do not require dilution and which result in a cured polymer adhesive with excellent mechanical properties and thermal stability. We are finding that these polymer systems make excellent candidates for the repair of military composite structures. The useful temperature limit for the BECy

polymer for the repair of military composites will be high because of the polymer's high T_g of greater than 500°F (260°C) and onset of decomposition above 750°F (400°C). The cyanate ester monomer also has near infinite room temperature stability (shelf life), facilitating reduced wastes due to spoilage compared to traditional thermosets. We are rheologically engineering these repair systems with the incorporation of nanosize alumina and silica particles (average diameter of 40 nm) for optimum crack filling and stability for repairs to withstand high loadings, environmental extremes and service temperatures.

It is believed that these repair resins will reduce the environmental hazards associated with current composite repairs and open up new repair opportunities specifically for high temperature composites, such as BMI matrix composites. In this paper, we review the toxicity of the cyanate ester/nanocomposite repair resin and its environmental impact. We start by discussing the toxicity of the base cyanate ester monomer. Next, we review some of the background and issues related to the synthesis of the relatively benign monomer. Then the toxicity of nanoparticles in general is reviewed. Finally, we report on our experiments using coupled pyrolysis-gas chromatography (GC)/mass spectrometry (MS) and thermogravimetric analysis (TGA)-MS experiments for the BECy monomer. Occasionally, we will refer to a baseline epoxy resin (a bisphenol-A/amine based epoxy, referred to as EPON 828) which is one of the resins we have selected as a benchmark system to which to compare the mechanical, adhesive, and volatility properties of our newly developed resin system.

2. Toxicity and handling precautions of cyanate ester monomers

Cyanate ester monomers are relatively low in toxicity[1]. Table 1 shows the oral, dermal and mutagenic test results of three commercial cyanate ester monomers, demonstrating their relatively low toxicity[2,3]. For comparison, the commonly used benchmark resin, EPON 828, is also listed in Table 1.

Table 1 Toxicity testing of cyanate ester monomers[2,3] and benchmark EPON 828 resin.

Sample	Acute oral LD_{50} (rat) (g/kg)	Acute dermal LD_{50} (rabbit) (g/kg)	Dermal irritation (rabbit)	Eye irritation (rabbit)	Dermal sensitization	Mutagenicity (Ames)	Inhalation LD_{50} (mg/m^3)
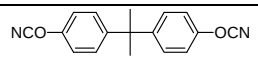 bisphenol A cyanate ester	> 2.5	> 2.5	None	-	Negative	Negative	>440
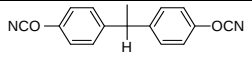 bisphenol E cyanate ester (BECy)	0.5-1.0	> 5.0	None	Mild**	Mild**	Negative	-
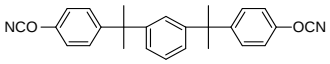 RTX-366	> 5.0	> 2.0	None	None	-	Negative	-
* 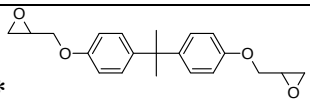 EPON 828 Epoxy	> 4.0	> 20.0	-	2mg/24h severe	Allergic	-	>2E10

* MSDS, "BISPHENOL A DIGLYCIDYL ETHER", Sigma-Aldrich.

** MSDS, "EX-1510 Liquid Resin", Tencate Ltd.

According to Table 1 and the MSDS data for the resins, the toxicity of BECy is much lower than the benchmark epoxy resin. Under conditions where exposure to vapors or mist is possible, BECy could cause respiratory tract irritation[4]. The long-term exposure may aggravate pre-existing eye, skin and respiratory disorders. However, the experiments of chronic effects on humans and animals are not established; the significance of mutagenic activity to man is still unknown. BECy is not a systemic carcinogen and is not listed as carcinogenic by the International Agency for Research on Cancer (IARC), National Toxicology Program (NTP), or Occupational Safety and Health Administration (OSHA).

The hydrolysis of cyanate ester does not produce hydrogen cyanide. Hydrolysis produces carbamates (or urethanes) which will rapidly liberate volatile decomposition products on heating, so shielding precautions should be taken if significant quantity of carbamate is suspected to be encapsulated in a resin during heating. Most cyanate ester

monomers contain multiple aromatic rings and have very low volatility. The single ring cyanate ester monomers, such as hydroquinone dicyanate, phenyl cyanate and low molecular weight alkyl and fluoroalkyl cyanates have a noticeable, sharp odor. Bisphenol E cyanate ester (BECy) monomer contains two aromatic rings and has very low volatility and no noticeable odor.

The curing reaction of BECy is autocatalytic and highly exothermic (700J/g). Overheating, non-uniform heating and overcatalyzing can cause uncontrollable exothermal reaction and should be avoided. The uncontrollable exothermal reaction may increase temperature locally in excess of 400°C along with smoke and char formation[5].

3. Issues in the synthesis of cyanate ester monomer

Organic synthesis of cyanate ester monomers can be traced back more than 100 years to a reaction of an alkoxide with cyanogen chloride[6]. This procedure and later attempts with aryloxides were not successful because the excess oxide reacted with organic cyanate to yield mixtures of imidocarbonate and cyanurates (Figure 1).

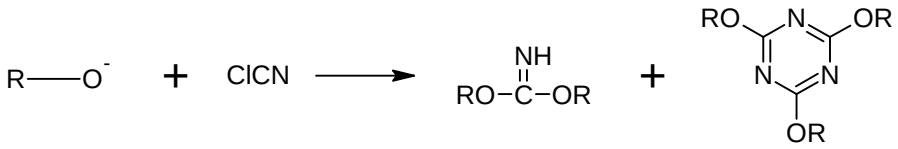

Figure 1. Chemical reaction of alkoxide with cyanogen chloride forming imidocarbonate and cyanurate

In 1960, an approach was successful when ortho-substituted phenols were used, and the first aryl cyanate was isolated[7]. The steric hindrance of substitution prevents the excess aryloxide from consuming the product under the reaction conditions (Figure 2).

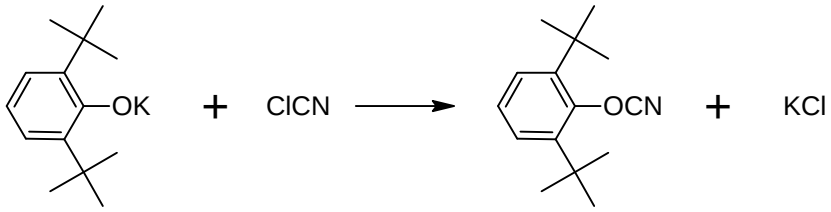

Figure 2. Chemical reaction between aryloxide and cyanogens chloride to yield aryl cyanate.

In 1963, a simple and efficient synthesis was reported when addition of a base to the phenol-cyanogen halide mixture was shown to avoid the excess oxide problem, and this

process was easily adaptable to an industrial scale[8,9]. A very large number of aryl and haloalkyl cyanates were readily synthesized in excellent yield and found to be remarkably stable[10]. Since then, most commercial cyanate ester monomers are prepared by the alcohol-cyanogen halide method.

Cyanogen halides, such as ClCN, BrCN, are highly toxic agents. They cause immediate injury upon contact with the eyes or respiratory organs. Symptoms of exposure are loss of consciousness, convulsions, paralysis, and death. ClCN is especially dangerous because it is capable of penetrating the filters in gas masks.

In 1987, Dow Chemical developed a synthesis where the cyanogen chloride is generated *in situ* and a polyfunctional cyante is formed, based on an addition of phenol and dicyclopentadiene[11]. Even with improvements in techniques and synthesis methods, the starting materials of cyanate ester monomer synthesis are highly toxic, which increases the cost of cyanate ester monomer and may have important impacts on the environment.

4. Toxicity of Nanoparticles

4.1 Introduction

Nanomaterials are defined as materials that possess at least one dimension of 100 nm or less. These materials have significantly different properties compared to their bulk counterparts, making them unique materials with a wide range of applications (e.g. carbon nanotubes, quantum dots, etc.). However, the same characteristics that lend these materials desirable properties may also impart adverse characteristics such as toxicity.[12] Steps have been taken to understand the adverse effects nanomaterials may inflict on our health and the environment, but there is still not a very extensive literature base on the topic.[13] Additionally, there are many conflicting findings concerning the same materials,[13,14,15,16] which may be partly due to the fact that there is no set standard for testing the toxicity of nanomaterials.[17]

Although logically, nano-sizes may facilitate transport within cells, this does not necessarily make nanomaterials toxic.[13] Because so much is unknown and toxicity behavior of nanomaterials is hard to extrapolate to behavior *in vivo*,[18] it is clear that much is still

unknown in the field of nanomaterial toxicology, and there is much work yet to be done to determine the exact toxicity of nanomaterials.

4.2 Mechanisms of exposure

The increased use of nanomaterials in industry will undoubtedly increase the unintentional, and potentially harmful, exposure during manufacturing and processing. It is also likely that nanomaterials will leach into the environment during the entire process from manufacture to disposal of products containing nanomaterials.[18]

The main methods of introducing nanomaterials into the body are through 1) inhalation, 2) ingestion, 3) the skin, and 4) injection.[18]

Inhalation of particles can be highly toxic.[15,16] Small particle sizes oftentimes give rise to higher deposition efficiencies and slower clearance rates. Because they have a very high particle-to-mass ratio, they can easily overload the body's natural mechanisms for clearance. The size of the particles can greatly affect their deposition location and retention within the lungs.[18] The respiratory system can also be a gateway to other body systems, which can be detrimental in the case of toxic particles. Nanoparticles have been shown to translocate from the lungs into the blood and circulatory system,[12,18] as well as via nerve endings, into the brain and nervous system.[12] Inhalation is a major mechanism by which nanomaterials may be introduced into the body. However, to be inhaled, nanoparticles must be in their solid, dry form, and since nanoparticles are often synthesized in the liquid phase, inhalation may not be as significant a problem as other forms of exposure, such as oral or dermal.[13,18]

When ingested, nanoparticles pass through the GI tract and are eliminated via urine and feces.[12,18] However, as they are able pass from the respiratory tract into the circulatory and nervous systems, it is possible that they may also be able to translocate from the GI tract into other body systems as well.

What happens to nanoparticles when they come in contact with the skin is also not completely understood.[15] Studies have shown healthy skin to be impermeable to nanoparticles,[12,15] however there are also conflicting studies that have found nanoparticles to be able to penetrate skin.[15] Damaged skin is also more susceptible to nanoparticle penetration.[12,18]

It must also be noted that the individual properties of nanomaterials such as size and surface chemistry, can drastically affect their properties *in vivo*.[18]

4.3 Factors that influence toxicity

There are many properties that can influence the toxicity of nanoparticles. The most logical property to consider is size. However, other properties, such as composition, surface properties, and solubility may also play a role;[12,17,19,20] however, it is still unclear which properties have the largest influence.

The smaller the size, the more easily a particle is able to be taken into a cell.[18] Due to their size, nanomaterials also have very high surface areas which may also have a strong influence on toxicity.[12,15,18,20] At the same time, studies have also shown that size does not influence the toxicity of nanoparticles.[14,16,21,22] It must be noted that in some of these studies, the nanoparticles agglomerated and therefore the actual particle sizes were significantly larger than the reported or advertised primary particle sizes. [14,19,20,22,23]

Literature with conflicting findings on the influence of the chemical composition of nanoparticles also exists. In one study, it was found that cytotoxicity did not depend on the chemical species,[21] whereas another study found cytotoxicity to be chemical composition dependent.[22] Other studies have shown that the shape of nanoparticles can also affect toxicity.[21] Toxicity may also depend on other factors not related to the specific nanomaterials, such as exposure time[14] and the cells involved.[23]

4.4 Mechanisms of toxicity

Mechanisms of nanotoxicity, while still not fully understood,[24] can be grouped into three main categories: 1) chemical, 2) mechanical, and 3) unknown.[17,19] Included in chemical mechanisms are factors such as composition, which may lead to the release of ions, which have been shown to effect cytotoxicity.[20,21] In addition, nanoparticles have been shown to form reactive oxygen species that can impose oxidative stresses on cells,[12,19,24] which can be also prove toxic. In one study with silica nanoparticles, a linear correlation was found between cell viability and reactive oxygen species.[14] Mechanical mechanisms include possible stresses that their nano-sizes, shape, or surface may inflict on cells.[17]

4.5 Silica (SiO_2) and Alumina(Al_2O_3) nanoparticles

Silicon dioxide, or silica, nanoparticles are currently used in a wide variety of industries and applications such as paints and viscosity modifiers.[14] As stated numerous times before, there are many studies that have presented conflicting findings regarding the toxicity of silica nanoparticles. Findings range from those that show silica to be non-toxic,[17] to semi-toxic,[19,23] to toxic.[14]

Although they have been shown to be non-toxic, and less toxic than other nanoparticles, the fact that certain forms of silica (e.g. crystalline) are known to be toxic after long-term accumulation, however, is still disconcerting. In one study,[25] silica nanoparticles were shown to be able to penetrate cells, but not necessarily the nucleus. Their ability to penetrate cells also varied cell to cell. Toxicity has been shown to increase with time and concentration in some studies as well.[14,25] In another study, nanoparticle silica was found to have less of an effect on fibrogenesis than micro-sized particles.[26] It was suggested that this was because the nano-sizes allowed the particles to translocate to different areas of the body and therefore were more diffuse than the microparticles. Studies on alumina nanoparticles have generally shown them to be non-toxic.[20,22,24] However, in one study, alumina nanoparticles were shown to inhibit root growth of several plant species.[16]

4.6 Conclusion

The data gathered thus far on nanomaterial toxicity is insufficient to conclude anything more than nanomaterials may be toxic. Different studies have shown contradicting results that warrant further investigation. Further investigation to determine factors that influence toxicity and mechanisms by which nanomaterials induce toxicity should be conducted to better understand the materials. In addition, before assessing the risk of nanomaterials, other things will need to be considered aside from the toxic effects, or hazard of nanomaterials, such as exposure and dose.[27] The risk of using nanomaterials cannot be fully assessed until conclusive data on all parts are examined.

5. Experimental Characterization of VOCs

5.1 Mass loss due to VOCs by ASTM and TGA

Throughout our SERDP research program we have evaluated the volatile content of various resin candidates and benchmark resins according to ASTM standard 1259-85. The ASTM standard calls for the heating of a certain geometry of material at 105 °C for ½ hour and measuring the mass loss. Thermogravimetric analysis (TGA) experiments under the same isothermal conditions were also performed as a concomitant measurement of the volatile content. [28] The isothermal TGA results are shown in Table 2. The BECy has just 0.7% volatile content (as defined by the ASTM standard isotherm for 30 min) while the butyl glycidyl ether (BGE) diluted epoxies had a volatile content of 24.8%. While the neat EPON 828 resin did have a lower volatile content than the neat BECy resin (0.4% vs. 0.7%), that system has a much higher viscosity and is not being considered as a suitable benchmark system unless it is diluted with the reactive diluent (BGE) so that the two resins have the same viscosity (for injection requirements). The last two columns in Table 2 are the time (and corresponding temperature) at which the sample is completely volatilized i.e., the entire sample is gone.

Table 2 Comparison of Volatile Content from TGA.

	TGA (105 °C for ½ h)	**TGA (ramp until 100% wt. loss)**	
	Change in wt%	Time (min)	Temperature (°C)
BECy	0.7	36.2	741
EPON	0.4	28.4	584
EPON/BGE	24.8	27.0	556

While the ASTM and TGA testing confirm that there is very little volatile content of the BECy resin at the 105 ° C isotherm (~0.7%), further analysis of the small volatile content was performed to determine the composition of the evolved gases using two different techniques: pyrolysis coupled with GC/MS measurements and TGA coupled with MS measurements.

5.2 Testing Method for pyrolyzer-GC/MS

The sample was analyzed by a CDS 5200 pyrolyzer and Varian 2200 GC/MS instrument. The Varian 2200 consists of a Varian 3800 GC and Varian 2200 Ion Trap MS. The MS has a scan range of 30-650 amu. Scan rate is dependent on scan range.

To obtain GC traces of the volatile gases evolving, 15.5mg sample was placed in the pyrolyzer (py) and heated to 105°C, holding for 30mins (similar to ASTM conditions) in helium atmosphere. During the trapping stage the Tenax TA was held at about 40°C, when the Tenax TA trap was desorbed and the GC trace obtained.

In the GC/MS system, helium was the carrier gas and the capillary column used was DB-5: 30m × 0.25mm × 0.25μm. The split ratio is 1:20, which means that for every 20 parts injected one part goes into the column and the rest travels out the exhaust and is not tested. The temperature of the transfer line was 300°C. The GC oven conditions used were as follows: initial temperature of 35°C for 5 min, ramped to 300°C at 8°C/min, holding for 10min. The transfer line needs to be heated to ensure that the sample travels through the column and is not stuck in the injection port. This high temperature may have caused the trapped gasses to further split into smaller fractions.

5.3 Testing Method for TGA-MS

TG/MS experiments were carried out on a TG/MS system consisting of a TA 2960 SDT interfaced with a Fisons BG Thermolab Mass Spectrometer using a heated capillary transfer line. In this system the sample was ramped very fast to 105°C, held at this temperature for 30 min, and then ramped to 500°C at a rate of 1 °C/min under 100ml/min nitrogen flow. The capillary transfer line was heated to 200 °C, and the inlet port on the mass spectrometer was heated to 150 °C. The MS unit is based on a quadrupole design and the mass scan ranged from 0-300 amu. The sample gas from the SDT was ionized at 70eV. The system was operated at a pressure of 1×10^{-5} torr.

5.4 Py-GC/MS Results

A complete list of all compounds detected by py- GC/MS is presented in Table 5.

The total number of compounds detected by py-GC/MS was 38. Yet, only five compounds made 98% of the total volatiles. These five compounds with most likely composition and relevant characteristics are summarized in Table 3.

Table 3 Volatile components of BECy present in greatest amounts. % volatile is based on the area of the GC peak compared to the total area.

Peak no	RT (min)	Compound	Formula	CAS	MW	% volatile	of total sample
4	7.01	Hexanoic acid, hexyl ester	$C_{12}H_{24}O_2$	6378-65-0	200	16.88	0.068%
8	10.39	3,5-Diamino-1,2,4-triazole	$C_2H_5N_5$	1455-77-2	99	76.28	0.305%
27	19.91	5-hydroxytryptophan	$C_{11}H_{12}N_2O_3$	4350-09-8	220	1.66	64ppm
28	20.29	Acetophenone, 4' -hydroxy	$C_8H_8O_2$	99-93-4	136	1.6	64ppm
35	29.52	4,4' -ethylidenediphenol	$C_{14}H_{14}O_2$	2081-08-5	214	1.65	66ppm
					total :	98.07%	0.4%

Concentration of the remaining 33 compounds were <0.4% each and most <0.1% each may have been fractioned from larger molecules when the volatile gas was injected into the GC at 300^{o}C.

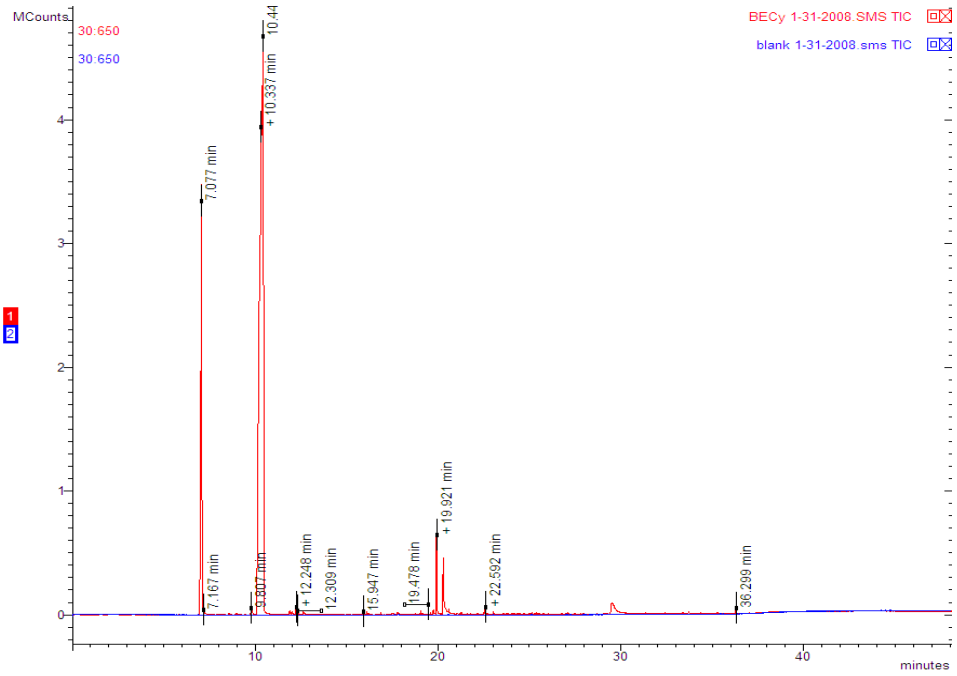

Figure 3 Total Ion Chromatogram for the sample

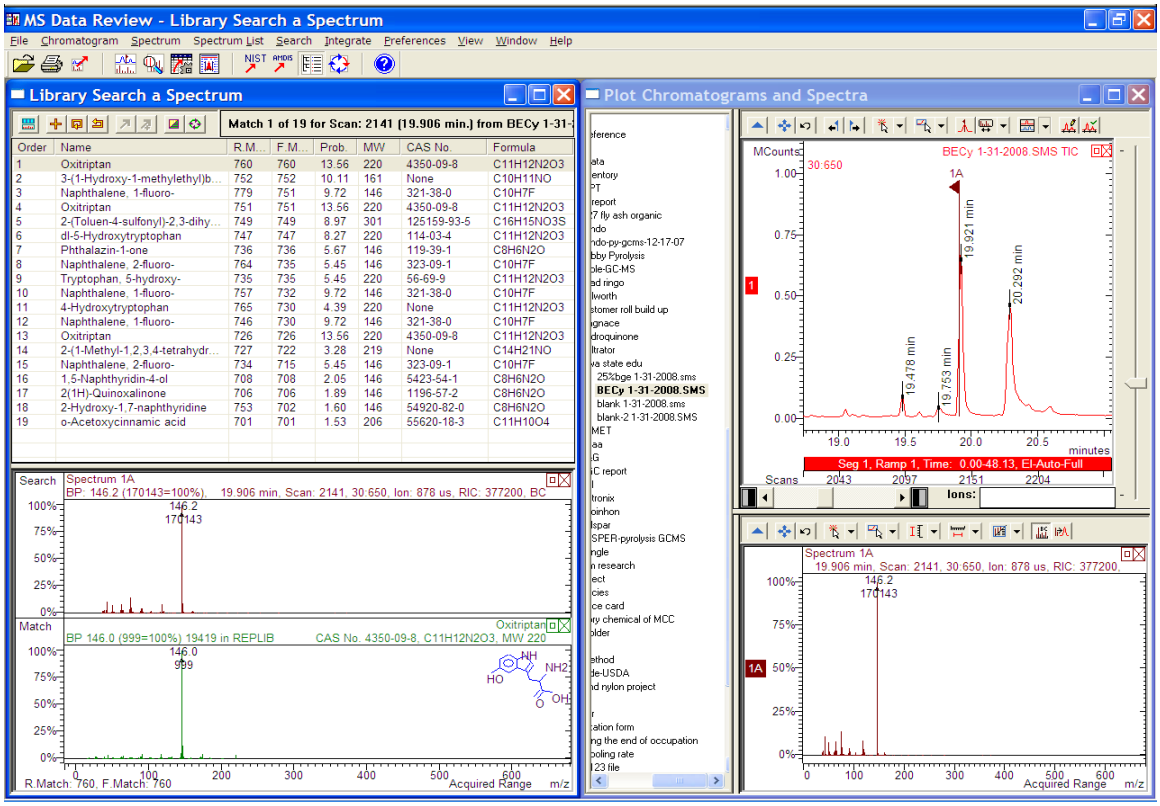

Figure 4 Example compound identification (Peak 27)

5.5 TGA-MS Results

For sample BECy, in the first stage, the mass no 16, 17 and 18 are evolving from the sample. The mass no 16 may be due to NH_2 and 17 and 18 may be due to evolution of water (OH and HOH). In the second and third stage mainly the mass no 16, 17, 18, 44, 50, 51, 52, 55, 61, 62, 63, 65, 66, 77, 78, 91, 92, 94, 107, 108 and 122 are evolving from the sample. Again the first three peaks may be due to NH_2 and H_2O evolution. The mass no 44 most likely represents evolution of carbon dioxide (CO_2, M_{wt} 44). The mass no 50, 51, 52, 77 and 78 may be due to the evolution of benzene and its fragments (C_6H_6, M_{wt} 78) whereas 65, 66 and 94 to that of phenol (C_6H_5OH, M_{wt} 94), and 91 and 92 may be due to evolution of toluene ($C_6H_5CH_3$ M_{wt} 92). The mass no 107, 108 and 122 may be due to the other higher molecular weight hydrocarbons that may have evolved from the resin or formed during the transfer of volatiles to MS at elevated temperature.

The MS data above does not disprove that the compounds listed in Table 1 are incorrect. Also, the NH_2 radical, and H_2O may be added to the list of volatile components at 105^oC.

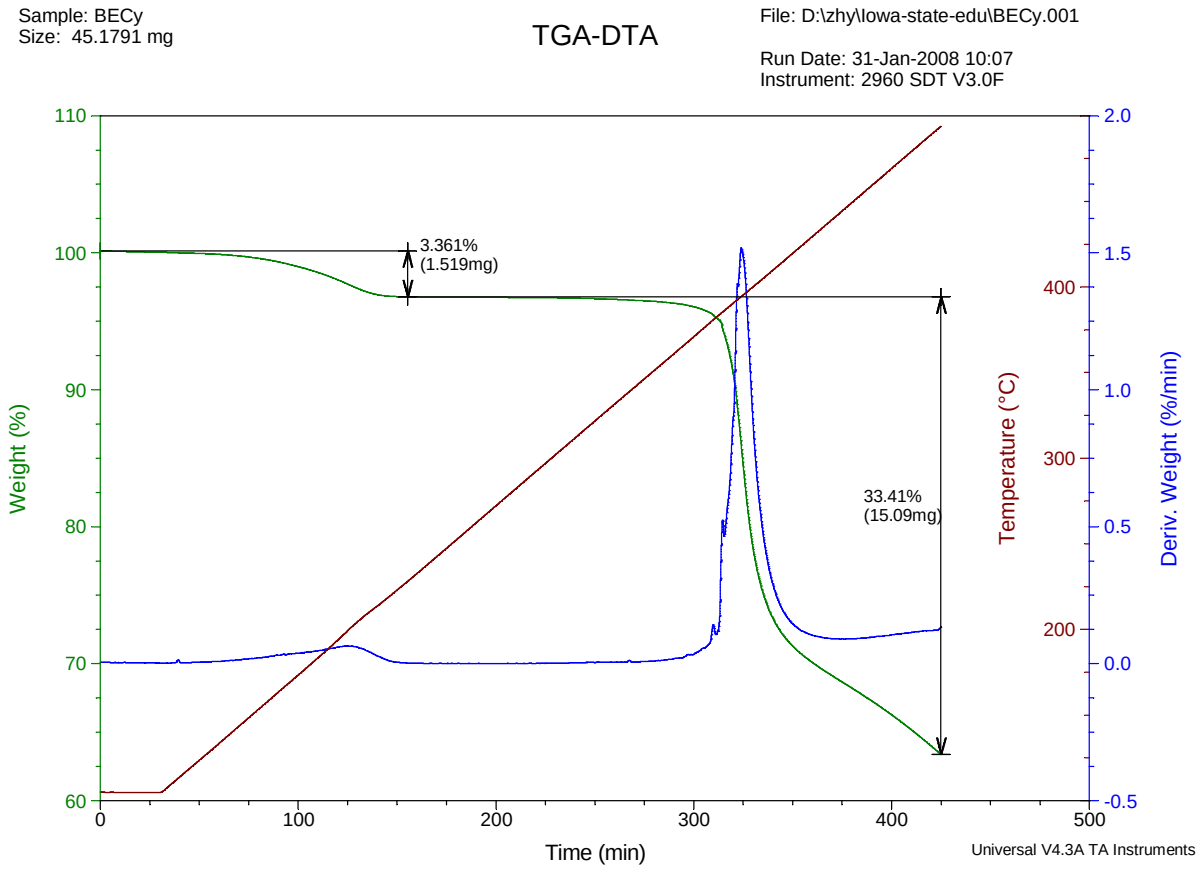

Figure 5 TGA plot of the BECy sample

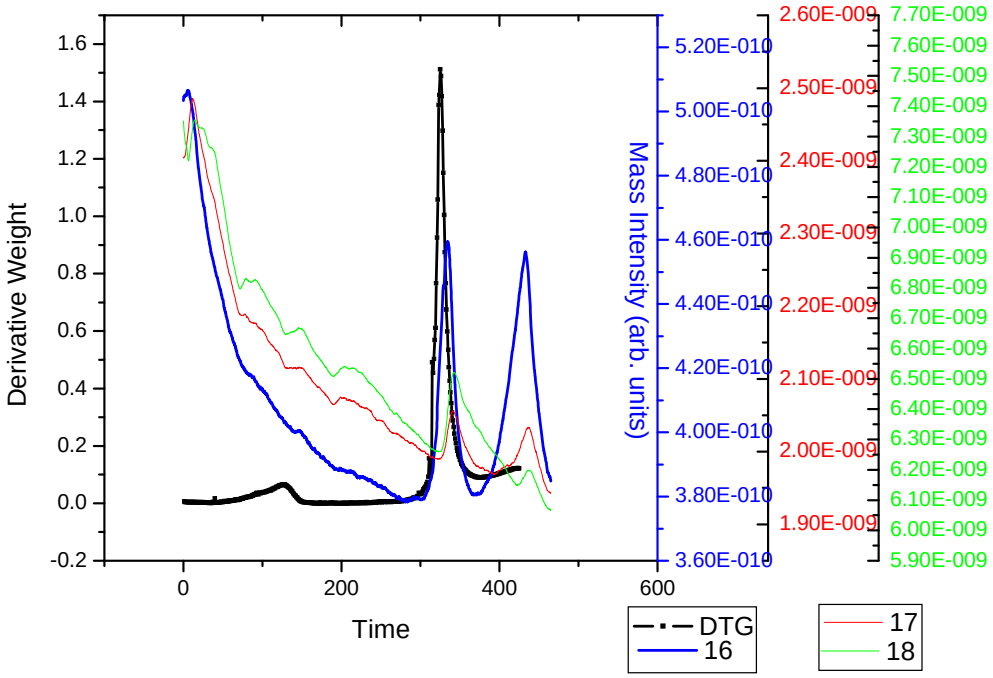

Figure 6 m/z = 16, 17 and 18 MS plot of BECy (Example)

It should be noted that GC and MS chemical assignments are based on the highest probability among possible compounds. Below, the structures of the five compounds with highest concentration in the volatiles are shown (see Table 3). These structures are similar to the monomer:

- Hexanoic acid could be formed by the opening of 6-member carbon ring.
- 3,5-Diamino-1,2,4-triazole and 5-hydroxytryptophan are composed of N, H, C and O all of which are found in the monomer,
- Acetophenone, 4'-hydroxyl is similar to half the monomer with hydroxyl group and carbonyl (C=O) may form from cleavage of cyanate (OCN) group,
- 4,4'-ethylidenediphenol is similar to the Bisphenol E monomer, with cyanate groups replaced by hydroxyl groups.

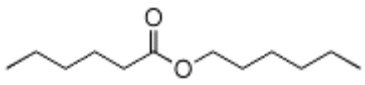

Peak 4 - Hexanoic acid, hexyl ester (hexyl hexanoate)

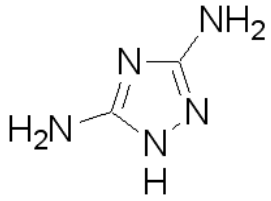

Peak 8 - 3,5-Diamino-1,2,4-triazole

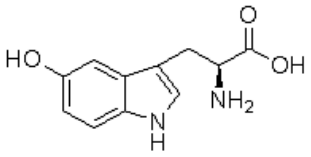

Peak 27 - 5-hydroxytryptophan

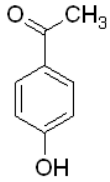

Peak 28 - Acetophenone, 4' – hydroxy

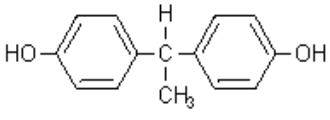

Peak 35 - 4,4' –ethylidenediphenol

5.6 Toxicity

The five compounds in Table 1 were researched for their toxicity. The following paragraphs summarize the information available in the literature with respect to their toxicity:

Hexanoic acid, also called caproic acid, is a fatty acid and a naturally occurring fragrance found in apple, melon, passion fruit, pear, sherry, strawberry, and tomato[29] A study of the toxicity of this acid states: "Conclusions of this criteria document (status December 2002): the acute toxicity of **caproic acid** is low; it is corrosive to the skin and eyes of rabbits; an occlusive patch test with 1% **caproic acid** on **human** volunteers did not show any sensitization; **caproic acid** is not mutagenic in the Salmonella mutagenicity test but is cytotoxic *in vitro*."[30]

3,5-Diamino-1,2,4-triazole. A synonym for this compound is Guanazole. This substance has been used in many clinical trials to treat cancer patients[31]. One study states[32]: "The pharmacokinetics of guanazole, (3,5-diamino-1,2,4-triazole) were evaluated in rats, mice and 3 cancer patients. In humans, IV doses ranging from 3.5-10 g/sq m were used. Half-life in blood was 1-2 hr. The drug was eliminated almost quantitatively in the urine in 24 hr. No metabolites could be detected in the perfusate or bile of the isolated perfused rat liver preparation, suggesting that the drug itself rather than a metabolite is responsible for antitumor activity."

5-hydroxytryptophan, or Oxitriptan, is "An aromatic amino acid with antidepressant activity. In vivo, 5-hydroxytryptophan (5-HTP) is converted into 5-hydroxytryptamine (5-HT or serotonin) as well as other neurotransmitters. 5-HTP may exert its antidepressant activity via conversion to serotonin or directly by binding to serotonin (5-HT) receptors within the central nervous system (CNS). Endogenous 5-HTP is produced from the essential amino acid L-tryptophan. Exogenous therapeutic 5-HTP is isolated from the seeds of the African plant Griffonia simplicifolia" [33].

Acetophenone, 4'-hydroxy is also known as 4'-hydroxyacetophenone, or Piceol. This substance has been found in the leaves of the Chilean plant *Lomatia hirsuta*[34], *and* may reduce inflammation[35]

No toxicity studies were found for 4,4' –ethylidenediphenol.

The MSDS sheets for each of the 5 major constituents were examined to gather more information on the toxicity of these compounds. The MSDS sheets do not provide much information in this regard. However, the type of personal protective equipment necessary to handle each compound is listed and summarized in Table 4.

Table 4 PPE required to work safely with the five compounds by the MSDS sheets

Compound	Personal Protective Equipment (PPE)
Hexanoic acid, hexyl ester	Respiratory: Not required. Use multi-purpose combination Hand: Protective gloves Eye: Chemical Safety goggles
3,5-Diamino-1,2,4-triazole	Respiratory: Air-purifying respirators or dust mask type N95 or type P1 Hand: Compatible chemical-resistant gloves Eye: Chemical safety goggles
5-hydroxytryptophan	Respiratory: Full-face particle respirator type N99 or type P2 Hand: Compatible chemical-resistant gloves Eye: Chemical safety goggles
Acetophenone, 4' - hydroxy	Respiratory: Air-purifying respirators or dust mask type N95 or type P1 Hand: Compatible chemical-resistant gloves Eye: Chemical safety goggles
4,4' -ethylidenediphenol	Respiratory: Air-purifying respirators or dust mask type N95 or type P1 Hand: Compatible chemical-resistant gloves Eye: Chemical safety goggles

5.7 Regulation

To find out whether the chemicals determined to be present in the sample by py-GC/MS were regulated, the document entitled "The Consolidated List of Chemicals Subject to Emergency Planning and the Community Right to Know Act" was referenced[36]. Only five out of the 38 chemicals listed in the table below were found in the list. All five chemicals found in the list had a concentration of less than 0.1% each in the evolved gas.

Table 5 Complete list of all peak assignments with the CAS number.

Peak No.	**Rt (min)**	**Compound**	**Molecular weight**	CAS #	Conc. %	Regulated
1	3.31	Propane, 2-cyclopropyl-	84	3638-35-5	0.03	
2	5.49	Toluene	92	108-88-3	0.02	Yes
3	5.83	Acetic acid, 2-methylpropyl ester	116	110-19-0	0.01	Yes
4	7.01	Hexanoic acid, hexyl ester	200	6378-65-0	16.88	
5	8.59	o-xylene	106	95-47-6	0.05	Yes
6	9.04	1,1'-bicycloheptyl	194	23183-11-1	0.05	
7	9.79	5-Octen-4-one, 7-methyl-	140	32064-78-1	0.34	
8	10.39	3,5-Diamino-1,2,4-triazole	99	1455-77-2	76.28	
9	11.88	Butanoic acid, butyl ester	144	109-21-7	0.04	
10	11.91	Dipropylene glycol monomehtyl ether	148	34590-94-8	0.03	
11	11.99	Dipropylene glycol monomehtyl ether	148	34590-94-8	0.06	
12	12.24	2-propanol, 1-(2-methyoxyproxy)-	148	13429-07-7	0.12	
13	12.31	3-Ethyl-3-hexene	112	16789-51-8	0.03	
14	12.63	Butyl carbamate	117	592-35-8	0.08	
15	14.25	2-Nonen-1-ol, (E)-	142	31502-14-4	0.01	
16	15.91	Cyclohexane, (3-methylpentyl)-	168	61142-38-9	0.01	
17	15.94	Cyclopentane, 1-pentyl-2-propyl-	182	62199-51-3	0.04	
18	16.1	Hydroxylamine, O-decyl-	173	298-79-1	0.04	
19	16.2	Cyclohexane, 1,1'-(1,2-dimethyl-ethanediyl)bis-,	222	54889-87-1	0.02	
20	16.24	Cyclodecanol	156	1502-05-2	0.01	

21	16.88	Cyclohexane, (1-methylethyl)-	126	696-29-7	0.04	
22	17.47	Hydroquinone	110	123-31-9	0.07	Yes
23	18.79	Cyclohexane, 1,1'-(1-methylpropylidene)bis-	222	54890-02-7	0.02	
24	19.05	1,7-dimethyl-4-(1-methylethyl)cyclodecane	210	645-10-3	0.05	
25	19.48	Cyclotetradecane	196	295-17-0	0.16	
26	19.73	1-n-Pentyladamntane	206	50782-11-1	0.12	
27	19.91	Oxitriptan	220	4350-09-8	1.66	
28	20.29	Acetophenone, 4'-hydroxy-	136	99-93-4	1.60	
29	21.27	Phenol, 2,4,6-tris(1-methylethyl)-	220	2934-07-8	0.03	
30	22.55	Diethyl phthalate	222	84-66-2	0.06	Yes
31	22.6	10-Heneicosene(c,t)	294	95008-11-0	0.09	
32	25.38	9-Nonadecene	266	31035-07-1	0.03	
33	27.08	Pentadecanoic acid, 14-methyl-, methyl ester	270	5129-60-2	0.04	
34	27.46	1,2-benzenedicarboxylic acid, butyl 2-methylpropyl ester	278	17851-53-5	0.02	
35	29.52	4,4'-ethylidenediphenol	214	2081-08-5	1.65	
36	32.41	Nonadecane	268	629-92-5	0.02	
37	33.71	1,2-benzenedicarboxylic acid, diisooctyl ester	390	27554-26-3	0.05	
38	36.29	2,6,10,14,18,22-tetracosahexaene, 2,6,10,15, 19, 23-hexamethyl-, (all-E)-	410	111-02-4	0.11	

6. Conclusion

As an integral part of developing a novel and environmentally friendly composite repair process, quantity and composition of the gasses evolving from BECy resin were

studied. In particular, protocol described in ASTM standard 1259-85 was followed. Total evolved gas was determined by heating the samples with prescribed geometry to 105 °C for 30 minutes and measuring the mass loss. As a benchmark comparison, EPON 828, and EPON 828 diluted with butyl glycidyl ether (BGE), to have the same injectable viscosity, were also tested. The BECy lost 0.7% compared to the butyl glycidyl ether (BGE) diluted EPON 828 which lost 24.8% of its mass. While the neat EPON 828 resin did have a lower volatile content (0.4% vs. 0.7%), it is not being considered as a suitable benchmark without the reactive diluent (BGE).

Chemical composition of the total evolved gases from BECY resin was studied by py-GC/MS and TGA/MS techniques. A total of 38 mass fractions were identified by MS. Of this total, five of them constituted the 98% of the total volatiles. Of the remaining 33 compounds, all but two had concentrations less than 0.1% each. The other two had concentration of 0.34 and 0.16% each. It should be noted that these concentrations represent 24 and 11 ppm of resin. Furthermore, It is certainly possible that the significant number of volatiles detected by the mass spectrometer might have formed during volatile gas transfer to MS at elevated temperature.

Identification of evolved gas fractions by mass spectroscopy is not a trivial task. Using the instruments database and the parent resin BECy's chemical structure, most probable compositions were assigned to each of the five most abundant volatiles. Literature was screened for toxicity assessment of the evolved gases. None of the five significant components was "regulated." Only five of the remaining 33 compounds were on the list of "regulated" compounds. Concentration of each of these compounds is 0.07% of total volatiles (or 5 ppm of resin) or less.

Literature on the toxicity of these "regulated" compounds is rather scarce and not specific. Therefore, accurate assessment of toxicity and permissible exposure levels is difficult if not impossible. However, it suffices to say that the limited study we have conducted on the amount of volatiles and their toxicity does not raise any immediate concern. Considering the fact that some of the volatile fragments may not even be evolved during heating to 105 °C but formed during the analysis step, may lower the potential toxicity concerns for the use of this resin for composite repair applications.

Toxicity and risks associated with the nanoparticles is a current topic of research. The few reports available in the literature are often inconclusive and conflicting. Although some concerns have been expressed for inhaling air born nanoparticles, toxicity does appear to be more associated with the chemical composition and crystal structure of the particles than their size. The reader is reminded that nano size clay particles have been handled by humans for millennia without an established health hazard. Similarly, colloidal gold has been injected into the human body for improving the condition of joints and other ailments. Toxicity of alumina nanoparticles suspended in liquids has not been properly evaluated but there is no obvious indication that they may pose serious health hazards.

Perhaps, it should be emphasized that the volatiles and toxicity assessment was limited in scope and depth, and was carried out by materials scientists not by an expert toxicologist. It might be prudent to have this report reviewed by toxicologists, and if necessary, additional work should be carried out before this repair technology is reduced to practice.

7. References

[1] I. Hamerton, "Chemistry and technology of cyanate ester resins", First edition, 1994 Chapman & Hall.

[2] Bogan, G. W., Lyssy, M. E., Monnerat, G. A. and Woo, E. P. (1988) *SAMPE J.*, **24**, 19.

[3] Kohn, J. and Langer, R., (1986) *Biomaterials*, **7**, 176.

[4] MSDS, "EX-1510 Liquid Resin", Tencate Ltd.

[5] Shimp, D. A., Christenson, J. R. and Ising, S. J., (1991), *Cyanate ester resins-chemistry, properties and applications, Technical Bulletin*, Ciba, Ardsley, NY.

[6] Crigat E. and Putter R., 1967, *Angew. Chem. Internat. Edit.*, **6**, 206.

[7] Stroh R and Gerber H., 1960, *Angew. Chem.*, **72**, 1000.

[8] Crigat E. and Putter R, 1963, German Patent 1, 195, 764.

[9] Crigat E. and Putter R, 1964, *Chem. Ber.*, **97**, 3012.

[10] "Chemistry and Technology of Cyanate Ester Resins", Hamerton I., Ed., Chapman and Hall, London, 282 (1994).

[11] Bogan G.W., Lyssy M.E., Monnerat G.A. and Woo E.P., 1988, *SAMPE J.*, **24**, 19.

[12] Andre Nel, et al. Toxic potential of materials at the nanolevel. Science. 311 (Feb 2006) 622.

[13] Vicki L. Colvin. The potential environmental impact of engineered nanomaterials. Nature Biotechnology. Vol 21 No 10 (Oct 2003) 1166-1170.

[14] Weisheng Lin, et al. In vitro toxicity of silica nanoparticles in human lung cancer cells. Toxicology and Applied Pharmacology. 217 (2006) 252–259.

[15] Roberta Brayner. The toxicological impact of nanoparticles. Nanotoday. Vol 3 No 1-2 (Feb-Apr 2008).

[16] L. Yang et al. Particle surface characteristics may play an important role in phytotoxicity of alumina nanoparticles. Toxicology Letters. 158 (2005) 122–132.

[17] Tobias J. Brunner et al. In vitro cytotoxicity of oxide nanoparticles: comparison to asbestos, silica, and the effect of particle solubility. Environmental Science and Technology. Vol 40 No 14 (2006) 4374-4381.

[18] Günter Oberdörster et al. Nanotoxicology: an emerging discipline evolving from studies of utlrafine particles. Environmental Health Perspectives. Vol 113 No 7 (July 2005) 823-839.

[19] Laura K. Adams et al. Comparative eco-toxicity of nanoscale TiO_2, SiO_2, and ZnO water suspensions. Water Research. 40 (2006) 3527–3532.

[20] Xiaoshan Zhu et al. Comparative toxicity of several metal oxide nanoparticle aqueous suspensions to zebrafish (Danio rerio) early developmental stage. Journal of Environmental Science and Health Part A. 43 (2008) 278–284.

[21] Akiko Yamamoto et al. Cytotoxicity evaluation of ceramic particles of different sizes and shapes. Journal of Biomedical Materials Research Part A. Vol 68A, Issue 2 (2003) 244–256.

[22] Andrew J. Wagner et al. Cellular Interaction of Different forms of aluminum nanoparticles in rat alveolar macrophages. Journal of Physical Chemistry B. 111 (2007) 7353-7359.

[23] Jenq-Sheng Chang et al. In vitro cytotoxicity of silica nanoparticles at high concentrations strongly depends on the metabolic activity type of the cell line. Environmental Science and Technology. 41 (2007) 2064-2068.

[24] Daohui Lin et al. Phytotoxicity of nanoparticles: Inhibition of seed germination and root growth. Environmental Pollution. 150 (2007) 243-250.

[25] Yuhui Jin. Toxicity of Luminescent Silica Nanoparticles to living cells. Chemical Research in Toxicology. 20 (2007) 1126–1133.

[26] Ying Chen et al. Comparing study of the effects of nanosized silicon dioxide and microsized silicon dioxide on fibrogenesis in rats. Toxicology and Industrial Health. 20 (2004) 21-27.

[27] Possible adverse health, environmental and safety impacts. Nanoscience and Nanotechnologies. (July 2004) 35-50.

[28] Kessler, Michael R., and Akinc, Mufit. Environmentally Benign Repair of Composites Using High Temperature Cyanate Ester Nanocomposites, Project WP-1580 FY07 Annual Report.

[29] http://www.thegoodscentscompany.com/data/rw1028161.html

[30] S. Hirzel Verlag, Birkenwaldstrasse 44, 70191 Stuttgart, Germany, 2005. Xi, 85p. http://toxnet.nlm.nih.gov/cgi-bin/sis/search/f?./temp/~JtglAj:1

[31] Toxnet. Toxicology Data Network. http://toxnet.nlm.nih.gov/cgi-bin/sis/search/r?dbs+toxline:@term+@rn+1455-77-2+@OR+@mh+%22+Guanazole+%22+@OR+@na+%22+Guanazole+%22+@OR+@ab+%22+Guanazole+%22+@OR+@kw+%22+Guanazole+%22

[32] Pharmacokinetics of guanazole in man. Clin. Pharmacol. Ther.; Vol 14 ISS Mar-Apr 1973, P264-270

[33] National Cancer Institute. NCI Drug Dictionary. http://www.cancer.gov/Templates/drugdictionary.aspx?CdrID=459776

[34] Simonsen, Henrik T. Anne Adsersen, et. al. BMC Complementary and Alternative Medicine 2006, 6:29.

[35] Alvarez, Maria Eugenia, Alejandra Ester Rotelli, et al. Il Farmaco 55 (2000) 502-505.

[36] http://www.epa.gov/ceppo/pubs/title3.pdf

Appendix B

Effect of alumina nanoparticles on the properties of low-viscosity cyanate ester adhesives for composite repair

Accepted for ANTEC conference 2009

Wilber Lio, Katherine Lawler, Xia Sheng, Mufit Akinc, and Michael R. Kessler
Department of Materials Science and Engineering, Iowa State University,
and Ames Laboratory, Ames, Iowa

Abstract

Polymer matrix composites (PMCs) are susceptible to microcracks and delaminations from impacts and thermal/mechanical loadings that greatly reduce their mechanical integrity. This is especially a problem for high-temperature PMCs because current repair resins have low glass transition temperatures (T_g's) that stem from the low prepolymer viscosities required of injectable resins. Bisphenol E cyanate ester has both a high cured T_g and low prepolymer viscosity, ideal for the injection repair of high-temperature PMCs. Alumina nanoparticles were incorporated to improve adhesive strength and engineer prepolymer viscosity. Lap shear tests were performed to evaluate the effects of alumina nanoparticles on the adhesive strength of the resin.

Introduction

Polymer composites are used in a wide range of applications, from airplanes to bicycle frames, and as the desire for stronger and lighter materials continues to grow, composites will be in ever-increasing demand. Composite materials, however, are susceptible to damage that can greatly compromise their mechanical properties. Depending on their applications, this can yield disastrous effects.

Defects in composites can be caused by various events that occur throughout a structure's lifetime. They may arise as a result of poor manufacturing techniques, or they may be introduced when a part is damaged while in service [1, 2]. The majority of in-service damage results from some form of impact. Cracks, dents, delaminations, and disbonds caused by impacts can lead to a dramatic decrease in mechanical properties. Low-velocity impacts can be especially troublesome because the presence and

amount of damage is often difficult to detect, yet can be greatly detrimental to the integrity of the part [1]—a 70% reduction in compressive strength has been reported in specimens that showed no visible damage [3]. For this reason, it is imperative for the integrity of composites to be properly maintained.

Resin-injection is a non-patch composite repair technique used to repair disbonds and delaminations within a composite. This is usually done by injecting a resin into the delamination zone, applying pressure to allow the resin to fully infiltrate the specimen, and heating the part to cure the resin (Figure 7). As simple as that sounds, there are many things that must be taken into account.

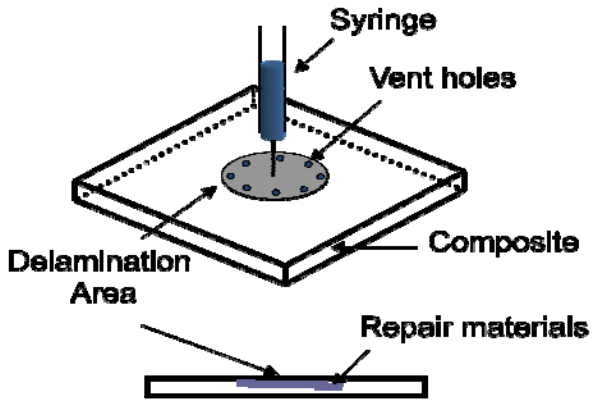

Figure 7. Resin-injection repair of composites**.**

One of the biggest challenges faced when designing an injection repair system involves resin viscosity. Injection repair is often limited to low-temperature composites because of the general trend for low-viscosity prepolymers to have low cured T_g's [4]. This trend is shown in Figure 8. A current problem in the field of composite repair thus lies in the resin-injection repair of high-temperature composites. High-temperature composite repair requires repair resins with high T_g's; however, because the high T_g's are usually accompanied by high prepolymer viscosities, these resins are very difficult to process, and as one can imagine, difficult to inject.

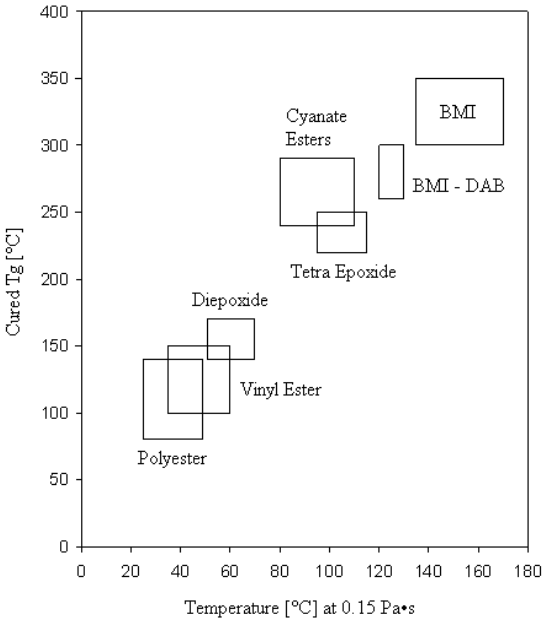

Figure 8. Polymer's T_g vs. temperature at which the monomer's viscosity is 0.15 Pa·s: most high-temperature resins in turn have high viscosities[4,5].

A unique type of cyanate ester monomer called bisphenol E cyanate ester (BECy, 1,1'-bis(4-cyanatophenyl)ethane) is one exception to this trend. The chemical structure of BECy is shown in Figure 9. BECy monomer has an extremely low viscosity between 0.09 - 0.12 Pa·s at room temperature [4], and yet, cured BECy has a T_g around 260 °C. These characteristics make BECy an excellent candidate for the resin-injection repair of high-temperature polymer composites.

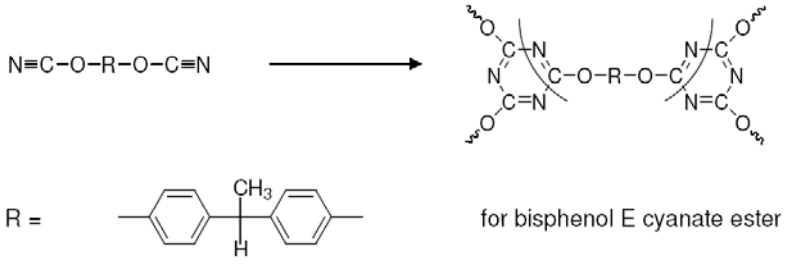

Figure 9. Chemical structure of bisphenol E cyanate ester and polymerization scheme.

Nanomaterials have not only been shown to increase adhesive strength by as much as 45% [6], but they have also been shown to drastically influence rheological properties. The majority of literature on the role of particles on rheology involves microparticle suspensions[7-11]. Aqueous alumina suspensions with sub-micron to micron-sized particles exhibit shear thinning behavior approaching a constant viscosity at high shear rates. The smaller the particle size, the higher the shear rate at which the limiting viscosity is reached. To explain the shear thinning behavior, it has been claimed that as shear rate is increased, floc networks are broken, releasing "entrapped" fluid[7,8]. Extrapolation of this model to nanoparticle suspensions implies that the viscosity of nanoparticle suspensions could result in a gel at zero shear and a low- viscosity liquid at high shear rates, or so-called thixotropic behavior. Rand and Fries[12] reported that as the particle size decreased, thixotropic behavior was much more pronounced due to increased interaction between the particle surfaces and fluid.

This behavior is attractive for resin-injection repair because the repair agents could be tailored to become shear thinning with the addition of nanoparticles. Shear thinning behavior is expected to allow easy injection into the damaged region and provide the suspension with sufficient integrity after injection until the monomer is cured.

The goal of this work is to evaluate the effect of nanoparticles on viscosity and adhesive strength for bisphenol E cyanate ester, a candidate resin for an optimized resin-injection repair process for composite materials.

Materials

The BECy monomer (EX1510 resin), purchased from Bryte Technologies, Inc. (Morgan Hill, CA), was used as received without further purification. The liquid phase organometallic-based catalyst, EX1510-B, was supplied with the resin.

An epoxy resin, EPON 828, was used as a benchmark comparison to the cyanate ester being investigated. The epoxy along with its curing agent, Epikure™ 3223, was purchased from Miller-Stephenson Chemical Company, Inc. (Morton Grove, IL). Butyl glycidyl ether (BGA) was used as a reactive diluent to lower the viscosity of the benchmark resin, and was purchased from Sigma-Aldrich (Milwaukee, WI).

Spherical alumina nanoparticles were supplied by Nanophase Technologies, Inc. (Romeoville, IL) as NanoTek aluminum oxide, which is γ-phase alumina (density of 3.6 g/cm^3) with an average particle size (diameter) of 48 nm and a specific surface area of 44 m^2/g. Before use, the nanoparticles were dried at 110 °C for 2 hr.

Methods

BECy/alumina nanoparticle suspensions containing 1 to 20 vol% alumina were prepared. BECy monomer was first weighed into a glass vial. Dried alumina nanoparticles were then weighed and added. The vial was then sealed and suspended in an ultrasonic water bath for 50 min. After ultrasonic treatment, the suspensions were stored in a desiccator for further characterization.

BECy/alumina nanoparticle suspensions were tested for rheological properties using a TA Instruments AR2000ex rheometer with a Peltier temperature control stage, utilizing a cone/plate geometry (45 mm diameter cone with 1° angle). A steady state flow test was conducted for each sample from shear rates of 0.1 to 500 s^{-1} (10 points per decade) at 25 °C. Before samples were loaded, suspensions were ultrasonicated for 5 minutes to ensure the particles were dispersed.

TEM samples were prepared by sectioning the cured BECy/alumina nanocomposites with an ultramicrotome to produce 50-60 nm thick sections which were placed on copper TEM grids. A JEOL 2100 transmission electron microscope (Tokyo, Japan) at an accelerating voltage of 200 kV was used.

Aluminum coupons and bismaleimide/carbon fiber (BMI) coupons for lap shear tests were machined to ASTM D 1002-05 and 5868-01 standards, respectively. The aluminum coupons were bead-blasted on the adhesive surfaces, and the BMI coupons sanded, to aid in adhesion. Lap shear specimens were prepared by applying resin onto one coupon, and applying adequate pressure to hold the second coupon in place during the cure cycle.

The resins for lap shear tests were mixed and cured in the following manner. For both BECy and BECy/alumina suspensions (2.5 vol.% alumina), catalyst was added in a 100:3 (resin:catalyst) weight ratio and cured in a convection oven with the following cure schedule: 1) heat from room temperature to 180 °C at a rate of 1 °C/min, 2) isothermally

cure at 180 °C for 2 hr, 3) increase temperature to 250 °C at 1 °C/min, 4) isothermally cure at 250 °C for 2 hr, and 5) cool to room temperature in the oven at a rate of 2 °C/min. The benchmark epoxy and curing agent were mixed in a 10:1 weight ratio and cured at 80 °C for 1 hr. The diluent BGE was added to the epoxy (25 wt.% BGE) in order to decrease its viscosity to the same level of that of BECy.

An Instron 5569 tensile testing machine (Norwood, MA) was used to perform lap shear tests. Spacers were used during tests to compensate for the inherent offset of the lap shear samples. Aluminum and BMI substrate samples were pulled at extension rates of 1.3 and 0.5 mm/min, respectively, until failure. High-temperature tests (conducted at 200 °C) were performed on aluminum substrate lap shear samples using an Instron SFL Heatwave temperature controlled chamber.

Results and Discussion

The dependence of viscosity on nanoparticle loading is shown in Figure 10. The viscosity of neat BECy was found to be 0.068 Pa·s and independent of shear rate. With increased alumina nanoparticle loading, the viscosity of the suspensions increased. In addition, the suspensions exhibit shear thinning behavior. The shear thinning became more pronounced as the volume fraction of particles exceeded 10 %. At 20 vol% loading, significant shear thinning was observed below 100 s^{-1} but at higher shear rates the material exhibited slight shear thickening behavior.

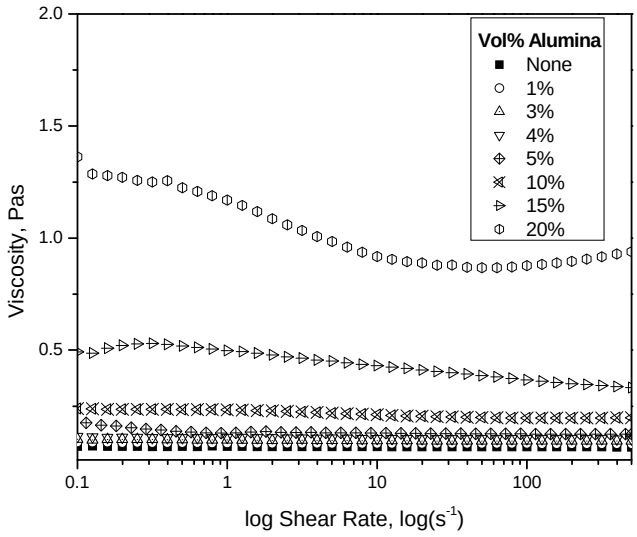

Figure 10. Viscosity vs. shear rate for BECy/alumina nanoparticle suspensions. The viscosity of the suspension increases greatly with particle loadings above 5 vol.%.

The viscosity of the BECy monomer was observed to be Newtonian: the viscosity was independent of shear rate. However, with higher volume fraction of solids, the viscosity increased and exhibited shear thinning behavior. This may be due to the interaction and flocculation of nanoparticles in the suspension. As the shear rate is increased, flocs are broken up, and the liquid becomes free to flow, resulting in a decrease in viscosity. This shear thinning behavior, seen in suspensions with 15 vol% nanoparticles or less, is promising for resin-injection applications. The resin is expected to be easy to inject because it has a low viscosity at high shear rates, and to remain in the damage zone (at a shear rate near zero) during cure.

TEM images (for example Figure 11) show that the particles are well dispersed in the matrix. White colored areas are due to particle pull-out during sectioning. The voids are elongated along the cutting direction.

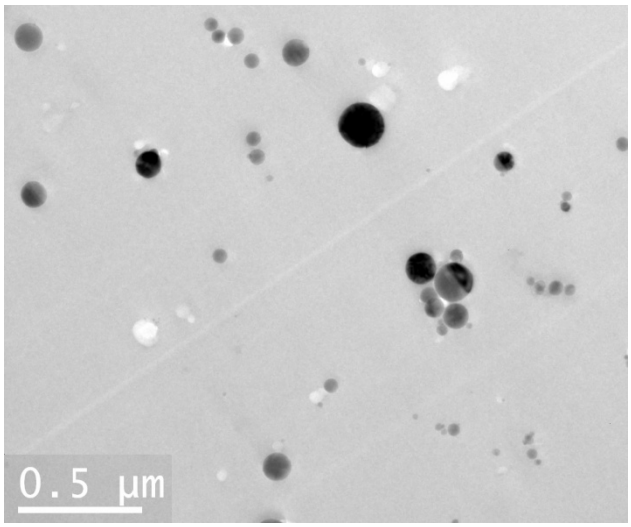

Figure 11. TEM image of cured BECy/2.5 vol.% alumina sample.

The lap shear test results are summarized in Figure 12 and Figure 13. Aluminum substrate samples were tested at room temperature as well as 200°C. At room temperature, both the neat BECy and BECy/alumina nanocomposite outperformed the benchmark epoxy. The BECy/alumina nanocomposite, however, was weaker than the neat resin. At 200°C, the failure stress of the neat BECy greatly exceeded that of the epoxy even more so than at room temperature.

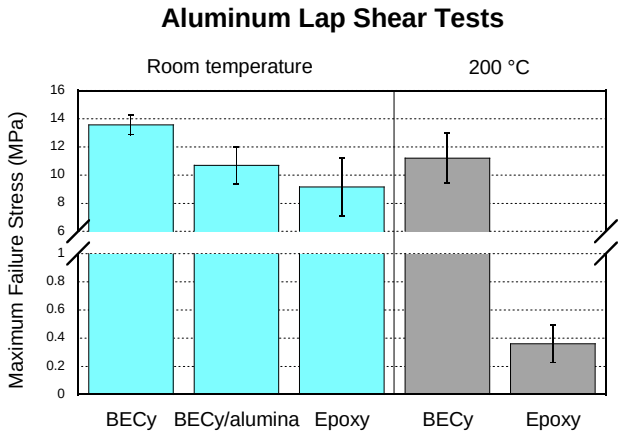

Figure 12. Lap shear test results at room temperature and 200°C on aluminum substrates.

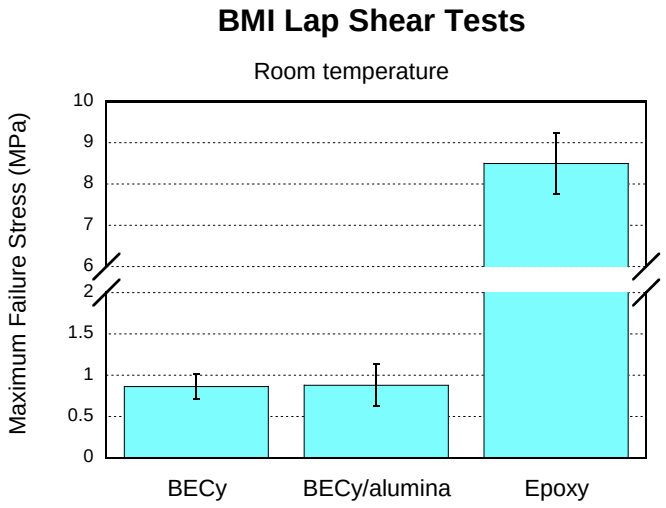

Figure 13. Lap shear test results at room temperature on BMI composite substrates.

On the other hand, the benchmark epoxy drastically outperformed both the neat BECy and nanocomposite at room temperature on BMI substrates. High-temperature tests on BMI substrates have yet to be conducted. The incorpoartion of alumina nanoparticles did not seem to effect the adhesive strength on the composite substrate.

The maximum failure stress of the BECy aluminum lap shear samples was 13.6 MPa. This is nearly 50% greater than the benchmark epoxy resin under the same conditions. At 200 °C, BECy outperformed the epoxy resin even more so than at room temperature. Oppositely, the maximum failure stress of the epoxy BMI lap shear samples was an order of magnitude greater than that of the neat BECy BMI samples.

The aluminum oxide layer on the surface of the aluminum substrates may be responsible for the exceptionally high adhesion of BECy on aluminum. It is possible that the surface hydroxyl groups promote adhesion by forming covalent bonds with BECy [5, [13]].

Possible explanations for the relatively poor adhesion of BECy on BMI include the lack of hydroxyl groups, poor wetting due to the surface energy, or perhaps, similar to grit blasting, as reported by Chin and Wightman[14], sanding of the BMI substrate could be detrimental to lap shear strength. In any case, further tests need to be conducted to fully understand these observations, including the investigation of different surface treatments.

The incorporation of alumina nanoparticles on adhesive strength was not very clear. There seems to be some sort of substrate dependence. The addition of alumina nanoparticles

in the lap shear samples on aluminum substrate showed a decrease in adhesive strength, whereas a slight increase in strength was observed in samples on BMI substrate. More tests are being conducted to determine exactly what the effects of alumina nanoparticles are on adhesive strength.

Conclusions

The effect of nanoparticle loading on the viscosity and adhesive strength of bisphenol E cyanate ester was evaluated. The addition of alumina nanoparticles increased the viscosity of resulting BECy/alumina suspensions and also rendered the suspensions shear thinning. This could be beneficial for resin-injection as the viscosity of the resin would be low during injection, and high afterwards, remaining stable within the delaminations.

Adhesive strength of BECy and BECy/alumina nanocomposites were also evaluated against a benchmark epoxy via lap shear tests. BECy was found to perform superior to the epoxy in aluminum substrate lap shear tests; however, performed inferior on BMI substrates. The effect of alumina nanoparticles requires further investigation.

Acknowledgments

The research described in this article was supported by a grant from the Strategic Environmental Research and Development Program (SERDP), under the "Environmentally Benign Repair of Composites Using High Temperature Cyanate Ester Nanocomposites" project (Project Number WP-1580). Thanks to Brian Richard for his help in preparing lap shear samples.

References

[1] Baker, A. A, *Composites Materials in Aircraft Structures*, Ed. D. H. Middleton, Addison-Wesley Longman, Limited, 207 (1990).
[2] W. J. Cantwell and J. Morton*, J. Strain Anal.*, **27,** 29 (1992).
[3] S.D. Bartus, *J. Adv. Mater.*, **39,** 3 (2008).
[4] D.A. Shimp and W. M. Craig, Jr., *34th Annual International SAMPE Symposium*, 1336 (1989).
[5] D.A. Shimp, *Chemistry and Technology of Cyanate Ester Resins*, Chapman and Hall, 282 (1994).

[6] K.T. Hsiao, J. Alms, and S.G. Advani, *Nanotechnology*, **14**, 791 (2003).
[7] G. Tari, M.F. Ferreira, and A.T. Fonseca, *Ceram. Int.*, **25**, 577 (1990).
[8] G. Tari, M.F. Ferreira, A.T. Fonseca, and O. Lyckfeldt, *J. Eur. Ceram. Soc.*, **18,** 249 (1998).
[9] M. Schneider, J. Claverie, C. Graillat, and T.F. McKenna, *J. Appl. Polym. Sci.,* **84**, 1878 (2002).
[10] A.A. Zaman, B.M. Moudgil, *J. Rheol.*, **42**, 21 (1998).
[11] A. Zupancic, R. Lapasin, and A. Kristoffersson, *J. Eur. Ceram. Soc.*, **18** 476 (1998).
[12] B. Rand and R. Fries, *CeramicTransactions*, **62**, 165 (1996).
[13] W.K. Goertzen, X. Sheng, M. Akinc, and M.R. Kessler, *Polym. Eng. Sci.,* **48**, 875 (2008).
[14] J.W. Chin and J.P. Wightman, *Compos. Part A-Appl. S.*, **27**, 419 (1996).